



**POLITECNICO**  
MILANO 1863

SCUOLA DI INGEGNERIA INDUSTRIALE  
E DELL'INFORMAZIONE

# Catalytic upgrade of pyrolysis vapors: acetic acid chain- growth reactions on $\text{TiO}_2$

TESI DI LAUREA MAGISTRALE IN  
ENERGY ENGINEERING  
INGEGNERIA ENERGETICA

Author: **Andrea Locatelli**

Student ID: 944667  
Advisor: Alessandra Beretta  
Co-advisor: Veronica Piazza  
Academic Year: 2021-22



## Abstract

The valorization of waste biomass is a resource for the current energy transition and a pillar of circular economy. However, the widespread use of bio-liquids is hampered by their negative features: poor stability, acidity, tendency to coking, limited calorific value. These negative factors are caused by the presence of C<sub>2</sub>-C<sub>4</sub> light oxygenates. In this context, the objective of this thesis is the study of light oxygenates catalytic C-C coupling reactions in order to increase C-chain length of bio-oil species while reducing the overall O/C ratio.

A model oxygenate and a model reacting system were chosen: acetic acid ketonization on TiO<sub>2</sub> catalyst. Carboxylic acids are in fact important light and undesired products of the pyrolysis of lignocellulosic biomass. Ketonization, then, is a reaction leading to the condensation of two molecules of acid with decarboxylation, then the loss of one C in the form of CO<sub>2</sub>. In this work, experiments were run in a lab-scale plant, using a traditional packed bed configuration where the catalyst was tested in powder form. The experimental campaign was divided into two parts. In the first one, experiments were run so that only ketonization reaction was taking place, avoiding secondary reactions. Acetone was thus the unique condensation product. To achieve this, maximum conversion and temperature during the experiments were set respectively at 50% and 300°C. The effect of both catalyst reduction pre-treatment and Ru addition in catalyst formulation were explored. In the second part, the catalytic system was pushed to more severe conditions (higher temperature and conversion), and the effect on products distribution over time on stream, Ru addition and H<sub>2</sub> co-feed were investigated. Under these operative conditions, both secondary reaction pathways from acetic acid and acetone, and deactivation phenomena were present. Indeed, heavy C<sub>6+</sub> products that are of great interest for fuel blending were formed, but their selectivity was seen decreasing with time. For this reason, carbon-deposits on spent catalyst were measured via TPO experiments. In conclusion, it has been shown that TiO<sub>2</sub> catalysts are able to successfully catalyse acetic acid ketonization. Moreover, at sufficiently high reaction temperature, secondary aldol condensation reactions were activated, together with cyclization and cracking routes. Indeed, heavy species in the fuel-range were observed among products, with C<sub>4</sub>-C<sub>12</sub> species reaching a global selectivity of 66% at 400°C. Challenges in terms of catalyst deactivation and difficult control of process selectivity emerged.

**Key-words:** acetic acid; ketonization; TiO<sub>2</sub>; chain-growth reactions; bio-fuels



## Abstract in italiano

La valorizzazione delle biomasse di scarto è una risorsa per l'attuale transizione energetica e un pilastro dell'economia circolare. Tuttavia, la diffusione dei bio-liquidi è ostacolata dalle loro caratteristiche negative: scarsa stabilità, acidità, tendenza al coking, limitato potere calorifico. Queste proprietà negative sono causate dalla presenza di ossigenati leggeri C<sub>2</sub>-C<sub>4</sub>. L'obiettivo di questa tesi è lo studio di reazioni catalitiche di C-C coupling su ossigenati leggeri al fine di aumentare la lunghezza delle specie, riducendo il rapporto O/C complessivo. La chetonizzazione dell'acido acetico su catalizzatori TiO<sub>2</sub> è stata scelta come sistema modello. Gli acidi carbossilici sono infatti prodotti indesiderati della pirolisi di biomasse. La chetonizzazione è una reazione che porta alla condensazione di due molecole di tale acido, con conseguente perdita di un C in forma di CO<sub>2</sub>. Gli esperimenti sono stati condotti in un impianto in scala di laboratorio, utilizzando una configurazione tradizionale a letto impaccato in cui il catalizzatore è stato testato sotto forma di polvere. La campagna sperimentale è stata divisa in due parti. Nella prima, gli esperimenti sono stati condotti in modo che avvenisse solo la reazione di chetonizzazione, evitando reazioni secondarie. L'acetone era dunque l'unico prodotto di condensazione. A tal fine, conversione e temperatura massime durante gli esperimenti sono state impostate rispettivamente al 50% e a 300°C. Sono stati esplorati gli effetti del pretrattamento di riduzione del catalizzatore e dell'aggiunta di Ru. Nella seconda parte, il sistema catalitico è stato portato a condizioni più severe (temperatura e conversione più elevate) e sono stati studiati gli effetti sulla distribuzione dei prodotti nel tempo, sull'aggiunta di Ru e sulla co-alimentazione di H<sub>2</sub>. In queste condizioni operative, erano presenti sia percorsi di reazione secondari da acido ed acetone, che fenomeni di disattivazione. Prodotti C<sub>6</sub>+ si sono formati, ma la loro selettività è diminuita con il tempo. Prove di TPO sono state svolte per quantificare i depositi carboniosi sui catalizzatori spenti. In conclusione, è stato dimostrato che i catalizzatori di TiO<sub>2</sub> sono in grado di catalizzare con successo la chetonizzazione dell'acido acetico. Inoltre, a temperature di reazione sufficienti, sono state attivate reazioni secondarie di condensazione aldolica, insieme a percorsi di ciclizzazione e cracking. In effetti, tra i prodotti sono state osservate specie pesanti nella gamma dei carburanti, con specie C<sub>6</sub>-C<sub>12</sub> che hanno raggiunto una selettività globale del 66% a 400°C. Sono emerse sfide in termini di disattivazione del catalizzatore e di difficile controllo della selettività del processo.

**Parole chiave:** acido acetico; chetonizzazione; TiO<sub>2</sub>; reazioni chain-growth; bio-fuels



# Table of contents

<b>Abstract</b> .....	<b>i</b>
<b>Abstract in italiano</b> .....	<b>iii</b>
<b>Table of contents</b> .....	<b>v</b>
<b>Introduction</b> .....	<b>1</b>
<b>1 State of the art</b> .....	<b>3</b>
1.1. Biomass-to-energy processes.....	4
1.2. Catalytic upgrade of pyrolysis vapours.....	6
1.2.1. Ketonization .....	7
1.2.2. Aldol condensation .....	10
1.3. Objective of the thesis work.....	10
<b>2 Experimental methods</b> .....	<b>13</b>
2.1. Description of the rig .....	13
2.1.1. Feed section .....	14
2.1.2. Reaction section .....	18
2.1.3. Analysis section .....	19
2.2. Catalyst preparation and characterization .....	26
2.2.1. Choice of the catalyst .....	26
2.2.2. Preparation of TiO <sub>2</sub> .....	26
2.2.3. Preparation of Ru/TiO <sub>2</sub> : dry impregnation.....	27
2.2.4. Catalyst characterization .....	28
2.3. Packed-bed Reactor.....	31
2.3.1. Reactor preparation and description.....	32
2.3.2. Sieving procedure.....	35
2.3.3. Leakage & pressure drops tests.....	35
2.3.4. Reactors summary .....	36
2.3.5. H <sub>2</sub> Pre-Treatment .....	38
2.4. Experimental procedure.....	38
2.4.1. Before the experiment.....	38
2.4.2. Experimental protocols.....	39
2.4.3. Shut-down .....	40

2.5.	Data processing.....	40
2.5.1.	Post-processing of the results .....	40
2.5.2.	Presentation of the results .....	44
<b>3</b>	<b>Catalyst characterization.....</b>	<b>47</b>
3.1.	Morphological analyses.....	47
3.1.1.	BET.....	47
3.1.2.	Mercury intrusion porosimetry .....	49
3.2.	TPR .....	51
3.3.	TPD.....	56
3.3.1.	CO <sub>2</sub> TPD .....	56
3.3.2.	NH <sub>3</sub> TPD .....	58
3.3.3.	Acetic acid TPD.....	60
3.4.	Characterization sum-up.....	63
<b>4</b>	<b>Experimental results .....</b>	<b>65</b>
4.1.	Blank Tests.....	65
4.1.1.	Regeneration effect .....	68
4.1.2.	H <sub>2</sub> co-feed effect .....	69
4.1.3.	Flow rate effect.....	71
4.2.	Acetic acid ketonization in the low-temperature range .....	72
4.2.1.	Pre-reduction effect .....	74
4.2.2.	Ru addition addition.....	77
4.2.3.	Ru precursor effect: Chloride vs Nitrate .....	80
4.3.	Acetic acid ketonization: high temperature analyses .....	81
4.3.1.	Temperature effect.....	84
4.3.2.	H <sub>2</sub> co-feed effect .....	93
4.3.3.	Ru/TiO <sub>2</sub> vs TiO <sub>2</sub> .....	99
4.4.	TPO.....	108
4.4.1.	Temperature effect.....	109
4.4.2.	H <sub>2</sub> co-feed effect .....	114
4.4.3.	Ru/TiO <sub>2</sub> vs TiO <sub>2</sub> .....	118
<b>5</b>	<b>Conclusions .....</b>	<b>121</b>
	<b>Bibliography .....</b>	<b>125</b>
	<b>List of Figures .....</b>	<b>129</b>
	<b>List of Tables .....</b>	<b>133</b>
	<b>List of symbols .....</b>	<b>135</b>
	<b>Acknowledgments.....</b>	<b>137</b>



# Introduction

The objective of this thesis is the experimental study of light oxygenates catalytic C-C coupling reactions; this process is studied as an interesting upgrading stage on pyrolysis vapors, with the aim of increasing C-chain length of bio-oil species while reducing the overall O/C ratio. The reaction mainly investigated was the ketonization of acetic acid and consecutive chain-growth reactions. Acetic acid was chosen as model of oxygenate and light carboxylic acid. The catalytic tests were performed in a pre-existing lab-scale plant using a packed bed reactor over  $\text{TiO}_2$  catalysts.

Chapter 1 explain the current state of the art regarding biomass application. After a brief overview, this part focuses particularly on the concepts behind C-C coupling processes and its main strengths.

Chapter 2 reports the description of the experimental setup. It illustrates the general rig layout and the characteristics of its components, the procedures for the preparation of catalysts and reactors, the description and procedures followed to carry out the experiments, and lastly the post-processing of experimental data collected.

Chapter 3 contains the results obtained during the catalyst characterization tests, to which the various catalysts used have been subjected.

Chapter 4 shows the results of ketonization experiments. It is divided into two main topics: firstly, a study of the reaction in a low conversion/temperature condition and then a switch to more severe ones (higher temperature and conversion).

Chapter 5 is assigned to conclusions, where the final thoughts of this thesis are discussed. In particular, there is a critical analysis of the results and a forecast of future goals.



# 1 State of the art

The push for a transition towards a low carbon economy is asking for a lower dependence on fossil fuels. Different technologies have been developed during the years to achieve this goal, with a particular attention to the exploitation of renewable energy sources. Hence, they have received strong attention not only from the scientific community but from the entire society in general. Throughout 2021, global energy demand and emissions increased by 5% compared to 2020, almost reaching pre-COVID-19 levels [1]. Renewable generation is projected to reach 80–90% of the global energy mix by 2050 as the global build-out rates for solar and wind grow by a factor of five and eight respectively, while annual investments in energy supply and production are expected to double by 2035, with almost all growth expected to come from decarbonization technologies and power, which will by 2050 exceed today's total energy investments [1].

Biomass is one of these renewable sources, together with wind, solar, geothermal, and hydro. Focusing on biofuels, their production growth reached 9.7% in 2018, the highest value since 2010 with a mean growth rate of 6.2% yearly from 2009 to 2019 [2]. Unfortunately like every other energy source the biomass suffered a big reduction in the global production due to the global pandemic (-6.3% [2]). However, by 2050, the share of sustainable fuels in the energy demand for transportation could be between 6% and 37%, depending on net-zero ambition levels across countries, as shown in Figure 1.1.

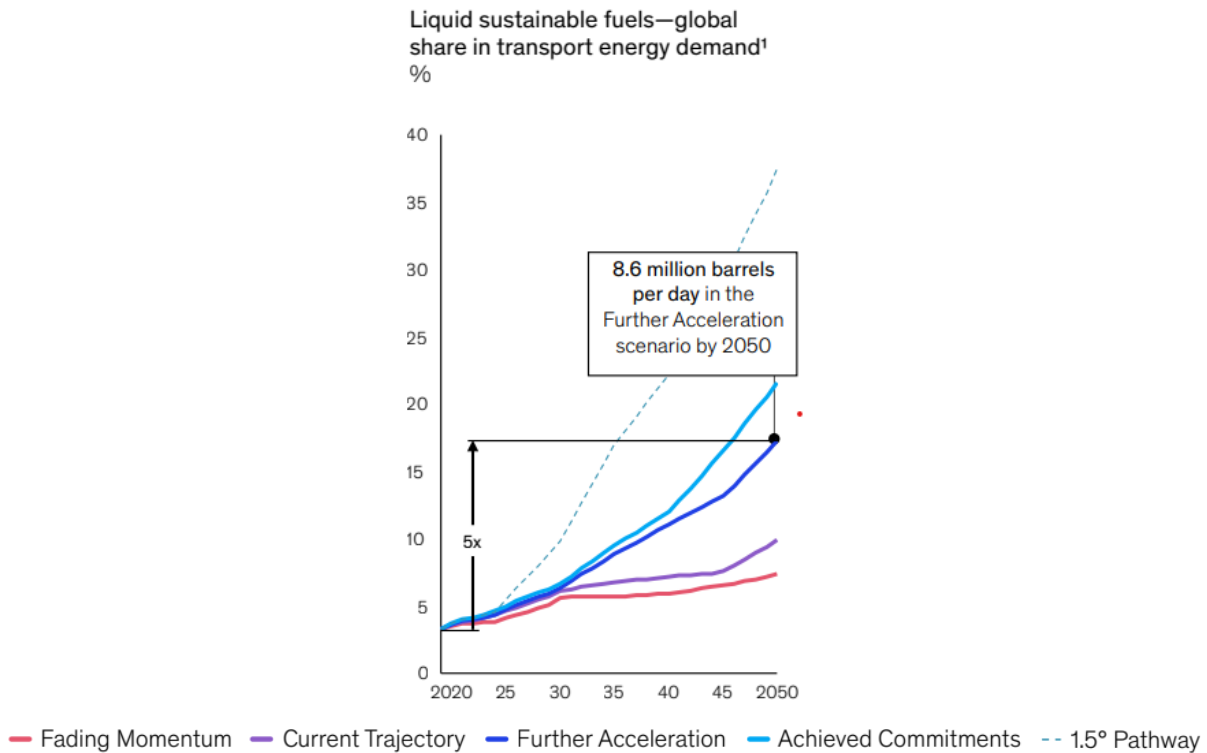


Figure 1.1 – Liquid bio-fuels projection to 2050

## 1.1. Biomass-to-energy processes

Biomass derives from organic material, like trees, plants, urban and agricultural wastes. Its sources are considered carbon-neutral: since they consume carbon dioxide during their lifetime through photosynthesis, their overall contribution to the increase of greenhouse gases is strongly lower if compared to hydrocarbons (although the energy used to process and transport the biomass may come from fossil). Besides their lower environmental impact, the increasing use of biomass-derived fuels would decrease the dependence from fossil fuels, thus also helping those countries that do not dispose of hydrocarbon sources on their own territory.

The main advantages of biofuels are no-sulphur content, no presence of polyaromatics and too heavy C-chain species (no toxicity, no treatment of heavy products), and a high cetane and octane number, making them a very suitable alternative to fossil ones. However, the main disadvantage of biofuels is energy density: to obtain a “small” amount of desired product, a large one of wastes/land has to be used, making it not so competitive for investors compared to other available technologies.

Biofuels can be divided into three generations, depending on its raw material sources. First-generation biofuels are produced directly from food sources, like sugarcane, corn starch and wheat. In this context, it is however important to use these resources in a responsible way and to tackle some issues: competition between food and energy

production, conversion of lands from forests, low sustainability of the conversion processes of biomasses themselves. Hence, regulations for energy production are necessary.

Second-generation biofuels (also called cellulosic biomass) instead derive from non-edible lignocellulosic biomass, such as grasses, wood, organic waste, food crop waste. The major issue of first-generation biomass, that is the dangerous boundary between energy and food production, is therefore solved when cellulosic fuels are employed.

Finally, third-generation biofuels come from special energy crops as algae, which present several benefits: higher yield than oleaginousness crops, no competition with agriculture, no need for herbicides and pesticides.

Several processes can be used to convert biomass to energy [3], which can be classified in two macro groups: thermo-chemical and bio-chemical processes:

- Bio-chemical processes: fermentation, aerobic digestion, transesterification
- Thermo-chemical processes: combustion, gasification, pyrolysis

Fermentation is the process responsible to produce bioethanol, that is an anaerobic process through which micro-organisms (bacteria or enzymes) break down sugar-containing biodegradable materials. The major sources of bioethanol are sugarcane, sugar beet and starch crops, but use of second-generation sources is gaining importance. Anaerobic digestion instead is used to produce biogas, where micro-organisms transform organic material into a gaseous mixture. Lastly, transesterification is used for the production of biodiesel, where vegetable oils are upgraded into more suitable material (higher cetane number) through the reaction of a triglyceride molecule into glycerol and methyl-esters.

For thermo-chemical processes, biomass can be simply burned to produce energy [3]. Wood and agricultural residues are employed to produce electricity and energy for space heating and industrial plants [4], [5]. Generally, biomasses with a low moisture content are employed.

Instead of directly burning biomass to produce energy, it is also possible to valorise it and produce components that can be subsequently used as chemicals or as fuels. A possible route for the production of syngas from biomass is the direct gasification. In this process, biomass is transformed into a gaseous mixture rich in synthesis gases in controlled conditions at high temperature (800-1300°C), in the presence of limited amount of oxygen and, sometimes, steam.

Lastly, pyrolysis is a thermal treatment, carried out with a limited or null amount of oxygen at relatively mild conditions (200-700°C) [4]. When biomass is subjected to pyrolysis three different phases are obtained: solid (charcoal), liquid (bio-oil or tar) and gaseous (fuel gas). By changing the operating conditions (e.g. temperature and contact time) yields towards these three phases change. The production of bio-oil is for instance favoured by Fast Pyrolysis (60-75 wt.% yield at 600-1000°C, short vapour

residence time 1-2s [4]). Bio-oil comprises a mixture of highly oxygenated compounds, water and char particles, that is mainly used as fuel [3], [6]. The bio-oil contain significant amounts of small carboxylic acids, which cause instability, corrosion during storage and transportation, can promote unwanted side reactions [7].

## 1.2. Catalytic upgrade of pyrolysis vapours

Bio-oils, produced by pyrolysis of lignocellulosic biomass, are multicomponent mixtures with high content of water and more than 300 oxygen-containing compounds, responsible for its well-known undesirable properties (high viscosity, high corrosivity, chemical instability, and incompatibility with conventional fuels and low heating value), which render bio-oils useless as a fuel. Important challenges lie in the elimination of all components that can lead to deterioration in biofuel quality, such as light oxygenates, C<sub>2</sub>-C<sub>4</sub> carboxylic acids, ketones, aldehydes. Besides them, the other main challenge in bio-oil upgrading is preservation of carbon in the product, with minimum hydrogen consumption [8].

Iliopoulou et al. [8] also propose bio-oil upgrading attempted by two main different approaches. The first one refers to down-stream treatment of bio-oil in separate catalytic units/processes using the condensed/collected organic phase of the bio-oil (including e.g., the catalytic hydrodeoxygenation (HDO) process with hydrogen under high pressures and the bio-oil coprocessing in existing refinery processes, like FCC). The second, and most promising approach, is the one using heterogeneous catalysts integrated into the fast pyrolysis process, commonly known as catalytic fast pyrolysis (CFP) of biomass. Development of such integrated multifunctional catalysts will offer the advantages of both HDO and cracking reactions at atmospheric pressure, without the requirements of pricey hydrogen or other reactive agents and/or other expenses (heating, high pressure, transfer costs, etc.), while they may be readily regenerated to remove deposits of coke. Development of robust, highly selective catalysts will help achieve the goal of producing drop-in fuels and petrochemical commodities from wood and/or other waste lignocellulosic biomass streams with all emerging industrial benefits. CFP is divided in:

- The “in-situ” upgrading, which refers to the fast pyrolysis of mixtures of biomass and catalyst, where the catalyst acts both as a heat carrier and as a reactive solid, thus resulting in the production of bio-oil with already modified-improved composition and properties
- The “ex-situ” or “two-stage” catalytic upgrading, where the pyrolysis vapours produced in the biomass pyrolysis are subsequently passed through a separate unit

The challenges in CFP of biomass are mainly focused on the development/optimization of advanced catalytic porous materials as efficient catalysts to produce bio-oils with tailored composition, suitable for direct use or further upgrading.

### 1.2.1. Ketonization

Among all the chemical reactions, the ketonization of carboxylic acids is one of the possible ways to upgrade pyrolysis vapours. Acetic acid is the component chosen for this thesis work, as it is the one who best approximate the conditions of the bio-oil produced by a pyrolysis process, due to both its acidic properties and the high O/C ratio. This means that a suitable catalyst has to be found firstly to start the investigations.

While known for many years, this reaction has recently gained significant attention due to its promising application in the production and upgrading of bio-oil. Ketonization is an effective method for acid upgrading since it converts two organic acids to a ketone and efficiently removes oxygen in the form of water and CO<sub>2</sub>. As a result, heating values of the bio-oil increase while the acidity decreases [7]. It also provides an attractive route for oxygen removal using the C-atoms within reactants, instead of added H<sub>2</sub> [9]. In ketonization of carboxylic acids, a larger ketone molecule is obtained along with CO<sub>2</sub> and H<sub>2</sub>O, as showed in Figure 1.2.

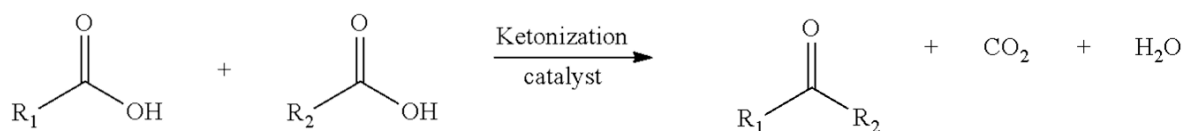


Figure 1.2 – Ketonization reaction

The ketones thereby produced (acetone if acetic acid is used) are a desirable building unit, since they can undergo further C–C coupling and hydro-deoxygenation to produce hydrocarbons for transportation fuels (e.g. via aldol condensation [7]).

From literature[10], we know that the reaction pathway for it mostly occurs for solid metals, metal salts and in the bulk of low lattice energy oxides (M = Ca, Mg, ...) when contacted with carboxylic acids at high temperatures (typically 350–500 °C). This means that a class of catalyst is already decided, the only thing missing is to choose what is better than others for the specific case of acetic acid conversion. Then, if we focus only on projects that investigated this particular reaction, we find that mainly three different catalysts were used:

1. Titanium dioxide (TiO<sub>2</sub>)
2. Ceric dioxide (CeO<sub>2</sub>)

### 3. Zirconium dioxide (ZrO<sub>2</sub>)

All of them have similar properties and highly activate only the desired reaction. Considering the process itself, it is assumed that the C-C coupling step is acknowledged by most as the rate-determining step. In the works by Wang et al. [11][9][12], that are one of our fundamental references, it was shown that the C-C coupling step has the highest free energy along the reaction coordinate for acetic acid conversion on anatase and rutile TiO<sub>2</sub>. This is probably the main reason why we also decided to adopt titanium dioxide as our catalyst.

Figure 1.3 and Figure 1.4 report the main pathways from literature [13] for the ketonization reactions catalysed by TiO<sub>2</sub>.

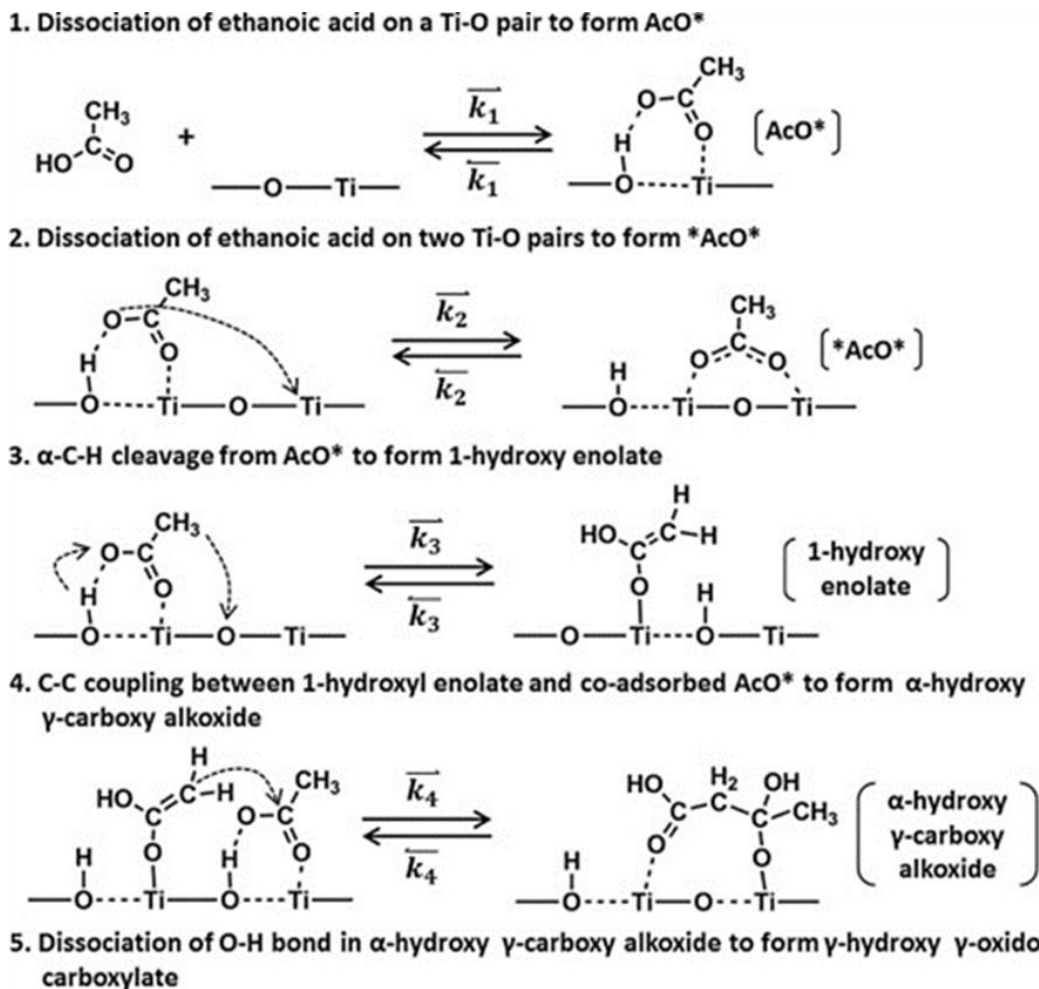
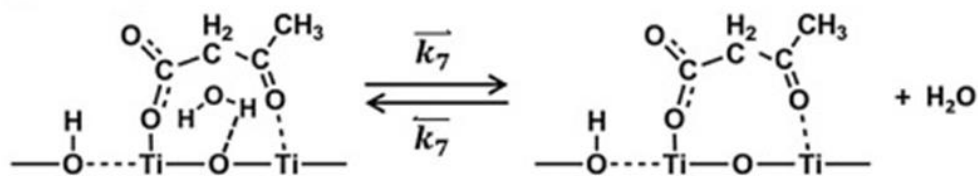
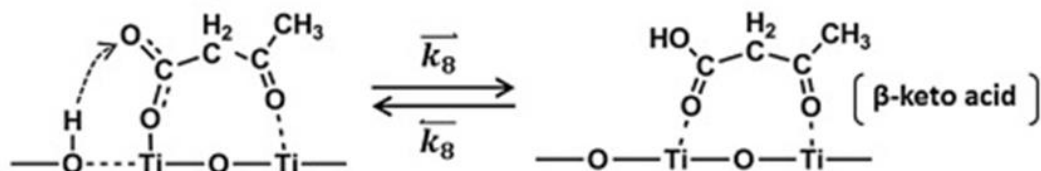
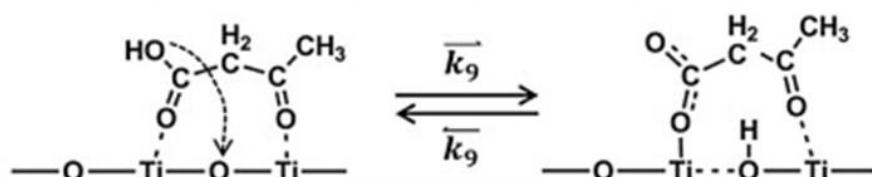
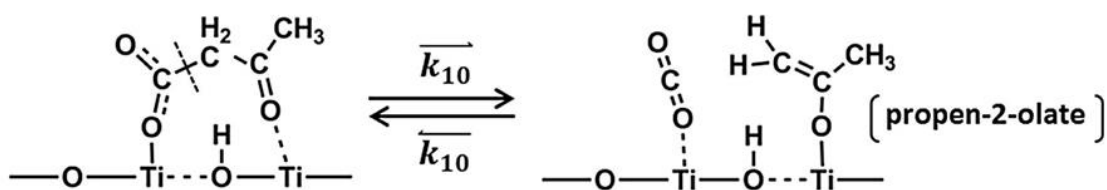
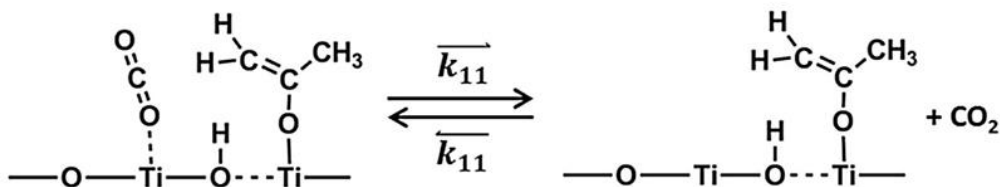


Figure 1.3 – Ketonization path of reaction Part. 1

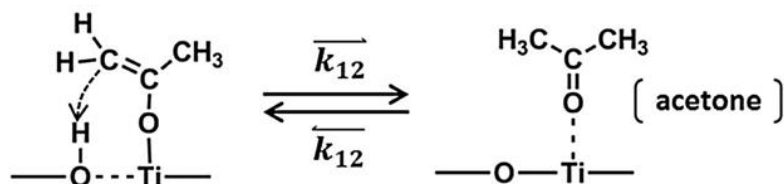


7. H<sub>2</sub>O desorption8. Protonation of  $\beta$ -keto carboxylate to form  $\beta$ -keto acid9. Dissociation of  $\beta$ -keto acid on a Ti-O-Ti structure

## 10. Decarboxylation to form propen-2-olate

11. CO<sub>2</sub> desorption

## 12. Protonation of propen-2-olate to acetone



## 13. Acetone desorption

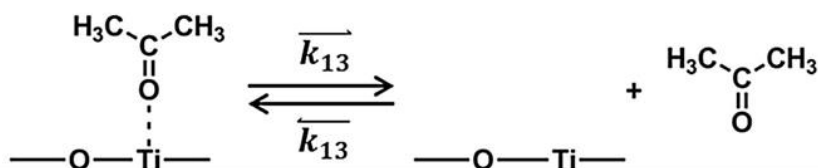


Figure 1.4 – Ketonization path of reaction Part. 2

### 1.2.2. Aldol condensation

Aldol condensation is another C-C coupling reaction. Here is studied as consecutive reaction to ketonization, as the species interested is its main product (i.e. acetone). In this case two  $C_n$  aldehydes or ketones react together and condense forming a  $C_{2n}$  aldehyde or ketone. An example of ketonization and aldol condensation chain-reactions is showed in Figure 1.5.

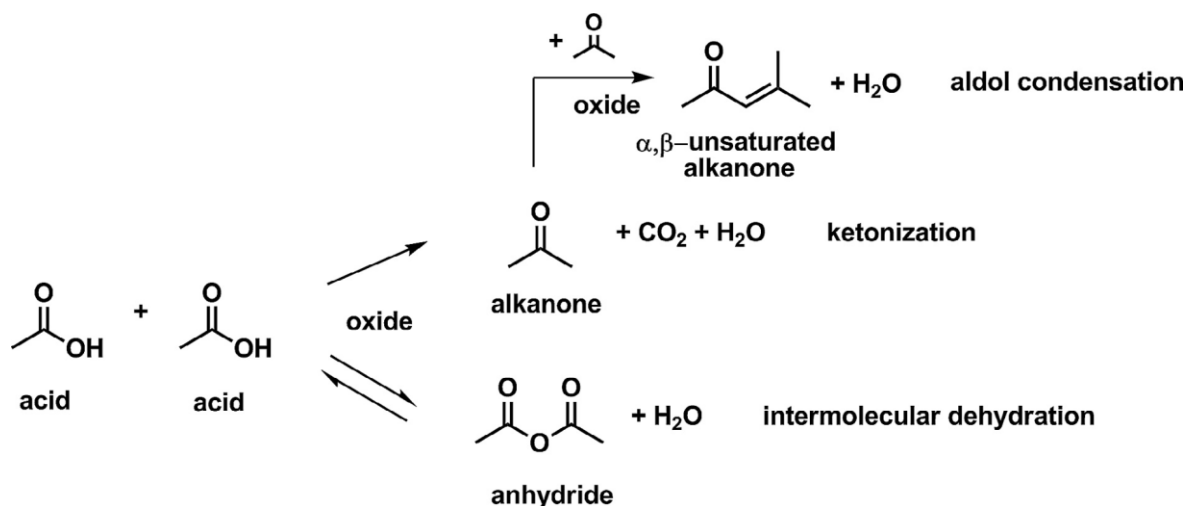
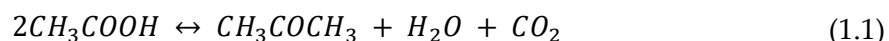


Figure 1.5 – Aldol condensation mechanism of aldehydes or ketones

## 1.3. Objective of the thesis work

Acetic acid ketonization reaction was experimentally investigated during this thesis work. In this specific case, when sufficient thermodynamics conditions are reached, two molecules of acetic acid react to form a molecule of acetone, plus one of  $H_2O$  and  $CO_2$ , as shown by Equation (1.1).



In order to do that an existing lab-scale plant was used to study this process that was designed and tuned in the previous work[14], that was defined as the starting point for this thesis. The experiments were carried out in a packed bed reactor where the catalysis was used in a powder form. Titania anatase was chosen as support material, and a commercial  $TiO_2$  anatase in powder form (Tronox) was used for the preparation. The model DT-51 D was chosen because it is the one with less sulphur content. The various catalysts used in this thesis have been subjected to characterization tests as BET, mercury intrusion porosimetry, TPD, and TPR, aiming to analyse their

morphological and chemical properties. Experimental campaign consisted of two main topics: firstly, a study of the reaction in a low conversion condition and then a switch to more severe ones (higher temperature and conversion). Since catalyst deactivation and carbon formation are typical issues connected to bio-derived oxygenates, an experimental protocol of TPO analyses was also performed. The objectives of the thesis were mainly two; firstly, better comprehend the chemical and morphological nature of  $\text{TiO}_2$  (and  $\text{Ru/TiO}_2$ ), since in the previous work Ru revealed to be an inhibitor of the reaction, contrary to what was reported in literature [12]. Secondly, investigate deeper the performance of  $\text{TiO}_2$ , that revealed to be the best performing catalyst at high temperature regions, where secondary reactions and low stability of the catalyst itself were observed.



## 2 Experimental methods

### 2.1. Description of the rig

The experimental tests that will be described in this thesis are heterogeneous catalytic processes, where reactants are fed in vapour phase and a solid catalyst is used. Those processes have been carried out in a testing unit which works completely under laboratory fume hood. Plant configuration was designed and calibrated during the previous thesis work [14].

The rig setup consists of three main parts which are connected by 1/8" stainless still pipelines:

- feed section
- reaction section
- analysis section.

This chapter provides the detailed description of this experimental setup and the experimental procedures followed on it for the tests performed for this thesis study.

Figure 2.1 and Figure 2.2 reports respectively a picture of the plant and its P&I diagram.

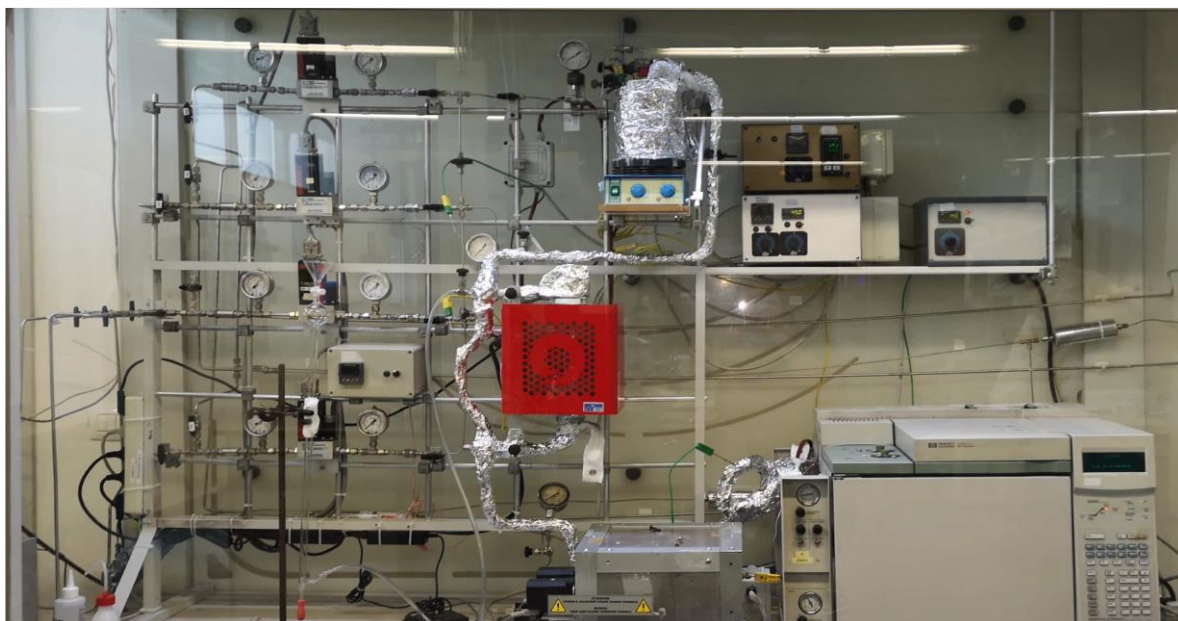


Figure 2.1 – Picture of the plant

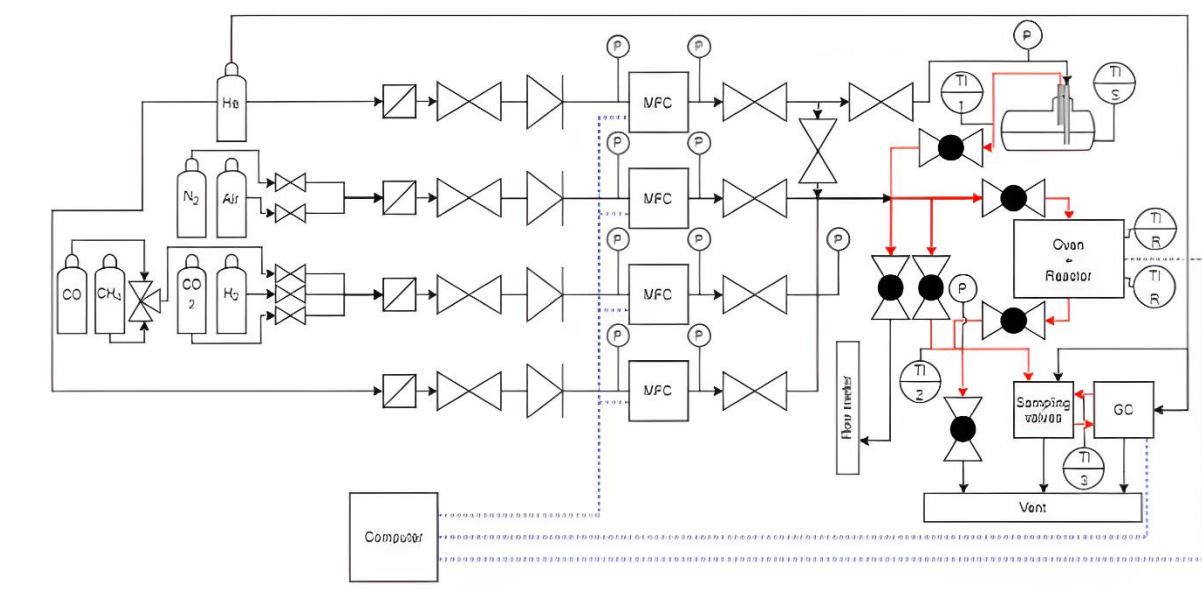


Figure 2.2 – P&amp;ID of the plant

### 2.1.1. Feed section

#### Gas phase

The reactants for these experiments were mostly gaseous species. Reactant gases came from pressurized cylinders placed either outside the laboratory ( $H_2$ ,  $CH_4$ ,  $CO$ ,  $CO_2$ ), or in the basement of the building (air, He). Instead, nitrogen ( $N_2$ ) was stored in a tank placed outside the building where it was kept in liquid state. For each gas, there was

an inlet line and a thermo-regulated valve which decreased the flow pressure from the one inside the cylinder (100-200 bar) to the line one (4-5 bar).

The rig had four lines with 1/8" diameters. They were used as follow:

- Two lines were used for the helium (complementary He and He sent to the saturator).
- One line was used for N<sub>2</sub> or air.
- One line for the co-feeding of H<sub>2</sub> (or eventually for CH<sub>4</sub> CO or CO<sub>2</sub>)

Each line had its own electronic MFC (Mass Flow Controller, model Brooks) and during the thesis exchanges between them were required, due to different experimental conditions. The MFC employed for the experiments were:

- Saturator and complementary helium lines were provided respectively with a 100 Nml/min and 300 Nml/min MFC
- Nitrogen line provided with a 50 Nml/min MFC or a 200 Nml/min one
- Hydrogen line provided with a 200 Nml/min MFC or a specific 50 Nml/min one for CO<sub>2</sub>

Moreover, for each line there were:

- an inlet valve to separate the lines and avoid back-flow
- two Bourdon spring gauges (6 bar) upstream and downstream of the MFC to control its operation
- a metal mesh filter (7 µm) to protect the instruments from impurities in the gases
- at least one interception valve before and after the MFC

Each MFC had to be calibrated before starting our experimental campaign: every manufacturer provides a configuration based on their testing gases, but since we did not send the same ones, the real flow rate going through the rig could result very different from the theoretical one. This happens because every gas has a different thermal conductivity.

Therefore, a manual procedure had to be carried out following these steps:

1. An initial opening (e.g. 5%) of the MFC was set
2. Using a gas bubble flowmeter, the real flow rate is measured with a chronometer (sensitivity 0,01s); an average of five measurements was considered
3. Previous steps must be repeated with an increasing opening until full aperture of the MFC valve is reached (e.g. steps of 5% each time).

An Opening-Flowrate plot was computed, from which a regression line was derived. Lastly, the curve's coefficients were collected and considered for the estimation of the real aperture to adopt during experiments:

$$F_i = a * [\text{opening}\%] + b \quad (2.1)$$

Where  $\dot{Q}$  is the flow rate, a and b the coefficients obtained by the regression line. Using Equation (2.1) it is then possible to obtain the theoretical flow rate. An example is seen in Figure 2.3.

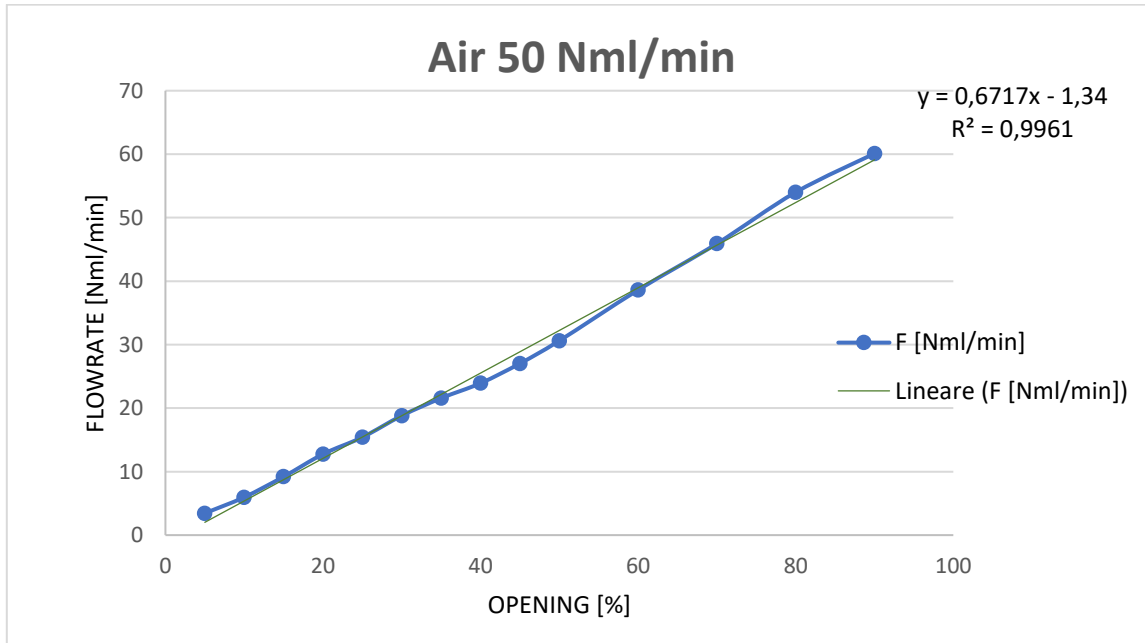


Figure 2.3 – Calibration result for air MFC

This procedure was repeated for all MFC all gases that were used. Notice that even if two different gases go through the same MFC, the procedure has to be performed two times, because every reactant is different from the others.

### Liquid phase

Differently from these gaseous species, acetic acid and acetone were stored in liquid phase. Therefore, we had to use a saturator.

A saturator works following the vapor-liquid equilibrium theory, allowing to extract the desired element in the vapor phase. Starting from the semi-empirical law of Antoine:

$$\log_{10}(p_i^0(T)) = A_i + \frac{B_i}{T + C_i} \quad (2.2)$$

Where pressure (p) and temperature (T) are expressed respectively in bar and K, while A, B and C are empirical coefficients for each species, reported in Table 2.1.



Antoine coefficients			
Species	A <sub>i</sub>	B <sub>i</sub>	C <sub>i</sub>
CH <sub>3</sub> COOH	4.68206	1642.54	-39.764
CH <sub>3</sub> COCH <sub>3</sub>	4.42448	1312.253	-32.445

Table 2.1 – Antoine coefficients table

In the liquid-vapor equilibrium, since all volatiles follow Equation(2.2), it is possible to define the partial pressure as:

$$p_i = \frac{p_i^0(T)}{p} \quad (2.3)$$

The gaseous molar fraction  $y_i$  can be defined as the product between partial pressure of the species to the one of the system, while liquid molar fraction  $x_i$  is equal to the ratio between amount of liquid species and solution. The flow rate of volatiles was then calculated as:

$$y_i = \frac{p_i^0(T)}{p} x_i \quad (2.4)$$

$$F_i = \frac{y_i}{1 - y_i} F_{He} \quad (2.5)$$

Where  $F_i \left[ \frac{Nml}{min} \right]$  is the flow rate of the i-species, and  $F_{He}$  is the He flow rate that is sent to the saturator. The amount of liquid that evaporated in the saturator depended on both He flux and saturator temperature. For this reason, an electric heating plate regulated by a T-controller (usually set to 45°C) was placed under the saturator. Moreover, the saturator was placed inside a water bath externally covered with glass wool, thermally homogenized by a magnetic stirrer to exploit the high thermal capacity of water, avoiding possible temperature oscillations.

To account for the deviation from the ideal Antoine equation, a correction factor  $f_c$  was needed. With this new term Equation (2.5) becomes:

$$F_i = \frac{y_i}{1 - y_i} F_{He} x_i f_c \quad (2.6)$$

### 2.1.2. Reaction section

After the feed section, all lines converge into one, that is then split into two different branches: one goes into the reactor, while the other defines the bypass line. The purpose of bypassing the reactor is that some procedure had to be performed outside of it (e.g. tuning of reacting mixture at the start of every experiment).

#### 2.1.2.1. Reactor

The reactor consisted of a quartz cylinder tube with an inlet and an outlet connection for the gas stream. The structure of the reactor bed, from the gas point of view, is shown in Figure 2.4.

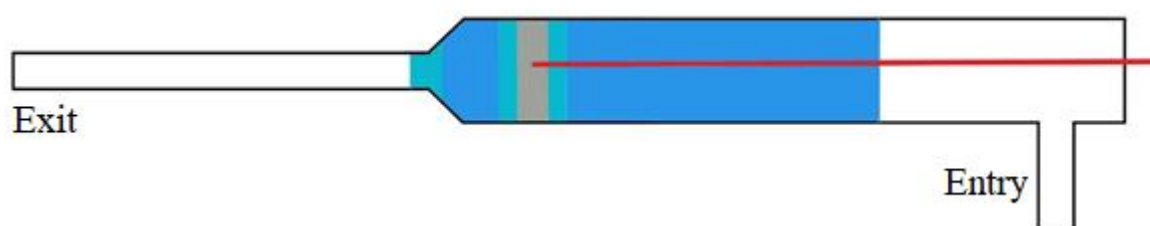


Figure 2.4 – Reactor scheme

A further explanation of reactor characterization will be provided in paragraph 2.3.

#### Oven

The reactor was inserted in a cylindrical furnace Carbolite TF1 11/32/150 with an internal diameter of 4.5 cm and length 23.4 cm. Temperature control was set by a control unit connected to the oven, with the possibility of remote control by a software.

A very important condition for all the experiments that were done, was keeping temperature constant along all the catalytic bed: having oscillations could have resulted into falsification of the results, because reactivity is highly influenced by thermodynamics. So, it was fundamental to always keep the catalytic bed in isothermal conditions. However, since the oven was not an ideal component, gradients of temperature were present, and only a small region was compatible with the isothermal property: through an investigation analysis during the previous thesis[14], that particular zone was found, as shown by Figure 2.5.

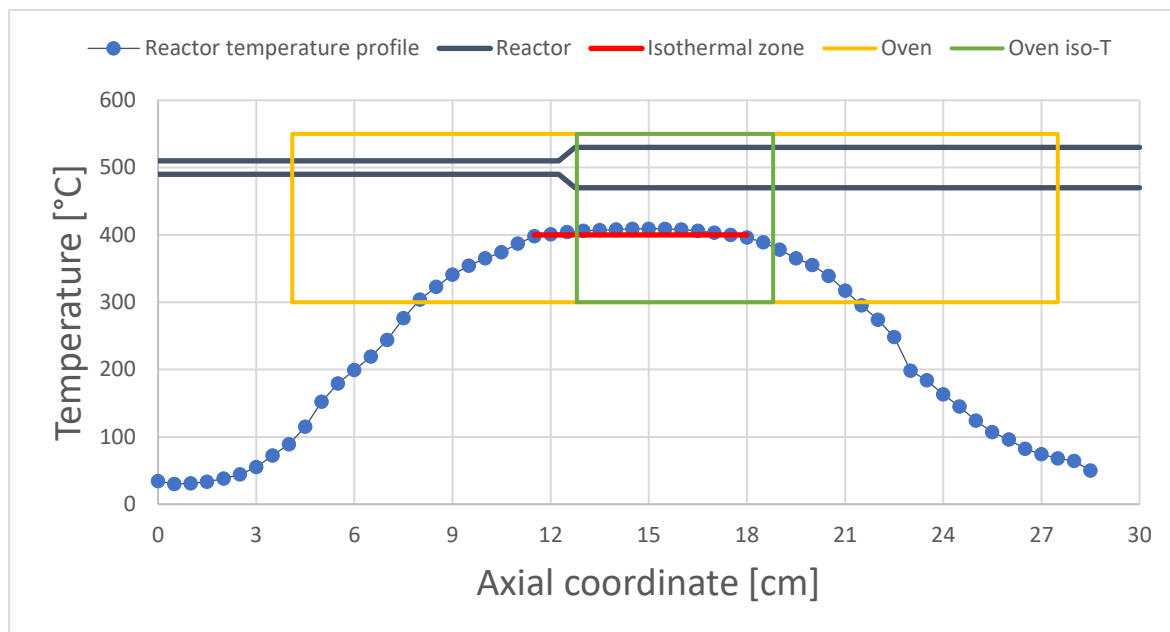


Figure 2.5 – Temperature profile of the reactor

### 2.1.3. Analysis section

During every experiment, it is required to monitor how much and which species are being produced: the reactants are known because they are chosen beforehand, but not their variation over time; also, not even products are known, as they come from a chemical reaction inside the reactor.

This requires the use of composition analysis tools, that for this thesis work were the following:

1. GC (Gas Chromatograph) + TCD (Thermal Conductivity Detector)
2. Micro GC +TCD
3. Offline GC + MS (Mass Spectrometer)

### GC

Reactants and products were analysed by the combination of a sampling unit and a GC (Hewlett Packard®, GC model 6890). Given the design of the unit, gases coming out of the reactor, or from the reactor bypass, could have gone directly to the vent or to the sampling unit of the GC: in order to ensure the second case, a needle valve was placed on the vent line. By closing this valve almost completely, pressure drops before the vent would increase so that the flow was directed to the sampling unit. A pressure gauge was installed to measure the backpressure provoked by the valve. It must be highlighted that the backpressure also affected the reactor and the saturator: caution must be exercised when closing the needle valve. In general, a backpressure of 0.1 bar was enough to obtain reliable GC analysis.

A sampling unit consisting of two sampling six-way valves (Figure 2.6) was used to send the mixture to the GC for analyses. These valves were placed within an oven, whose temperature was controlled by a thermocouple placed inside it. It was possible to select the desired set point by means of a gearbox. Usually, the temperature of the valves was set to 150 °C, to avoid any possible condensation of the gases.

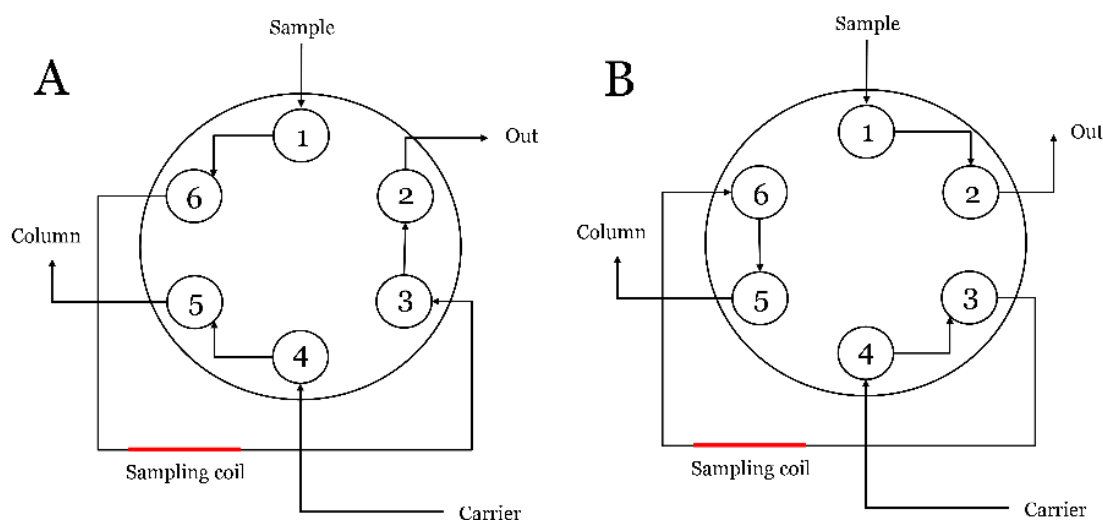


Figure 2.6 – Scheme of the valve positions, A and B

The valves worked with a two-phase position mechanism: at start (position A), the gas mixture from the reaction section passed through a sampling coil and then went out while the carrier gas (He) went to the column. Then, when the mixture had to be injected, a switch to position B happened, where the carrier gas passed in the sampling coil and dragged the gas mixture from the reaction section to the column. Therefore, when a GC analysis was run, the position of the valves was switched, one by one, from position A to position B. Valve position was manually selected with an electronic switch.

The GC was provided with two capillary columns which were covered internally by two different solid species that had different affinities with the different molecules passing through it. The solid tended to form bonds with the gases, but these are re-brought into the solution by the carrier gas. The final effect was a slowdown of the species and the greater the gas-solid affinity was, the greater the slowing down effect. Therefore, they came out of the column separated and at different times. In this way it was possible to define the “retention time” as the time needed by a given species to pass through the column.

The GC was provided with two TCD (Thermal Conductivity Detector): they consisted of a Wheatstone bridge on which one resistance was connected to a flow of carrier only (reference material), while the other one to the flow coming out of the column. Because the two resistances were subjected to flows with different thermal conductivity they cooled differently, giving out different voltage results, because resistivity is dependent

on temperature. The resulting voltage signal is called chromatogram. Figure 2.7 shows an example of a chromatogram produced by the GC for an analysis during an experiment.

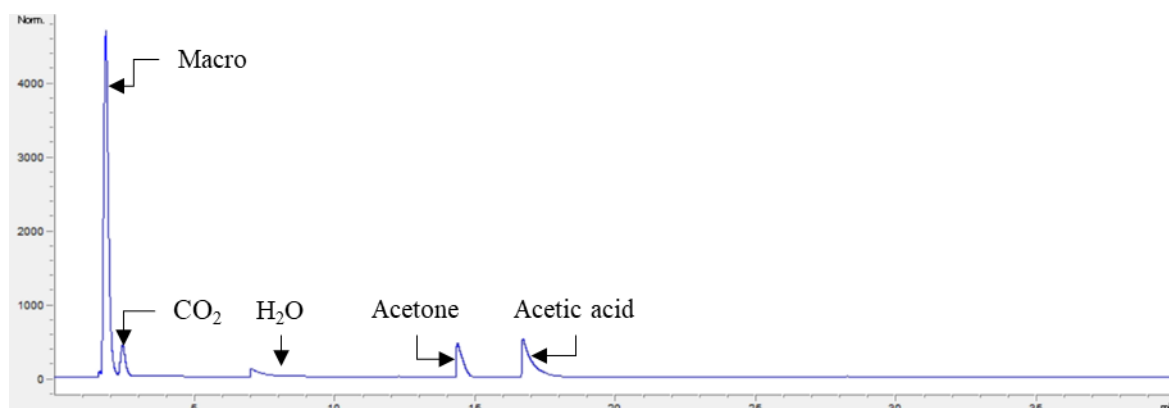


Figure 2.7 – Example of resulting chromatogram

The procedure explained before is then clear:

- the “base-line” voltage signal is produced when the carrier gas (He) reaches the detector
- instead, every peak that is found represents a different species that exited the column, thus giving a higher voltage than the reference

As said previously, the GC was provided with two different capillary columns:

- Molecular sieves column (column A): it uses helium (He) as carrier gas. It was able to separate  $N_2$ ,  $O_2$ , CO and  $CH_4$ ;  $H_2$  was also seen as a negative peak when its concentration was sufficiently high
- PoraplotQ column (column B): it used helium (He) as carrier and it could separate  $CO_2$ ,  $H_2O$ , acetone, acetic acid and heavier component from  $N_2$ ,  $O_2$ , and CO. This means that the retention time was the same for  $N_2$ ,  $O_2$ , CO and  $CH_4$  species (therefore the need to have a specific column for those species)

Specifications and operative conditions of the two columns are provided Table 2.2.

GC columns		
Specifications of the columns	Molecular sieves	PoraplotQ
Coating thickness	50 [ $\mu\text{m}$ ]	20 [ $\mu\text{m}$ ]
Length	30 [m]	25 [m]
Internal diameter	0.53 [mm]	0.53 [mm]
Maximum temperature	350 [ $^{\circ}\text{C}$ ]	250 [ $^{\circ}\text{C}$ ]

Table 2.2 – GC columns specifications

Temperature and pressure of capillary columns during the GC analysis must be decided. For this reason, a method must be created (or chosen if already available):

with the help of a dedicated software (ChemStation Rev.A.10.02 developed by Agilent Technologies®) the condition of each analysis could be set. This was related to timing reasons: if we did not directly accelerate the process, a very long time would have passed before every product exited the column, because retention time depends on temperature, pressure and type of element. Since pressure was fixed, the only other variable remained temperature: the higher it was, the faster every element would have detached from the capillary. However, if temperature increased too much over a small period of time, the distinction of each peak was lost (macro-peaks)

Therefore, there was the need for a trade-off between duration and precision. The criteria behind this search were in order of importance:

- All the species must be seen
- All the peaks must be well divided (if possible)
- Analysis time must be minimized

Once all these criterions were evaluated, the method was chosen. For our objectives, the following steps were created:

1. 5 min at 45°C
2. Ramp rate 15°C/min until 160°C
3. 8 min 20 s at 160°C (total 21 min)

Reactants' analyses were carried out until point 3; in the case of products, instead, the analysis was longer:

4. Ramp rate 15°C/min until 230°C
5. 39 min 20 s at 230°C (total 65 min)
6. Cooldown to step 1

While for pressure, these parameters were adopted:

- Molecular sieves column head pressure: 25 kPa
- PoraplotQ column head pressure: 50 kPa

A picture of GC-TCD is shown in Figure 2.8.



Figure 2.8 – Picture of GC-TCD

### 2.1.3.1. Micro-GC

Another gas chromatograph was used during the project when fast analyses were needed. Indeed, in the GC above, analyses duration time was too long.

Therefore, a Micro GC Fusion Gas Analyzer® made by Inficon™ was adopted.

Working principle was the same as the previous GC, with the advantage of having reduced time of analysis, lower gas volume analysed, and automated sample injection through a pump installed into the micro GC.

The MGC was provided with two different columns, whose behaviour is shown in Table 2.3.

Micro GC Fusion Columns				
Column name	Column type	Length [m]	Diameter [mm]	Elements detected
<b>Rt®-Molsieve 5A</b>	Capillary (PLOT)	10	0,25	He, N <sub>2</sub> , H <sub>2</sub> , O <sub>2</sub> , CH <sub>4</sub>
<b>Rt®-Qbond</b>	Capillary (PLOT)	12	0,25	Heavier components

Table 2.3 – Columns characteristics for Micro GC Fusion

Also in this case a correct method had to be set, following the same criteria used for the GC:

- Column A (Molsieve): 180s at fixed temperature of 70°C
- Column B (Qbond): 200s at fixed temperature of 180°C
- Total analysis time: 200s
- Column pressure: 25 psi for both cases

A picture of the Micro-GC is shown in Figure 2.9.



Figure 2.9 – Picture of Micro-GC

### Offline composition analysis GC-MS

Both GC explained were provided with TCD detectors; hence, they were not able to associate the peaks found in chromatographs to certain species

Therefore, another fundamental tool was needed to complete the analyses when peak-species assignment was not clear: the GC-MS.

The main differences between the ones previously mentioned were:

- The columns coating was done with different materials (Table 2.4)
- The method was different
- At the exit of the column there was not a TCD but a MS (Mass Spectrometer) detector
- It was not integrated with the plant, meaning that a mixture sample had be taken and injected manually (offline analysis)

As mentioned, a manual sample must be collected from the plant and injected into the GC-MS. Therefore, a sampling point was installed after the reactor line. Here the gases that exited from the reactor could be sampled by a vapor gas syringe of 1 ml, moved to the GC-MS and then injected in its columns.



During this thesis only one of the columns was used. Table 2.4 shows its characteristics.

GC-MS column characteristics	
Column name	HP-5MS
Coating thickness [ $\mu\text{m}$ ]	0.25
Length [m]	30
Internal diameter [mm]	0.25
Maximum temperature [ $^{\circ}\text{C}$ ]	350

Table 2.4 – GC-MS column characteristics

The mass spectrometry worked in the following way: a hot filament (1200 K) was capable of thermally ionize the gas that met it. The ions produced were captured by a detector which was capable of measuring the mass and the quantity of each ion. Every substance had a certain combination of ion's mass over charge ( $m/z$ ) that could be thermally generated which are reported in NIST MS Search 2.0 (a library integrated in the GC-MS software Enhanced Data Analysis). Thanks to the contribution of both the GC (separation of the species) and the MS detector (ions measurement) it was possible to draw a chromatogram in function of time and number of masses detected. An example of association between library and species detected is shown for acetic acid in Figure 2.10.

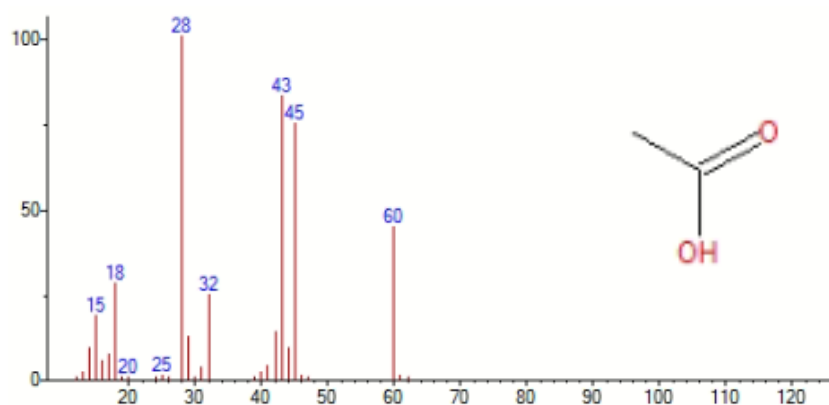


Figure 2.10 – Acetic acid recognition from GC-MS analysis

In this thesis, the GC-MS was used only to identify the unknown species that were present during the high conversion reactions. It wasn't used to find quantitatively the gas composition so there was no need to calculate again the response factors for every species (Paragraph 2.5.1).

As for the method adopted, the procedure was the following:

- Initial oven temp: 40°C
- Ramp rate of 10°C/min from initial temperature up to 110°C
- Ramp rate of 12°C/min from 110°C to 300°C
- Analysis run time: 30,83 minutes

A picture of the instrument used is shown in Figure 2.11.



Figure 2.11 – Picture of GC-MS

## 2.2. Catalyst preparation and characterization

### 2.2.1. Choice of the catalyst

Since the aim of this project is to evaluate the performance of the ketonization reaction, the first step to do was to choose which type of catalyst was needed. An overview on this matter was already provided in Paragraph 1.2.

For the sake of the experiments, two types of catalyst were particularly considered:

1.  $\text{TiO}_2$
2.  $\text{Ru/TiO}_2$ , where Ru was added as a doping element to the  $\text{TiO}_2$

This section will explain exactly how these two catalysts were prepared.

### 2.2.2. Preparation of $\text{TiO}_2$

Titania anatase was chosen as support material. The reason was that the titania provides acid-basic couples that are necessary in order to increase the reaction rate [13]. A commercial  $\text{TiO}_2$  anatase in powder form (Tronox) was used for the preparation of all the bed. The model DT-51D has been chosen because it was the one with the lowest sulphur content.

A calcination in air was carried out to remove all volatiles and pre-treat the material. Maximum temperature was set at 400°C, which is the maximum temperature reached

during the experiments: this was done in order to prevent changes of the material during the tests.

Calcination procedure was the following:

1. controlled heating from  $T_{amb}$  to  $T = 400^{\circ}\text{C}$  with a rate of  $1^{\circ}\text{C}/\text{min}$
2. permanence at  $400^{\circ}\text{C}$  for 3 hours
3. controlled cooling from  $T = 400^{\circ}\text{C}$  to  $T_{amb}$  with a rate of  $2^{\circ}\text{C}/\text{min}$ .

### 2.2.3. Preparation of Ru/TiO<sub>2</sub>: dry impregnation

Once anatase TiO<sub>2</sub> powder was ready, ruthenium, must be added if Ru/TiO<sub>2</sub> was to be prepared. The technique of dry impregnation (or incipient wetness impregnation) was employed: this methodology consists in impregnating drop by drop the powders of the support with an amount of solution equal to the pore volume of the support itself. Operating in this way, any loss of active element was prevented, and the exact amount of Ru deposited on the catalyst is known. To do this, two different Ruthenium precursors were considered:

1. Ruthenium (III) chloride hydrate (39 wt. % Ru, Johnson Matthey)
2. Ruthenium (III) nitrosyl nitrate solution (1.4 wt. % Ru, Alfa Aesar)

Regarding the methodology of the process for RuCl<sub>3</sub>, firstly the mass of ruthenium ( $m_{Ru}$ ) necessary to reach the desired final percentage  $\omega_{Ru}$  was calculated as:

$$m_{Ru} = \frac{m_{TiO_2} * \omega_{Ru}}{1 - y_{Ru}} \quad (2.7)$$

Where  $m_{TiO_2}$  is the mass of support that is subjected to impregnation.

The required amount of  $m_{sol}$  was then evaluated, using the mass fraction of ruthenium in the solution  $\omega_{Ru,sol}$ :

$$m_{sol} = \frac{m_{Ru}}{\omega_{Ru,sol}} \quad (2.8)$$

From BET measurements, it was possible to evaluate the pore volume  $V_{pores, specific}$  of the support. The amount of impregnating solution  $m_{salt}$  must be diluted to reach a volume  $V_{pores}$  equal to pore volume, according to dry impregnation procedure.

$$V_{pores} = m_{TiO_2} v_{pores,specific} \quad (2.9)$$

It was also important to check if the solution met the solubility limit. Otherwise, multiple impregnations had to be performed.

The impregnation procedure consisted in a slow dripping of the solution onto titania powders by periodically mixing the sample with a spatula so that all the liquid is

absorbed homogeneously by the powders. The dripping is stopped when the dropped volume is equal to pore volume, hence when:

$$V_{dropped} = V_{pores} \quad (2.10)$$

The procedure was carried out using a 5 ml graduated flask, in which the correct amounts of water and Ru were mixed. Lastly, the mixture was taken with a 1 ml graduated pipette. Concentration set (%wt of Ru) on the impregnated catalysts were respectively fixed at 1% (Ru nitrosyl nitrate) and 3% (RuCl<sub>3</sub>).

Pictures taken during the procedure can be observed in Figure 2.12.

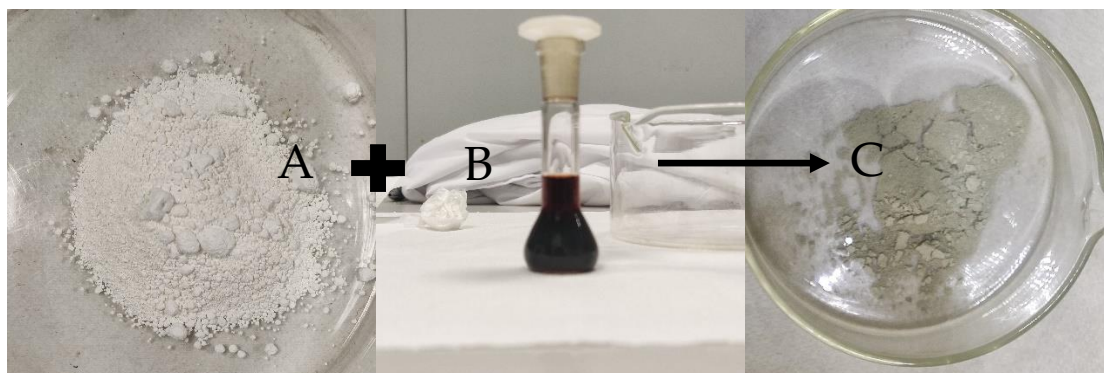


Figure 2.12 – Dry impregnation for Ru/TiO<sub>2</sub> from nitrate solution. TiO<sub>2</sub> (A), Flask with nitrate solution (B), impregnated Ru/TiO<sub>2</sub> (C)

#### 2.2.4. Catalyst characterization

A key aspect of experimental research also lies in understanding what the properties and characteristics of the catalyst used during the campaign are: it is also important to characterize the catalyst before testing (fresh) and after testing (spent), so an understanding of its properties is obtained not only for the initial ones, but also when it has undergone experiment tests. That is the reason why different catalyst analysis' types were performed.

##### Morphological analyses: BET

The catalysts were subjected to adsorption/desorption of N<sub>2</sub> analyses, then streamlined by BET isotherms (Brauner, Emmet, Teller). The isotherms could provide information concerning morphological and structural properties of the catalyst, through the study of adsorption and desorption of N<sub>2</sub> at 77.15 K (-196°C). With this technology, the superficial area and the pore volume could be determined. The instrument used for the measurements was a *Micrometrics Tristar 3000*.

### Morphological analyses: Hg Porosimetry

Mercury intrusion porosimetry, also called Hg porosimetry, is an analytical technique that allows to measure some characteristics of a material attributable to the presence of pores, including total volume of pores, pore diameter and surface area. In this sense, Hg porosimetry is very similar to BET because they aspire to reach the same goal, however they differ for their scope of application: while BET focus more on smaller elements (due to N<sub>2</sub> usage), Hg porosimetry is usually more useful for a bigger point of view. This technique consists in introducing into the material mercury at high pressure, that is necessary to counteract the surface tension of the liquid which alone would not allow it to penetrate inside the pores of the material. The pore size can be determined from the liquid pressure value.

### TPR

Temperature programmed reduction (TPR) is a material characterization process commonly used in catalysis studies to examine the surface chemistry of metals and metal oxides under varying thermal conditions.

In a typical TPR experiment, the catalyst is tested in a system known as a fixed bed reactor. A reducing gaseous mixture such as hydrogen (H<sub>2</sub>) is then made to flow across the catalyst under gradually increasing thermal conditions. As T increases, H<sub>2</sub> consumption is monitored. A highly sensitive detector continually analyses the chemical difference in concentration at the outlet, producing an accurate picture of the maximum or peak reduction rate of the catalyst.

The protocols used for TPR experiments were carried out in two different ways, as two different tools were used.

First ones were performed on a TPDRO 1100 (Temperature Programmed Desorption Reduction Oxidation) by ThermoQuest®, external to the grid.

In this case, operating conditions were:

- Packed bed reactor,  $m_{\text{cat}}$  of 100mg
- 20 NmL/min with a concentration of 5% H<sub>2</sub> in Ar
- Temperature ramp rate of 10°C/min up to 1000°C, plus 5 minutes hold at the end

The second ones instead were operated inside another testing rig with gas-phase analysis in online MS and IR (Infrared spectroscopy), with the following conditions:

- Packed bed reactor,  $m_{\text{cat}}$  of 60 mg
- 100 Ncc/min of 4% H<sub>2</sub> in He
- Temperature ramp of 10°C/min up to 800°C

## TPD

A temperature programmed desorption (TPD) is the technique that allows one to study the interaction of reaction gases with solid surfaces, thereby being a powerful tool for both the evaluation of active sites on catalyst surfaces and the understanding of the mechanisms of catalytic reactions including adsorption, surface reaction and desorption.

In a typical TPD experiment, the catalyst is tested in a system known as a fixed bed reactor. The procedure consists in the adsorption of a reaction (or probe) gas on the catalyst surface until saturation point is reached. Then, the catalyst is heated at a linear heating rate under a carrier gas flow.

Every test was performed following the same procedure:

1. After a stabilization of the gas mixture, a switch to reactor line occurred, with an adsorption of the gas flow followed by a stabilization of the flow concentration back to normal; required time about 40 minutes (Adsorption phase)
2. Once the adsorption completed, all gases lines were closed except for inert ones, in order to remove physically all the species deposited on the catalyst; required time about 50 minutes (Purge phase)
3. Then, a ramp rate of temperature started; required time about 1 hour (TPD phase)

Three different TPD tests were performed during the work, as three probe gases were used: CO<sub>2</sub>, NH<sub>3</sub> and Acetic acid.

For CO<sub>2</sub>, test conditions were the following:

1. Adsorption: room temperature, 100 Nml/min of 1%CO<sub>2</sub>, 10%-5% N<sub>2</sub> in He
2. Purge: room temperature, 100Nml/min with 10%-5% N<sub>2</sub> in He
3. TPD: 50-30 Nml/min where He was reduced until 50-30Nml were reached; ramp rate of 10°C/min until 600°C.

Ammonia TPDs instead had the following changes:

1. Adsorption: 0,2% NH<sub>3</sub> in He/Ar mixture with 100 NmL/min total flowrate, at 100°C for 1h
2. Purge: 100 NmL/min He for 1h45min at 100°C
3. TPD: 100 NmL/min, from 100°C to 600°C with 10°C/min ramp rate and final hold at T<sub>max</sub>

Lastly, for Acetic acid TPD the same procedure explained above was applied but with the following changes:

1. Adsorption: 100 Nml/min of 3% Acetic acid, 5%N<sub>2</sub> in He, room temperature, required time ~35 min

2. Purge: 100Nml with N<sub>2</sub> fixed as before and He changed to compensate for the acid absence, room temperature, required time ~25min
3. TPD: 30 Nml/min where He was reduced until 30Nml were reached; ramp rate of 1-5°C/min until 600°C, required time ~60 min

## TPO

Temperature programmed oxidation (TPO) is a material characterization process that heats a sample of an element or compound during its oxidation reaction.

In a typical TPO experiment, the catalyst is tested in a system known as a fixed bed reactor. The procedure this time performs a linear heating rate of the reactor under an oxidating gas flow (i.e. air), measuring all the components that desorb.

For this thesis, TPO was used to understand qualitatively and quantitatively the C-deposits formation on spent catalysts.

Regarding the tests' procedure, the following instructions were adopted:

- Flow rate of 25Nml/min of 100% Air
- Temperature ramp rate of 2°C/min until 600°C for all reactors.
- All catalysts tested were previously subjected to a ketonization reaction for 4.5 hours.

## 2.3. Packed-bed Reactor

The main element of the plant is the reactor, where all processes and studies occur. It is then very important to understand why we chose a particular type of configuration and how its preparation was performed.

In the chemical field, there are multiple types of catalytic reactor configurations, but usually we can classify them into the following main categories:

- Packed-bed reactors: the catalytic bed is fixed in position and the reagents go through it. It is the simplest one, and it is modelled as a PFR (Plug Flow Reactor)
- Moving bed reactors: opposite to the packed ones, here the catalytic bed is dragged along the reactor to achieve better heat exchange and efficiency. A bit more complicated than the packed bed, with its own pros and cons, it is again a PFR
- Fluidized bed reactors: intermediate configuration between the two, where there is a better and prolonged contact between catalyst and reagents due to a continuous re-mixing given by balancing gravitational forces of molecules and dragging force of the current. It is usually the best configuration for heat



exchange and efficiency, however it is modelled as CSTR (Continuous Stirred Tank Reactor)

Figure 2.13 shows these catalytic reactor's types.

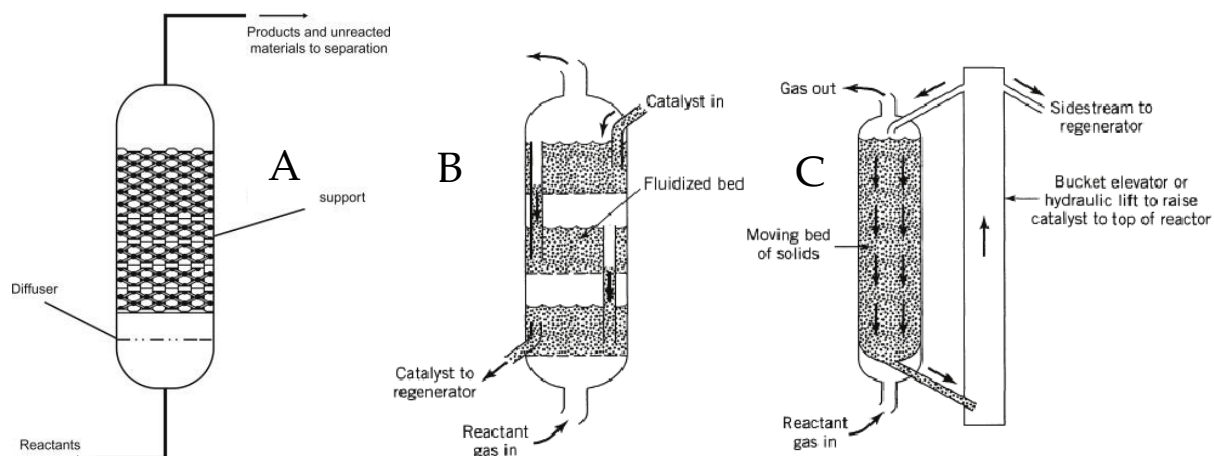


Figure 2.13 – Catalytic bed reactors: Fixed(A), Fluidized(B) and Moving(C)

Since the objective of this thesis work was to easily understand what was happening and how the interested reactions evolved over time with temperature, a traditional packed bed quartz reactor was adopted, while the catalyst was tested in the form of powder.

### 2.3.1. Reactor preparation and description

The reactor consists of a quartz cylinder tube with an inlet and an outlet connection for the gas stream, placed vertically inside the oven. The structure of the reactor bed is represented in

Figure 2.14 (from the gas point of view).



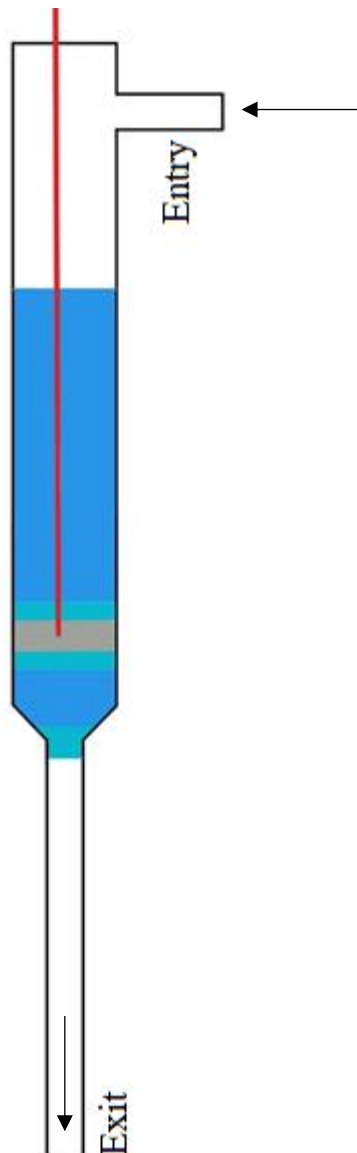


Figure 2.14 – Reactor scheme

Dimensions of the reactors were:

- Total length: 32 cm
- Tail length: 12.5 cm
- Nozzle: 2 cm
- Internal diameter in reaction section: 1.1 cm

Instead, from a structural point of view, six different layers could be defined:

- Column of quartz grains, height around 5 cm, grains size between 500-850  $\mu\text{m}$ , used to increase the turbulence and homogeneity of the feed and to avoid homogeneous reactions before reagents meet the catalyst (Blue)

- Layer of quartz wool, height around 5 mm used to separate the different layers (Light blue)
- Catalytic bed, as powder with a mesh of 140-200 (i.e. 75-106  $\mu\text{m}$ ), mass ranging from a minimum of 150mg to a maximum of 300mg (between 6-8 mm), (Grey)
- Layer of quartz wool, height around 5 mm used to separate the different layer (Light blue)
- Column of quartz grains, height around 1.5 cm, grain size between 500-850  $\mu\text{m}$ , used to lift the catalytic bed into the isothermal region of the oven (Blue)
- Layer of quartz wool, length around 5 mm placed at the shrinkage of the reactor in in order to prevent the motion of the bed when exposed to the gas flow (Light blue)

One K-type thermocouples (0.5 mm in diameter) was placed in the middle of the catalytic bed and it was used to control the temperature in the oven (Red).

The reactor preparation procedure was carried out as follows:

1. Place around 4 mm of quartz wool at the shrinkage of the reactor
2. Put around 1,5 cm of quartz grain (500-850  $\mu\text{m}$ )
3. Place around 4 mm of quartz wool over the quartz grain
4. Measure the desired amount of catalytic powder and place it inside the reactor as carefully as possible
5. Tap gently the reactor with a spatula in order to reduce the void fraction of the bed
6. Place around 4 mm of quartz wool on top of it and let it rest for 30 minutes
7. Measure the height of the catalytic bed (powder + quartz wool)
8. Insert a thermocouple in the centre of the catalytic bed until touch the upper quartz wool layer
9. Mark the thermocouple at a known distance by keeping a reference on the quartz reactor
10. Put around 5 cm of quartz grain on top of it
11. Close the cup of the reactor and check if the mark on the thermocouple has moved

Previously, step 8 was carried out inserting the thermocouple until the quartz wool layer under the catalytic bed was reached; then, to correctly place it, it was moved up by half of catalytic bed height. However, critical problems were not considered: by doing this, preferential channels for the gas flow could be created, with also the possibility of piercing the quartz wool layer. This could have resulted firstly in too much void space, creating a pathway on which the gas would have been obliged to flow, and secondly breaking of the quartz wool that could lead to catalyst dispersion.

### 2.3.2. Sieving procedure

As mentioned before both the catalyst powder and the quartz grain were used with a specific mesh dimension. In order to achieve that, a sieving procedure using a shaker from Sassuolo Lab S.R.L. was performed. The sieve was divided into at least four components:

- A cap used to prevent the loss of the powder from the top
- At least two layers of sieve placed in an increasing order of the grid diameter: 75  $\mu\text{m}$  (200 mesh) and then 106  $\mu\text{m}$  (140 mesh)
- A bottom cup to collect all the small part

Before using the sieves, powders were dried at 120°C for at least 20 minutes. Also, the sieves themselves were heated up in the same oven to increase the performance of the procedure: TiO<sub>2</sub> in particular was very difficult to sieve because of its hydrophilic nature that caused the creation of a thin coating layer on the sieve surface, hindering the mechanism. After this, the powders must be placed on top of the first sieve, so that the shaker was capable of separating the various grain thanks to mechanical vibration and gravity.

### 2.3.3. Leakage & pressure drops tests

After every reactor was mounted, two pre-experiment tests had to be performed. Firstly, it was important to avoid any possibility of gas leakage from the reactor: this could have led to falsification of the results and mandatory repetition of the test, resulting in a loss of precious time and effort. Secondly, no pressure drops had to be present inside the reactor, otherwise the flow could have been obstructed from reaching the catalyst surface or also create preferential channels.

In order to avoid those two problems, the procedure here below was adopted:

1. Slightly open the mass flow controller of an inert gas
2. Open only the valve at the inlet of the reactor (the bypass valve is already open)
3. Slowly close the bypass and then close the mass flow controller when the pressure inside the reactor reaches around 0.2 bar
4. Check if pressure remains constant or not: in the former case there is no leakage, while in the latter there is a leak that must be found with the help of a liquid detector
5. Once the check is done, open slightly the valve at the end of the reactor (the pressure must slowly decrease, otherwise we could have a plugging effect)
6. Once the pressure reaches 0 bar open it completely
7. Using again an inert gas, gradually increase the aperture of the MFC to check if there are pressure drops into the reactor

If either one of those two tests came out positive, a repetition of reactor assembly (leaks) or creation (pressure drops) must be done.

### 2.3.4. Reactors summary

It is then convenient to make a summary recap of all the reactors prepared during this thesis work. It is important to notice that all of them will be called from now on with the acronym "NSx", where "NS" stands for the initials (Name, Surname) of the operator while "x" for the reactor's number, as shown in Table 2.5.

Reactors Summary Table			
Reactor Name	Catalyst Type	Mass [mg]	Experiment
AL2	1 wt% Ru/TiO <sub>2</sub> (N)	300,3	Ketonization
AL3	TiO <sub>2</sub>	302,4	TPR
AL4	TiO <sub>2</sub>	300,2	Ketonization
AL5	1,2 wt% Ru/TiO <sub>2</sub> (Cl)	185,8	Ketonization
AL6	Quartz	305,8	Blank
AL7	TiO <sub>2</sub> Fluka	301,3	Ketonization
AL8	TiO <sub>2</sub>	300,3	Ketonization
AL9	1 wt% Ru/TiO <sub>2</sub> (N)	269,5	Ketonization
AL10	TiO <sub>2</sub>	305,8	Ketonization
AL11	TiO <sub>2</sub> DT-51D	149,3	Ketonization
AL12	TiO <sub>2</sub> Degussa	89,3	Ketonization
AL13	TiO <sub>2</sub> DT-51D	206,6	Ketonization
AL14	TiO <sub>2</sub> DT-51D	200,6	CO <sub>2</sub> TPD
AL15	1 wt% Ru/TiO <sub>2</sub> (N)	199,7	Acetic Acid TPD
AL16	TiO <sub>2</sub>	200,6	CO <sub>2</sub> TPD

<b>AL17</b>	TiO <sub>2</sub>	151,9	CO <sub>2</sub> TPD
<b>AL18</b>	TiO <sub>2</sub>	149,3	CO <sub>2</sub> TPD
<b>AL19</b>	TiO <sub>2</sub>	150,1	Acetic Acid TPD
<b>AL20</b>	3 wt% Ru/TiO <sub>2</sub> (Cl)	199,1	Acetic Acid TPD
<b>AL21</b>	TiO <sub>2</sub>	150,2	Acetic Acid TPD
<b>AL22</b>	Quartz	301,3	Blank Test
<b>AL23</b>	TiO <sub>2</sub>	152,8	Acetic Acid TPD
<b>AL24</b>	TiO <sub>2</sub>	200,2	Ketonization+TPO
<b>AL25</b>	TiO <sub>2</sub>	205,2	Ketonization+TPO
<b>AL26</b>	TiO <sub>2</sub>	200,7	Ketonization+TPO
<b>AL27</b>	TiO <sub>2</sub>	200,7	Ketonization+TPO
<b>AL28</b>	TiO <sub>2</sub>	200	Ketonization+TPO
<b>AL29</b>	TiO <sub>2</sub>	200,1	Ketonization+TPO
<b>AL30</b>	3 wt% Ru/TiO <sub>2</sub> (Cl)	199	Ketonization+TPO
<b>AL31</b>	TiO <sub>2</sub>		Ketonization+TPO
<b>AL32</b>	3 wt% Ru/TiO <sub>2</sub> (Cl)	199,8	Ketonization+TPO
<b>AL33</b>	TiO <sub>2</sub>	200,1	Ketonization+TPO
<b>AL34</b>	3 wt% Ru/TiO <sub>2</sub> (Cl)	200,3	Ketonization+TPO

Table 2.5 – Reactors summary

In the table, only reactors that were tested in the plant presented in this thesis work are reported. Other tests were performed with different plants and reactors, but they will only be cited in chapter 4, as a full explanation would result superfluous and inaccurate

### 2.3.5. H<sub>2</sub> Pre-Treatment

A pre-treatment process for the catalyst had to be performed before every test on which it was needed. In particular, a reduction in H<sub>2</sub> environment was performed, with the following operating conditions:

- GHSV: 6000 NL/h/kg<sub>cat</sub>
- Flux: 100% H<sub>2</sub>
- 3-step temperature variation:
  1. Firstly, 10°C/min rate from room temperature up to 400°C
  2. Then, a hold of 1hour
  3. Lastly, there was a cooldown of the oven with again a rate of 10°C/min until temperature was at least lower than 50°C.

## 2.4. Experimental procedure

### 2.4.1. Before the experiment

A set of consecutive steps must be performed before initiating any activity on the rig to ensure proper safe working conditions. All of them will be listed in order of execution.

#### Start-up of the rig

Start-up is the first step that has to be performed:

1. The suction hood is turned on to avoid gas leakage to the working environment.
2. Then, the reagent cylinders placed outside the building and the valves placed upstream and downstream of the pressure reducer are opened. The reducer is typically set to 4 bar for ordinary gases and 5.5 bar for transport gases.
3. Next, the shut-off valves are opened at the entrance to the system lines.
4. At this point, heating tapes must be turned on. Then the GC is set into the desired method.

#### Flow measurement

Once the heating tapes have reached the operating temperature, the reacting mixture is prepared. The desired flow rate of each gas is set by adjusting proper openings of MFC. Each flowrate is then also measured by means of a bubble flow meter as an additional check. For using the bubble flow meter, it is necessary to open the flow meter valve and close the bypass one. Time measurements are taken with a chronometer (sensitivity 0.01 s) and an average of five measurements is calculated. To

bring the measurement unit back to NmL, the flow temperature is also measured. Then the flow rate is given by the equation:

$$F_i \text{ [NmL/min]} = \frac{V_{measured} \text{ [mL]} \cdot 273.15 \text{ [K]}}{t_{average} \text{ [min]} \cdot T_{measured} \text{ [K]}} \quad (2.11)$$

This procedure is repeated for every gas that is going to be used during the experiment. Once all the gas flows have been checked, all the brooks are opened, and the helium carrier is sent to the saturator in order to collect acetic acid. Because the saturator has high inertia, to reach faster the equilibrium, the flow of the helium is strongly increased (around 80% of the maximum flow that the brooks can provide) and then slowly decreased until the right flow is reached.

Once the reacting mixture is ready, GC analyses in the bypass line have to be performed to check if the mixture we have set respects the target concentrations that were previously fixed.

#### 2.4.2. Experimental protocols

After all the checks, the real experiment could start. During the project, protocols were adopted, depending on the type of test. Characterization tests have already been reported in paragraph 2.2.4, while the remaining procedures are here explained.

##### Acetic acid ketonization

It consisted in the composition analysis of products at different increasing set points of temperature for the ketonization reaction of acetic acid.

Standard procedure was:

- GHSV: 20000 NL/h/kg<sub>cat</sub>
- Flux: 3% Acetic acid, 10% N<sub>2</sub> in He

Investigated effects regarded the influence of Ruthenium presence, Ru precursor type and pre-reduction process over the reaction.

##### Blank Test

Blank tests were carried out using Quartz instead of TiO<sub>2</sub> (same catalyst mesh of 140-200). The experimental procedure was the same as the one used for ketonization tests.

Tests were performed to ensure if regenerated quartz from previous tests could lead to higher reactivity and C-deposits on the reactor column. In addition, reactivity changes in the presence of hydrogen and increased flow rate were also evaluated.

### 2.4.3. Shut-down

Once the test finished, the oven set point is lowered to zero. When the temperature on its screen is lower than 175°C, the oven can be switched off safely. The mass flow controllers and shut-off valves are then closed in reverse order with respect to the opening one. However, the inert gases (He and N<sub>2</sub>) are left open for a few minutes and allowed to flow into the reactor in order to cleanse and cool it. After that, the reactor is isolated by opening the bypass valve and closing both the upstream and downstream valve, so that the catalyst is left in an inert environment. At this point, flow controllers and the valves on the inert lines can be closed. Then, it is possible to close the system inlet valves, the ones straddling the pressure reducer and finally the external tanks of the reactants. The lines heating tapes and the hood can now be switched off. Finally, the GC is set in the shut-down method which is called "Spegnimento".

## 2.5. Data processing

### 2.5.1. Post-processing of the results

#### Response factor

As it was explained before, the chromatograph given by the GC represents each species' peaks, measured with a voltage difference. However, since we want an estimation of the molar flow, we must convert these voltage signals into actual quantities. The solution resides in the area of each peak: they are proportional to their quantity, meaning that a bigger area leads to a bigger amount of the same element. However, to convert areas into concentrations it is necessary to introduce  $\alpha_i$ , also known as response factor, which is defined as follows:

$$\alpha_i = \frac{\dot{N}_i/\dot{N}_{\text{ref}}}{A_i/A_{\text{ref}}} \quad (2.12)$$

Where  $N_i$ ,  $N_{\text{ref}}$  are the volume or molar fluxes of the  $i$ -component and reference [NmL/min],  $A_i$  and  $A_{\text{ref}}$  are the areas [ $\mu\text{V}\cdot\text{s}$ ] of the peaks of the  $i$ -species and reference. The response factors, obtained from a gas chromatograph calibration, establish a direct proportionality between the flows and the areas, therefore allowing to evaluate the flows of each species if the reference flow is known. For this thesis work, N<sub>2</sub> was used as reference.

The procedure used to calculate the response factor for gaseous species was the following:

- Set the molar fraction of the gaseous species that must be calibrated



- Measure the flow of that species together with N<sub>2</sub> (reference) and He (complement) accordingly
- Perform the GC analysis of the mixture (in order to reduce the experimental error, the analysis is performed three times and averaged)
- Find the response factor that allow the molar fraction calculated to be equal to the measured one

To better evaluate the response factors, three different molar fractions (1, 3 and 5%) were considered, and the results were averaged.

A different procedure was adopted for acetic acid and acetone because their flow rate was not controlled with an MFC. Since the amount was not known, we could not check calculated molar fraction with measured one. Instead, one thing that was surely known was the combustion reaction of both components in air. Thus, the controlling parameter to find the response factor became the carbon balance.

The method used was:

- Set the molar fraction of the species that must be calibrated
- Measure with the flowmeter the flow of the air (whose N<sub>2</sub> is used as reference) and He (both complement and carrier) accordingly
- Burn the reagent inside the reactor
- Perform the GC analysis of the gas mixture from the reaction section (in order to reduce the experimental error, the analysis is performed three times and is used the mean result)
- Find the response factor that allow to close the carbon balance

It is worth mentioning that in order to follow this second procedure all the possible products of the combustion of the liquid must already be calibrated (i.e. CO<sub>2</sub>).

Table 2.6 reports all the response factors used during this thesis work in the GC analyser.

Response factors Table		
Column	Species	$\alpha_i$
<b>A (Molecular sieves)</b>	H <sub>2</sub>	50,175922
	O <sub>2</sub>	1.009749
	N <sub>2</sub>	1.000000
	CH <sub>4</sub>	1,370939
	CO	0,808217
<b>B (Plot U)</b>	Macro	1,000000
	CO <sub>2</sub>	0,816540
	Light comp.*	0,750000
	H <sub>2</sub> O	1,400779
	Medium comp.*	0,750000
	Acetone	0,486746
	Acetic Acid	0,657115
	Heavy comp.*	0,65

Table 2.6 – Response factors table for GC

“x\* components” classification refers to all the possible species between the upper and lower defined element of the table: for example, “medium components” refers only to the species found between water and acetone residence time. For all these three categories, an estimation of their response factors was done based on the ones already available. Of course, a check of the C balance was also performed and verified.

#### Calculation of molar flows from chromatograph

The molar flows of reactants and products were calculated from the GC analyses.

As previously said in the response factor section, to do this a reference species must be chosen, so that all results are normalized to a single parameter. Nitrogen, an inert species fixed at 5-10% in all the tests of this thesis work, was used as internal standard. Nitrogen peak is detected by both the columns of the gas chromatograph. However, Column B (Poraplot Q) does not separately detect N<sub>2</sub>, O<sub>2</sub>, CH<sub>4</sub> and CO, and it combines

them in a single macro-peak. Even if they are insignificant in all the experiment, to isolate them, it is necessary to resort to the signal of column A and to evaluate the fraction of the area under the macro-peak relative to nitrogen:

$$x_{areaN_2} = \frac{A_{N_2}^A}{A_{N_2}^A + A_{O_2}^A + A_{CO}^A} \quad (2.13)$$

An average fraction on three consecutive chromatographic analyses was evaluated, in order to have a solid estimation:

$$x_{areaN_2}^{average} = \frac{x_{areaN_2}^{analysis\ 1} + x_{areaN_2}^{analysis\ 2} + x_{areaN_2}^{analysis\ 3}}{3} \quad (2.14)$$

The area of the “apparent” nitrogen in signal B can be therefore calculated:

$$A_{N_2app}^B = A_{macro}^B * x_{areaN_2}^{average} \quad (2.15)$$

Since nitrogen was chosen as the reference species, it was necessary to use its area to normalize the areas under the peaks of all the other components detected by the gas chromatograph. For the signals of column B the apparent nitrogen area just calculated was used, while for column A the measured nitrogen area was directly employed:

$$f_i = \frac{A_i}{A_{N_2app,N_2}} \quad (2.16)$$

Again, for each species the average ratio was then considered:

$$f_i^{average} = \frac{f_i^{analysis\ 1} + f_i^{analysis\ 2} + f_i^{analysis\ 3}}{3} \quad (2.17)$$

It was also necessary to estimate the response factor  $\alpha_i$  of each species: this parameter account for the different sensitivity of the detector towards a specific component when compared to the reference (whose response factor is fixed to 1). During the calibration procedure, a mixture with known composition is sent to the gas chromatograph and response factors are estimated. Since these factors depend on the temperature of the analysis and on the composition of the mixture that reaches the chromatograph, the calibration procedure must be carried out in conditions similar to the system of interest.

Once all  $f_i^{average}$  and  $\alpha_i$  are known, it is possible to evaluate the flowrate starting from (2.12):

$$\dot{N}_i = f_i^{average} \alpha_i \dot{N}_{N_2} \quad (2.18)$$

The flowrate of inert species (i.e.  $N_2$  and He) is instead fixed with the one measured at the start of the experiment.

Once all of this is done, we can finally evaluate the important results, such as:

1. Molar fraction:

$$y_i = \frac{\dot{N}_i}{\dot{N}_{TOT}} \quad (2.19)$$

2. Conversion of reactants:

$$\chi_j = \left( \frac{\dot{N}_j^{in} - \dot{N}_j^{out}}{\dot{N}_j^{in}} \right) * 100 \quad (2.20)$$

3. C selectivity:

$$\sigma_{C,i} = \frac{\dot{N}_i^{out} * n_{C,i}}{\dot{N}_{C,conv}} \quad (2.21)$$

Where  $\dot{N}_{C,conv}$  accounts for the carbon atoms that converted from reactants into products

$$\dot{N}_{C,conv} = \sum_{j=1}^{NR} (\dot{N}_j^{in} - \dot{N}_j^{out}) * n_{C,j} \quad (2.22)$$

4. C balance:

$$B_C = \frac{\sum_{i=1}^{NS} \dot{N}_i^{out} * n_{C,i}}{\sum_{i=1}^{NS} \dot{N}_i^{in} * n_{C,i}} \quad (2.23)$$

All these calculations and operations were performed in a specific worksheet using Microsoft Excel©.

### 2.5.2. Presentation of the results

Experimental results had to be shown in terms of balances, conversion of reactants and composition of the outlet products. They were represented as function of either temperature or TOS (Time Of Stream). Also, C-selectivity graphs were plotted.

The software used for this task was OriginLab 9 Pro©. Figure 2.15 shows a typical representation of the results obtained.

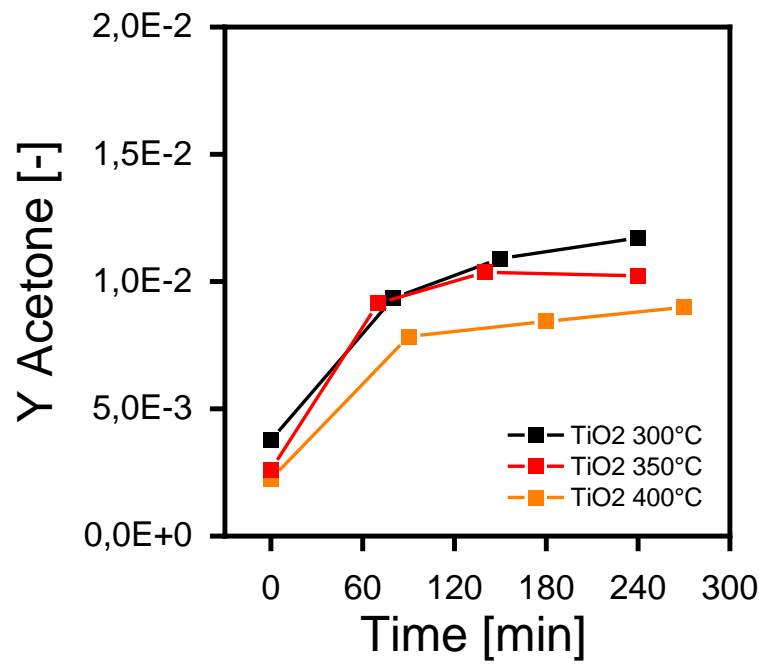


Figure 2.15 - Example of Origin graph



## 3 Catalyst characterization

### 3.1. Morphological analyses

This section reports the results of N<sub>2</sub> adsorption/desorption measurements that allow to characterize the key morphological properties. All experimental procedures have already been explained in chapter 2.

The morphology of the catalyst is characterized in terms of:

- Surface area: area per unit catalyst weight, a parameter that is strictly related with the overall activity of the catalyst, since it indirectly measures the overall surface that is available for the interaction between catalyst and gas mixture
- Pore volume: volume of the catalyst's pores where gas mixture can diffuse
- Pore diameter: diameter of pores

Aim of the characterization was to understand if the ketonization reaction could lead to the obstruction of active sites due to carbon deposition of the products or a morphological change of the catalyst.

#### 3.1.1. BET

BET analyses were performed on samples of TiO<sub>2</sub> calcined at 400°C:

- a) a fresh sample (that did not undergo any type of reaction),
- b) a sample of TiO<sub>2</sub> unloaded from the reactor after high temperature ketonization test for prolonged time (4.5h) with a reacting mixture of 66 Nml/min of 3% Acetic acid, 10% N<sub>2</sub> in He.

Figure 3.1 shows the results obtained in terms of cumulative pore volume and its derivative over the average diameter during desorption.

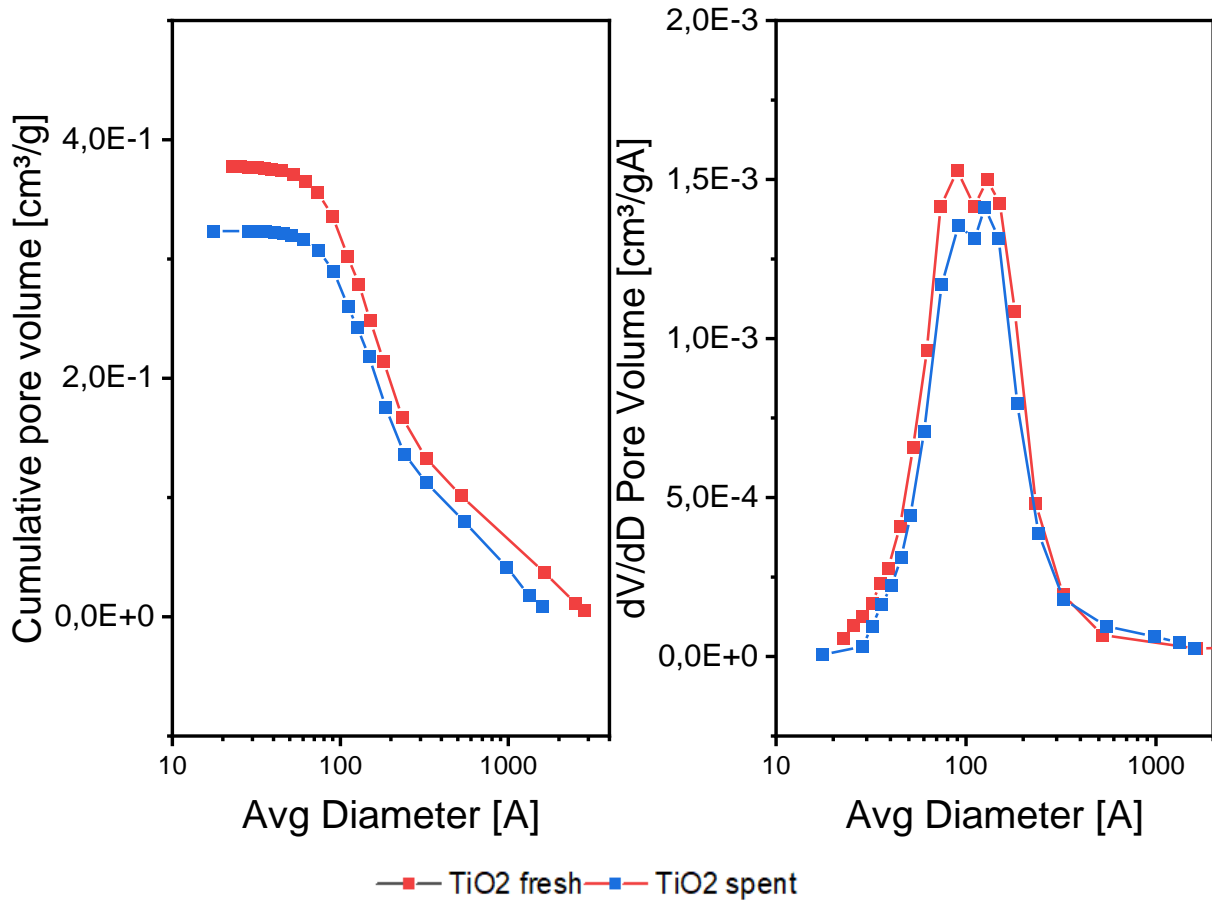


Figure 3.1 – BET results comparison between TiO<sub>2</sub> fresh and TiO<sub>2</sub> spent

The curves of cumulative pore volume obtained by N<sub>2</sub> adsorption/desorption cover the range of micro and mesopores. The total pore volume of the fresh catalyst was larger than the spent catalyst (0.38 vs 0.32 ml/g), although with comparable average pore diameter; the differential curve provides the pore volume distribution and show two contributions centered at 9 and 13 nm for both samples. The comparison reported allows to appreciate that the spent catalyst shows a lower amount of the smaller pores, with diameter below 10 nm.

Consistently, the BET surface area amounts to 80 and 65 m<sup>2</sup>/g for the fresh and spent sample, confirming that after reaction conditions the catalyst pore structure is subject to an important modification, likely due to the partial occlusion of pores.

Table 3.1 instead reports the quantitative data from the analyses.



<b>BET results on TiO<sub>2</sub> DT-51D</b>				
<b>Property investigated</b>	<b>TiO<sub>2</sub> fresh</b>		<b>TiO<sub>2</sub> spent</b>	
<b>BET surface area</b>	80.3	[m <sup>2</sup> /g]	64.9	[m <sup>2</sup> /g]
<b>BJH desorption cumulative pore volume of pores</b>	0.38	[cm <sup>3</sup> /g]	0.32	[cm <sup>3</sup> /g]
<b>Pore diameters of the bimodal distribution (From desorption curve)</b>	9 & 13	[nm]	9 & 13	[nm]

Table 3.1 - BET results test for TiO<sub>2</sub> fresh and TiO<sub>2</sub> spent

### 3.1.2. Mercury intrusion porosimetry

The same catalysts were also tested with mercury intrusion measurements, to better understand the meso- and macro-pores morphology: in fact while N<sub>2</sub> adsorption/desorption allows to investigate micro/meso-pores, Hg porosimetry is used to detect larger pore sizes.

Figure 3.2 reports porosimetry results in terms of cumulative pore volume and its derivative over average diameter. Since porosimetry is a destructive test, only the phase of intrusion is informative.

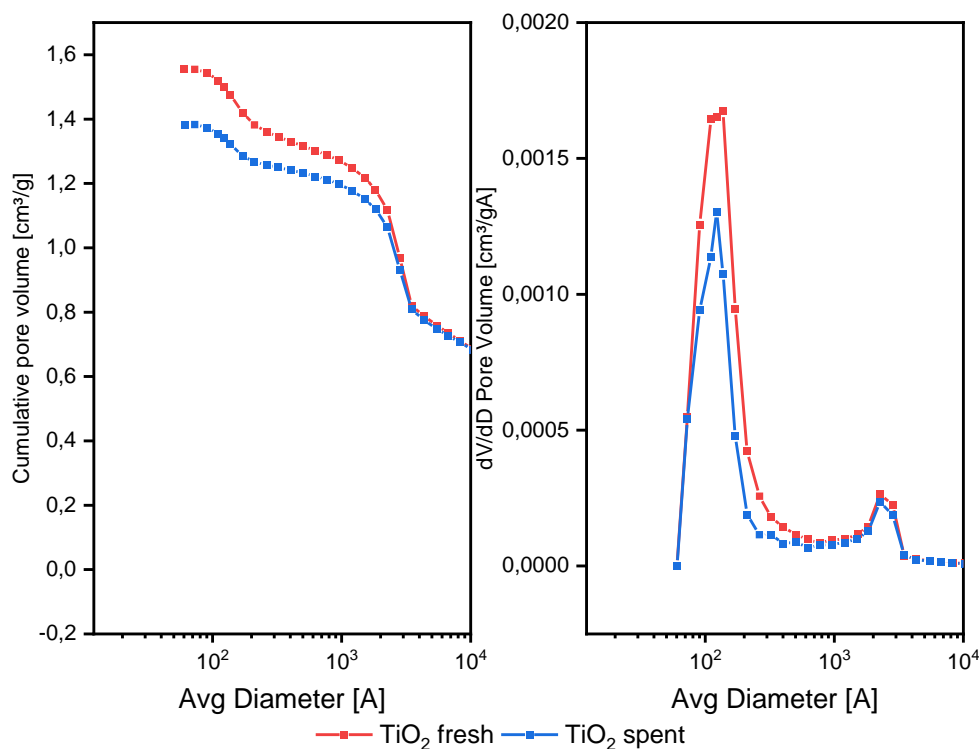


Figure 3.2 – Hg porosimetry on TiO<sub>2</sub> fresh and TiO<sub>2</sub> spent

The curves of cumulative pore volumes consist of different contributions; in particular the volume of Hg uptake to 0.85-0.9 ml/g corresponds to the filling of the measuring cell results and needs to be subtracted from the analysis. Indeed, in correspondence with the pore size of about 300 nm, the integral pore volume curve shows a discontinuity with a sharp increase of the slope. It is reasonable to associate this point with the true initial filling of the catalyst porosity.

It is deduced that the overall pore volume measured by Hg intrusion amounts to about 0.55 ml/g for the fresh sample and 0.45 for the spent catalyst. The differential curves  $dV/dD$  allow to better identify an additional pore contribution in the range of macropores, with average diameter in between 200 and 300 nm.

Data are detailed in Table 3.2.

TiO <sub>2</sub> spent/fresh comparison		
Property	TiO <sub>2</sub> fresh	TiO <sub>2</sub> spent
Mesopore diameter [nm]	14,5	13,7
Mesopore volume [cm <sup>3</sup> /g]	0,22	0,15
Intergranular distance [nm]	280	275
Macropore volume [cm <sup>3</sup> /g]	0,53	0,44

Table 3.2 - Hg porosimetry results on TiO<sub>2</sub> spent and TiO<sub>2</sub> fresh

In conclusion, both  $N_2$  adsorption/desorption measurements and Hg penetration concur to support the hypothesis that the reaction conditions modify the morphology of the catalysts; in particular a partial blockage of the smaller pores would lead to reduction to the total pore volume (especially at the expense of smaller pores) and reduction of the total surface area.

### 3.2. TPR

Temperature Programmed Reductions were performed on the catalysts tested during this thesis work. The technique of TPR is useful to evaluate several important factors, in particular the catalyst components reducibility and the effective content of the metal phase.

Tests were performed on the TPDRO 1100 (Temperature Programmed Desorption Reduction Oxidation) by ThermoQuest©, along with the procedure explained in paragraph 2.2.4. All catalyst were previously calcined at  $400^\circ\text{C}$  in air.

Figure 3.3 reports the results obtained, in terms of  $H_2$  consumption (mV of the detector) over temperature for  $TiO_2$  and  $Ru/TiO_2$  coming from two different precursor ( $RuCl_3$  and Ru-Nyrosyl-Nitrate).

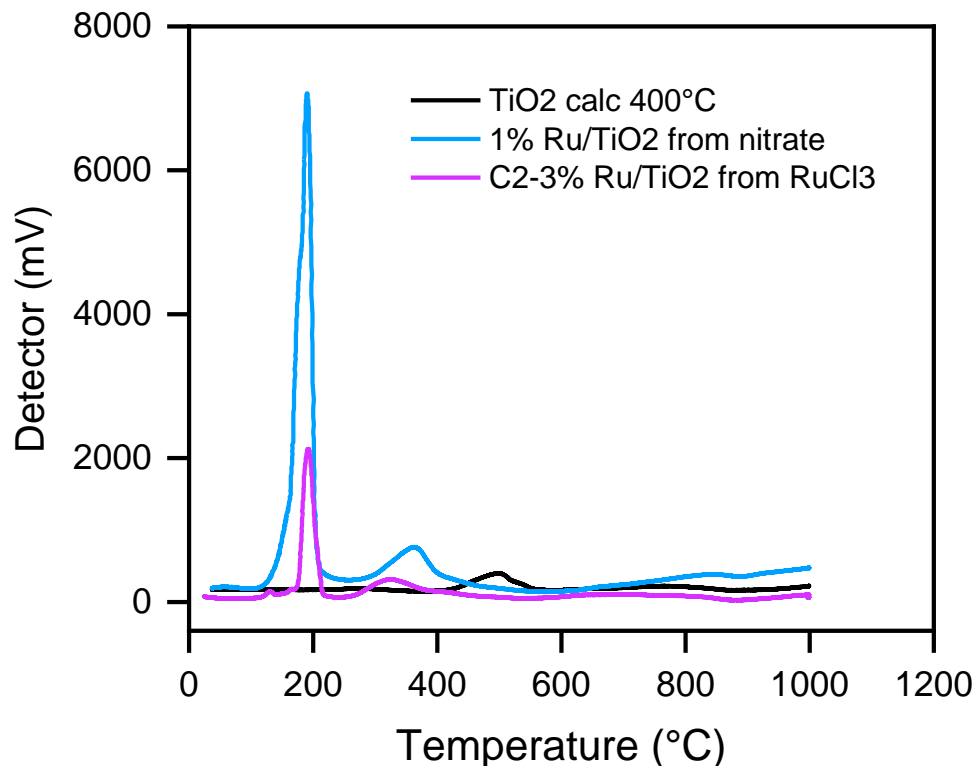
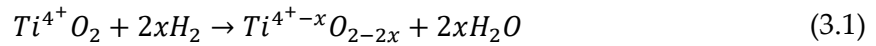


Figure 3.3 - TPR results on  $TiO_2$  and  $Ru/TiO_2$

For  $\text{TiO}_2$ , it is observed that a peak of  $\text{H}_2$  consumption is found between  $400^\circ\text{C}$  and  $600^\circ\text{C}$ . Both  $\text{Ru}/\text{TiO}_2$  curves instead show two in the range from  $250^\circ\text{C}$  to  $400^\circ\text{C}$  and an important sharp peak that starts at  $150\text{-}180^\circ\text{C}$ .

The addition of ruthenium shows two different effects: firstly, the peak found on  $\text{TiO}_2$  results anticipated, and secondly an additional sharp one emerges.

As reported by Shin et al.[15], the peak found in the range from  $400^\circ\text{C}$  to  $600^\circ\text{C}$  for  $\text{TiO}_2$  was associated with the formation of oxygen vacancies due to partial surface reduction with  $\text{H}_2$  spillover. This reaction can be explained with a stoichiometry of the form:



Shin et al.[15] also proposed that the additional peak caused by ruthenium addition was attributed to its reduction.

For  $\text{RuCl}_3$ , the process caused the reduction of  $\text{RuO}_2$  into metallic  $\text{Ru}$ , as shown by Equation (3.2):



While for  $\text{Ru}$  coming from Nitrosyl Nitrate the reaction considered is a bit more complicated, because more reduction reactions take place at the same time. This is also confirmed by the higher amount of  $\text{H}_2$  consumed.

The results proved the reduction procedure correct, because all  $\text{Ru}$  oxide is converted below the  $400^\circ\text{C}$  threshold at which pre-reduction is carried out.

To quantify the amount of hydrogen consumed, it was necessary to integrate the curves over time. However, the ratio of  $\text{H}_2$  moles to area was not 1:1, but could be defined by an F-factor, as shown by Equation (3.3):

$$F = \frac{n_{\text{H}_2}}{A_{\text{H}_2}} \quad (3.3)$$

Where  $n_{\text{H}_2}$  is the number of  $\text{H}_2$  moles, while  $A_{\text{H}_2}$  is the area of  $\text{H}_2$  curve in TPR.

Since the factor changes over time, it is never fixed: it is necessary to recalibrate it from time to time, and to do this a test is carried out with a known mass of copper oxide according to the reaction in Equation (3.4):



From the mass of  $\text{CuO}$  (all consumed) one can easily find the moles of  $\text{H}_2$ , and with the area the factor  $F$  for those given operating conditions is found. Then, under the same conditions, TPR is carried out and the result is plotted. By integration of the curve

and the factor found above, the hydrogen consumption for the test can be calculated using Equation (3.3). Lastly, to find the moles of Ru that reacted with hydrogen, Equation (3.5) is used:

$$n_{Ru} = \frac{k_{Ru}}{k_{H_2}} * n_{H_2} \quad (3.5)$$

Where  $k_i$  is the stoichiometric coefficient of the reduction reaction of Ru.

The integration results reported that:

- Ru/TiO<sub>2</sub> from RuCl<sub>3</sub> had an estimated load of 1,35 wt% instead of the theoretical 3% that was set during preparation
- Ru/TiO<sub>2</sub> from Ru-Nitrosyl-Nitrate conserved the theoretical load of 1 wt%

However, because the procedure is more a qualitative one, theoretical amounts were kept.

The same TPR measurements were repeated in order to better comprehend the nature of reduction reactions observed with TiO<sub>2</sub>. For this reason, gas-phase composition was analyzed during TPR tests. All of them were performed using the second procedure previously explained: packed bed reactor with catalyst in the form of powders, and analysis with a MS (Mass Spectrometer) and IR analyzer.

Figure 3.4 and Figure 3.5 reports the species found by MS and IR in terms of concentration over time.

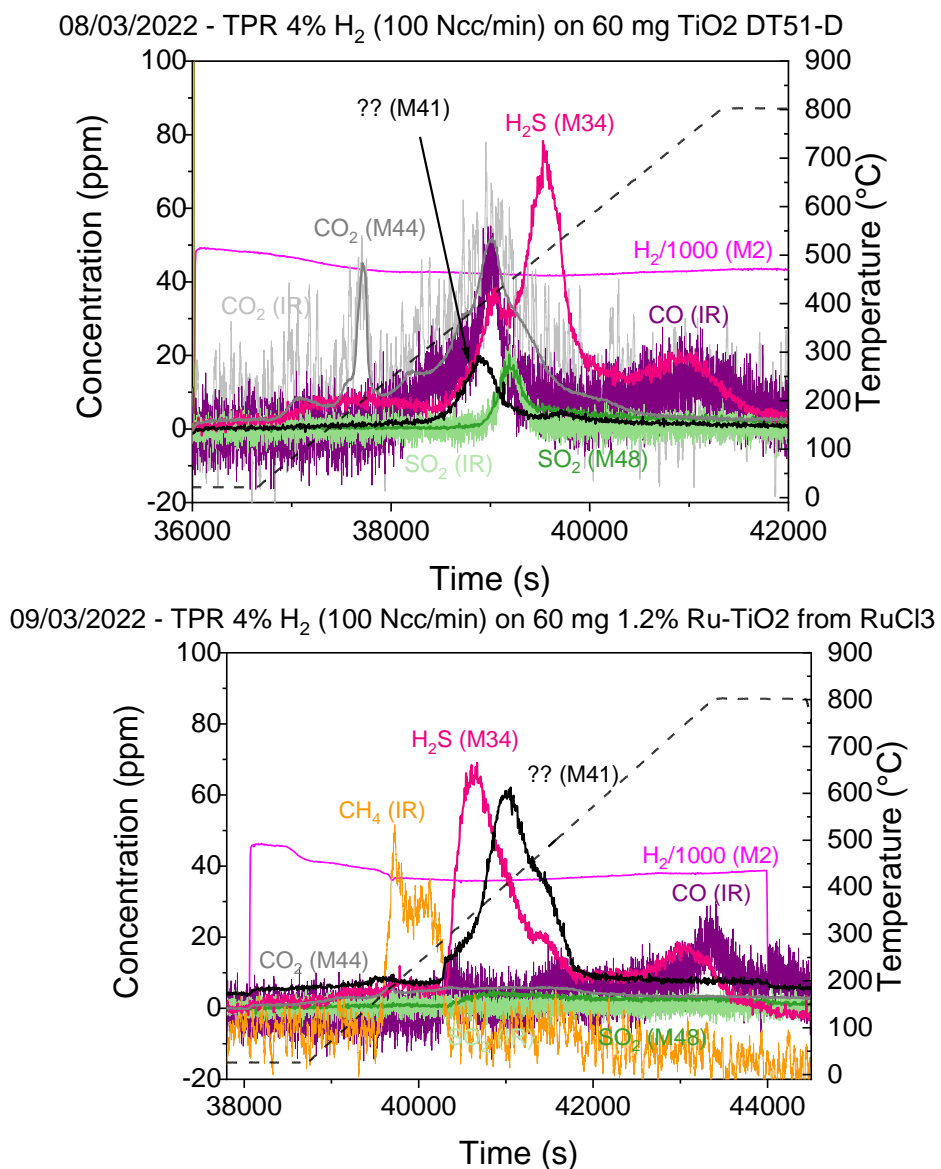


Figure 3.4 - Analysis of the gas-phase composition during TPR tests over the sample of TiO<sub>2</sub>, Ru/TiO<sub>2</sub> from chloride and nitrate Ru precursors. (Part 1)

10/03/2022 - TPR 4% H<sub>2</sub> (100 Ncc/min) on 60 mg 1% Ru-TiO<sub>2</sub> from nitrates

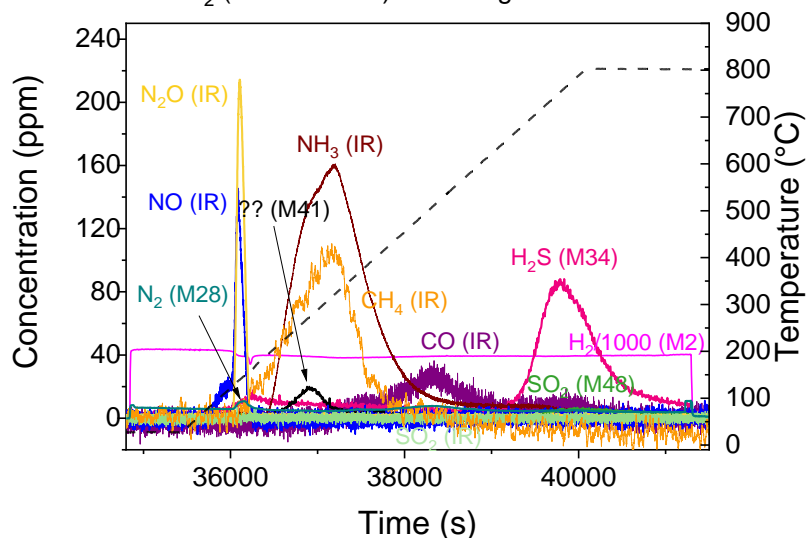


Figure 3.5 – Analysis of the gas-phase composition during TPR tests over the sample of TiO<sub>2</sub>, Ru/TiO<sub>2</sub> from chloride and nitrate Ru precursors. (Part 2)

In the Fig., it can be observed that different species were found for the different cases: TiO<sub>2</sub> reported the presence of CO<sub>2</sub>, CO, H<sub>2</sub>S, SO<sub>2</sub>, while Ru/TiO<sub>2</sub> (Cl) had also CH<sub>4</sub>; lastly, Ru/TiO<sub>2</sub> (N) showed also the presence of nitrates like NO, NH<sub>3</sub> and N<sub>2</sub>. An unknown species has also been found, but it probably refers to some other impurity of the material

The interesting thing is that the reduction of the catalyst surface clearly shows the removing of impurities. Indeed, in the case of TiO<sub>2</sub> the peak that was found at 400-600°C coincides with the emergence of H<sub>2</sub>S and SO<sub>2</sub>, that signifies a sulfur removal.

Moreover, the addition of Ruthenium, once again, demonstrate that the peak anticipation of the first tests results into an anticipated release of H<sub>2</sub>S and SO<sub>2</sub>, because they are found around 250-300°C. CH<sub>4</sub> presence is probably due to the methanation property of Ru, that is also used as main catalyst for that kind of process.

Lastly, the presence of nitrates for Ru(N) is correlated to the precursor reduction that, as said above, results in more reactions respect to the Ru(Cl) case. CO<sub>2</sub> and CO presence are probably related to the fact that some impurities that go through combustion are also present.

In conclusion, the importance of the pre-treatment process in H<sub>2</sub> has been clearly proved and enhanced, because not only it causes the reduction of Ru, but also helps in sulfur and other impurities removal.

### 3.3. TPD

The last part of the characterization tests were various TPD (Temperature Programmed Desorption), carried out using 3 different species as gas probes:

- CO<sub>2</sub> and NH<sub>3</sub> to quantify and characterize respectively basic and acid sites
- Acetic acid to test its own reactivity

#### 3.3.1. CO<sub>2</sub> TPD

To measure the quantity of basic sites, three different conditions were tested for TiO<sub>2</sub>, that are shown in Table 3.3. For clarity purposes, “fresh” means a catalyst that did not undergo a pre-treatment procedure, while “reduced after ket” refers to a catalyst that was subjected to a ketonization reaction up to 300°C and then reduced; “reduced” instead refers to a pre-treatment procedure in H<sub>2</sub> before the actual test was carried out.

Catalyst tested with CO <sub>2</sub> TPD	
Catalayst type	Mass [mg]
TiO <sub>2</sub> fresh	156
TiO <sub>2</sub> reduced	151,9
TiO <sub>2</sub> reduced after ket	152,8

Table 3.3 – Catalyst tested with CO<sub>2</sub> TPD

Figure 3.6 instead reports the results obtained in terms of CO<sub>2</sub> moles (normalized to catalyst mass) with temperature increase.



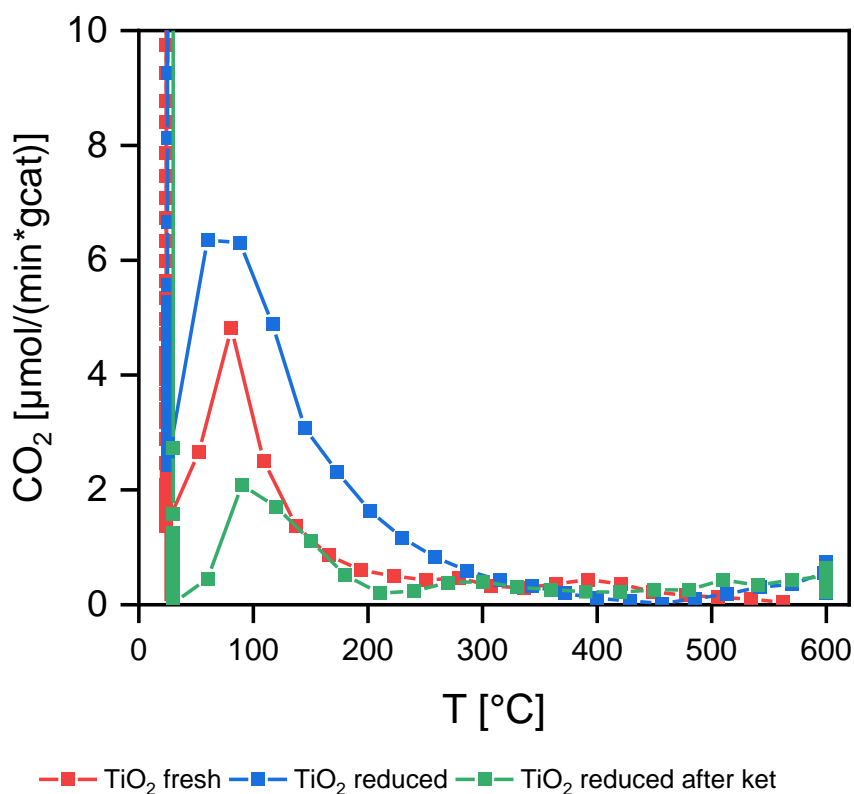


Figure 3.6 – CO<sub>2</sub> TPD results for TiO<sub>2</sub> fresh, TiO<sub>2</sub> reduced and TiO<sub>2</sub> reduced after ket. Finally, integration results to obtain the total CO<sub>2</sub> desorbed were performed, and are reported in Table 3.4.

Integration Results of CO <sub>2</sub> TPD tests	
Catalyst type	CO <sub>2</sub> [mmol/g <sub>cat</sub> ]
TiO <sub>2</sub> Fresh	0,021
TiO <sub>2</sub> reduced	0,034
TiO <sub>2</sub> reduced after ket	0,019

Table 3.4 - Integration results for CO<sub>2</sub> TPD tests

Consistent with literature [16][17], only weak basic sites were found on the catalyst, because all the CO<sub>2</sub> adsorbed was then desorbed by thermal treatment between room temperature and 200 °C. An important thing to notice however is that TiO<sub>2</sub>, when reduced, showed an increased amount of basic sites. The same thing does not happen

for the reduction after a ketonization test, possibly meaning that some sites that should have been activated during reduction were not available, maybe because ketonization deposited some products on the catalyst surface.

It is also important to note here that  $\text{CO}_2$  in the presence of reducible oxides may adsorb in defects on the catalyst surface, and this may not be an accurate representation of the number or strength of basic sites, as reported by the work of Pham et al.[7] already cited.

As a more general conclusion, the  $\text{CO}_2$  adsorption/desorption test seems to identify the pre-treated  $\text{TiO}_2$  as the surface that is more prone to interact with an acidic and O-rich molecule as  $\text{CO}_2$ . Notably the carboxylic group of acetic acid is the functional group that is closest to the full oxidation state of  $\text{CO}_2$

### 3.3.2. $\text{NH}_3$ TPD

$\text{NH}_3$  TPDs were carried out on another testing rig due to a more suitable configuration. The analyses were coupled with a mass spectrometer to correctly identify each species found during the test, and in particular mass 15 ( $\text{NH}_3$ ) was monitored. Operating conditions were set at a temperature of  $100^\circ\text{C}$ , with a ramp rate

The same catalyst configurations tested with  $\text{CO}_2$ -TPD were used also for  $\text{NH}_3$  ones, so that results could compare acid and basic sites for the same catalyst type.

Figure 3.7 reports the results obtained in terms of ppm of  $\text{NH}_3$  over temperature for the three cases studied.

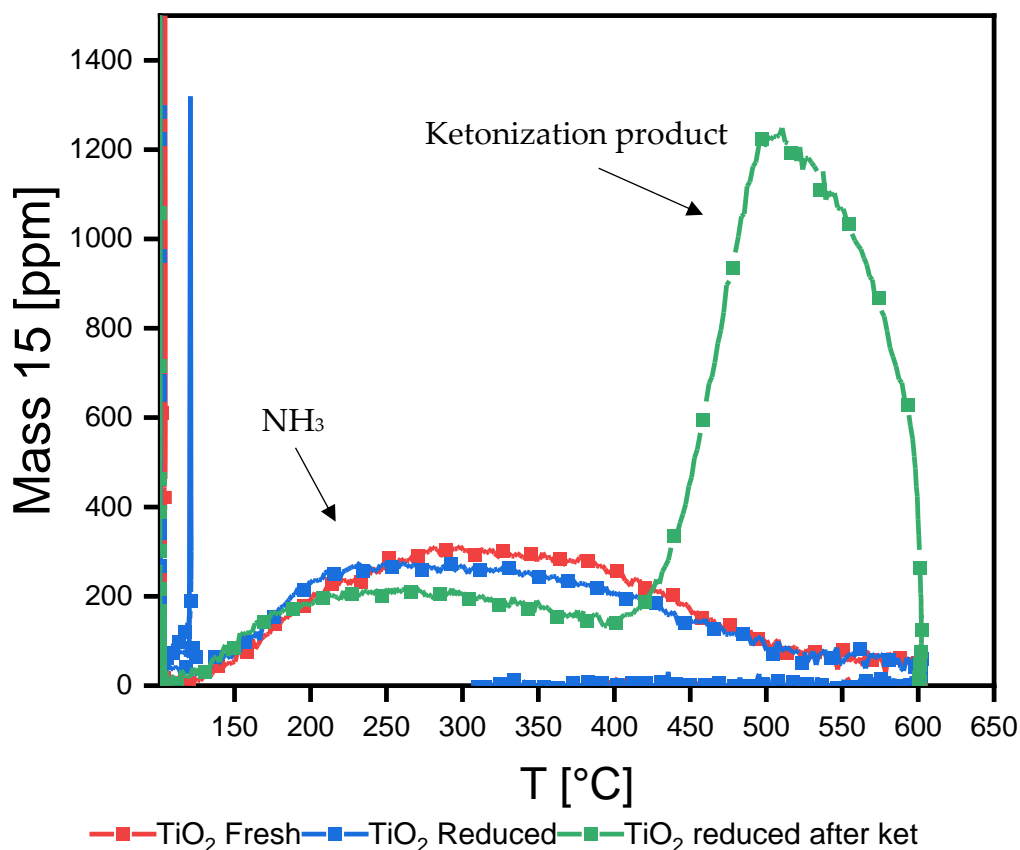


Figure 3.7 - NH<sub>3</sub> TPD results on TiO<sub>2</sub> fresh, TiO<sub>2</sub> reduced and TiO<sub>2</sub> reduced after ket

It is immediate to notice that TiO<sub>2</sub> reduced and fresh show a similar behaviour, with the fresh catalyst desorbing NH<sub>3</sub> at slightly higher T (curve is higher at higher temperature) while reduced TiO<sub>2</sub> has more weaker ones (curve lower at lower T). Instead, the TiO<sub>2</sub> fresh that was subjected firstly to ketonization and then reduction show a lower amount for both cases, while a very important second peak emerges after 400°C.

For TiO<sub>2</sub> reduced, also H<sub>2</sub>S and CO<sub>2</sub> were observed during the analysis.

Again, the curves have been integrated in time to obtain the total amount of NH<sub>3</sub> desorbed, and the results are shown in Table 3.5.

Integration results of NH <sub>3</sub> TPD			
NH <sub>3</sub>	TiO <sub>2</sub> fresh	TiO <sub>2</sub> reduced	Spent TiO <sub>2</sub> reduced after ket
Adsorbed [mmol/g <sub>cat</sub> ]	0,372	0,358	0,271
Desorbed [mmol/g <sub>cat</sub> ]	0,244	0,168	0,140

Table 3.5 – Integration results of NH<sub>3</sub> TPD

Comparing  $\text{NH}_3$  with  $\text{CO}_2$ , it is noticed that the first one desorbs this time for a bigger range of temperature (up to  $500^\circ\text{C}$ ), indicating stronger acid sites than the basic ones. Moreover, also the integration shows higher quantities desorbed, indicating not only that these sites are stronger, but also more numerous than the basic ones (values are one order of magnitude greater).

Regarding  $\text{NH}_3$ ,  $\text{TiO}_2$  reduced has lower ammonia desorbed because probably, due to the reduction process, acid sites not only reduced, but also became weaker: the curve shifted to the left, but quantity also decreased. For the spent case instead, it is noticeable that quantity at the start is lower, as the curve is below the other two: C-deposition probably happened, and some sites were not reachable by  $\text{NH}_3$ . It must be noted that the products have acidic properties, but they could not desorb before a certain temperature threshold was reached.

This exact phenomenon originates the second peak found for the spent  $\text{TiO}_2$ , that is clearly not related to the acid sites of the catalyst, but something else: because it was the only case where we experienced it, other components (formed during the ketonization) deposited on our catalyst that were released as temperature increased. It could possibly be that this unknown species is associated with  $\text{CH}_3$  molecules (mass 15) originated by the cracking of adsorbed species on the catalyst surface..

As shown in literature, the presence of acid and basic sites is a fundamental requirement for ketonization, otherwise the reaction will not be as promoted by other catalysts.

### 3.3.3. Acetic acid TPD

TPD on acetic acid were done to understand what happens when our catalyst adsorbs it, since it is the main reactant of all our tests and investigations on the improvement of pyrolysis vapours. The objective was to understand the influence of Ru addition during catalyst preparation. For this reason, three different catalysts were tested, that are reported in Table 3.6. For the sake of clarity, (Cl) will indicate a chlorine precursor, while (N) a nitrate one, as two different sources were used to obtain Ru (see Paragraph 2.2).

Catalysts tested with Acetic acid TPD	
Catalyst type	Mass [mg]
<b>TiO<sub>2</sub> reduced</b>	150,9
<b>Ru/TiO<sub>2</sub> (Cl) reduced</b>	149,1
<b>Ru/TiO<sub>2</sub> (N) reduced</b>	150,2

Table 3.6 – Catalysts tested with Acetic Acid TPD

Analyses were carried out using the GC and monitoring the outlet composition, that is reported in Figure 3.8, in terms of moles (normalized to catalyst mass) over temperature increase.

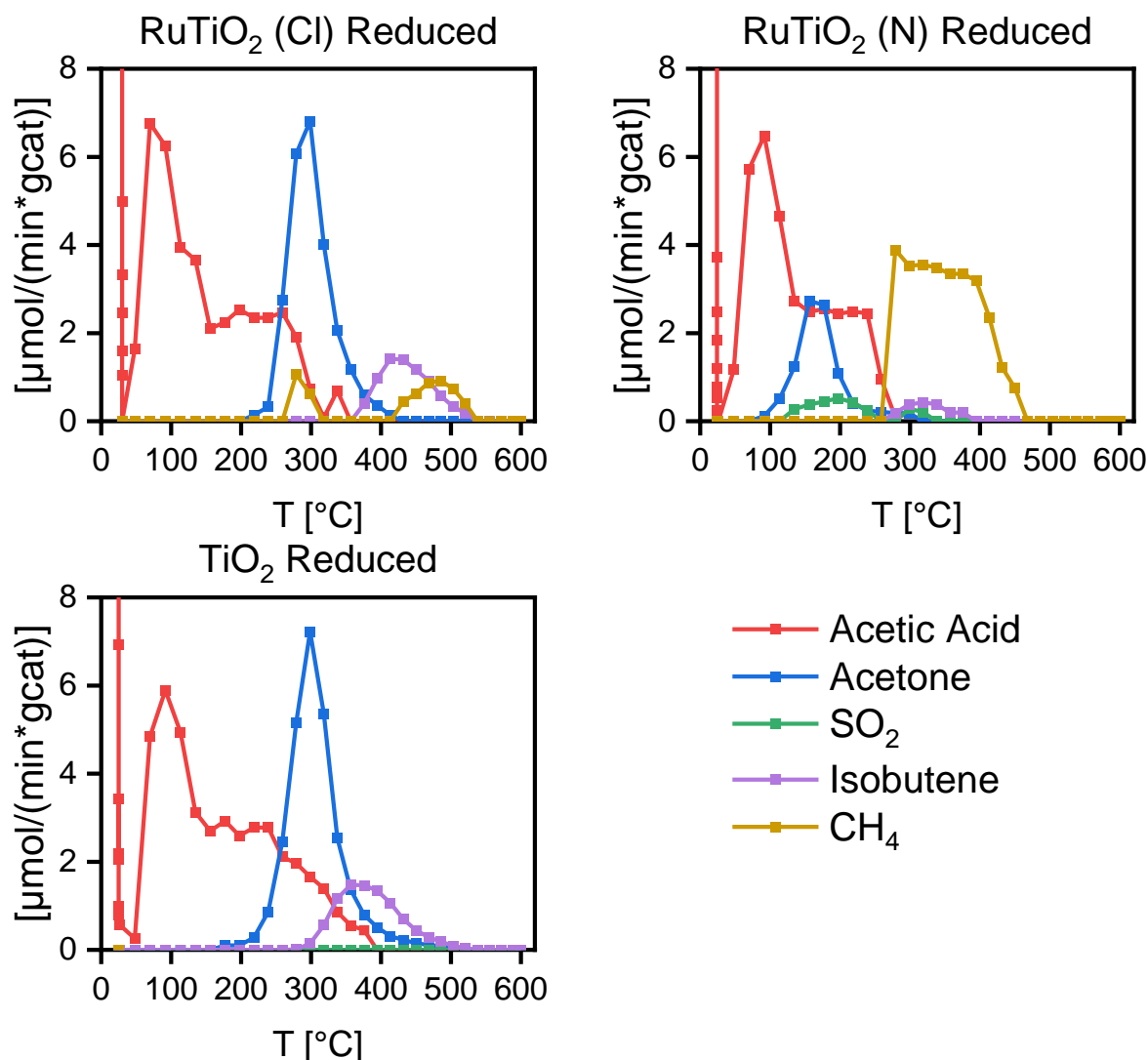


Figure 3.8 - Acetic Acid TPD on  $\text{TiO}_2$ ,  $\text{Ru}/\text{TiO}_2$  (Cl) and  $\text{Ru}/\text{TiO}_2$  all reduced

From the graphs, different observation can be made. If we consider  $\text{TiO}_2$ , Acetic acid immediately desorbs until 400°C; at 200°C acetone is found up to 500°C, with a maximum peak at 300°C; at 300°C isobutene emerges, with a broad peak that max out at 350°C and it extinguishes at 500°C.

For  $\text{Ru}/\text{TiO}_2$  (Cl) instead, things are different: acetic acid terminates at 350°C, isobutene is shifted of 50°C to the right, while  $\text{CH}_4$  is also found at 270°C and from 400°C to 550°C; lastly, traces of  $\text{SO}_2$  were observed from the chromatograph around 150-250°C

$\text{Ru}/\text{TiO}_2$  (N) is also different from the other two: acetone is anticipated at 100°C, with a peak at 150°C and much lower quantity; same things happen for isobutene, that is found from 250°C;  $\text{CH}_4$  emerges as the same time but it remains very high in quantity until 450°C; lastly,  $\text{SO}_2$  this time is detectable, meaning that a higher quantity desorbed.

All C-species found have been integrated in time, as shown by Table 3.7.

Integration results of C moles for each species			
Species	Ru/TiO <sub>2</sub> (N) reduced [mmol/g <sub>cat</sub> ]	Ru/TiO <sub>2</sub> (Cl) reduced [mmol/g <sub>cat</sub> ]	TiO <sub>2</sub> reduced [mmol/g <sub>cat</sub> ]
Acetic Acid	0,206	0,238	0,237
Acetone	0,057	0,147	0,166
Isobutene	0,021	0,088	0,108
CH <sub>4</sub>	0,086	0,017	0,000
Total amount			
C species	<b>0,371</b>	<b>0,490</b>	<b>0,511</b>

Table 3.7 - Integration results for Acetic acid TPD

The first important conclusion that is immediately seen is that acetic acid, although it was the only reactant used, is not the only component found: this means that other reactions took place as temperature increased.

In particular, it can be clearly said that at least ketonization happened: when temperature conditions were enough, conversion from acetic acid into acetone started. Moreover, in the case of nitrate precursor, the temperature threshold is quite lower than the other two, implying that acetic acid is more prone to conversion.

Another major discovery is that isobutene is present because a cracking reaction took place. Faba et al.[18] reported that two acetone molecules combine into an intermediate C<sub>6</sub>, that then cracks into an acetone molecule and isobutene, as shown in Figure 3.9.

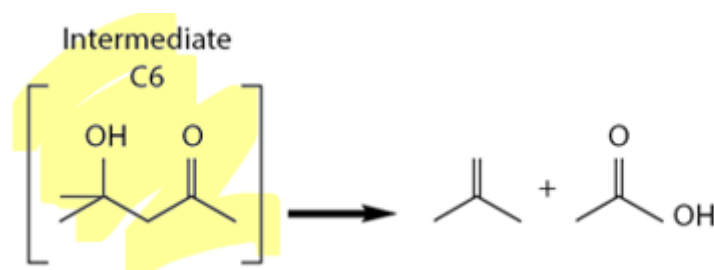


Figure 3.9 – Cracking mechanism of intermediate C<sub>6</sub>

This is a very important discovery, because it highlights that at higher temperature regions, secondary reactions are present, while acetic acid is no more selective to ketonization alone.

CH<sub>4</sub> presence can be attributed to the addition of Ru, as this metal is widely used in methanation processes because it is able to better catalyze the reaction thanks to its hydrogenation properties[16].

Lastly, SO<sub>2</sub> presence is found only for the Ru cases: it is possible that the metal addition is able to partially remove more impurities from the catalyst as temperature increase.

A quantification of the amount of carbon species desorbed is important to understand if the three catalysts have very different reactivity to acetic acid. The integration results however show that for all three cases quantities are in the same order of magnitude. RuTiO<sub>2</sub>(N) has the lowest amount due to the lower amount of acetone (around 0,1 mmol/g) and isobutene desorbed, probably meaning that nitrate precursor is less sensitive to acetone conversion and cracking reactions.

### 3.4. Characterization sum-up

Morphological measurements show that high-temperature ketonization experiments lead to partial pore blockage, probably due to the accumulation of carbon species.

TiO<sub>2</sub> is an acidic medium but after reducing pre-treatments develops basic sites that can be titrated with CO<sub>2</sub> adsorption. Adsorption/desorption of NH<sub>3</sub> shows instead the presence of modest acidic sites.

Adsorption/desorption of acetic acid shows that the minimum activation temperature of the reaction is about 200°C and it is only marginally affected by the presence of Ru. The desorption of acetic acid is accompanied by the primary formation of acetone and the secondary formation of isobutene, which can be explained by the cracking of a C<sub>6</sub> compound (condensation of acetone). In the presence of Ru, high-temperature cracking reactions could lead to the formation of CH<sub>4</sub>.





## 4 Experimental results

Experimental results obtained performing acetic acid ketonization tests on TiO<sub>2</sub> catalysts are presented and discussed in the present chapter. Tests were carried out in a lab-scale experimental rig which was developed during the previous thesis [14], where experimental procedures and preliminary results on acetic acid ketonization on Ru/TiO<sub>2</sub> were also discussed. Instead, in the present thesis work, the investigation on acetic acid ketonization on TiO<sub>2</sub> was extended: on one side the effect of catalyst reduction pre-treatment was explored to maximize the activation of ketonization reaction in the low-temperature range; on the other, high temperatures were better investigated, addressing secondary chain-elongation reactions and monitoring catalyst activity and stability.

### 4.1. Blank Tests

When heterogenous catalytic processes are studied, the impact of (undesired) homogenous reactions must be assessed and controlled. For this purpose, blank ketonization tests were performed; in these experiments the quartz reactor was filled with quartz grains and particles (no catalyst) and the same volumetric flowrates used for catalytic experiments (later shown in chapter) were chosen. Also, the feeding composition was kept equal to the standard one (3% Acetic acid, 10% N<sub>2</sub> in He). Moreover, in the previous thesis work [14] it was already observed that the column of quartz grains before the catalytic bed was turning black after the exposure to several ketonization tests; this indication suggested that carbon deposition took place in certain condition. In order to quantify this phenomenon, a campaign of blank tests was planned, where the effect of regeneration procedure, H<sub>2</sub> co-feed and total inlet flow rate were analysed.

An example of this is shown in Figure 4.1, where the difference of before/after an experiment is undeniable.

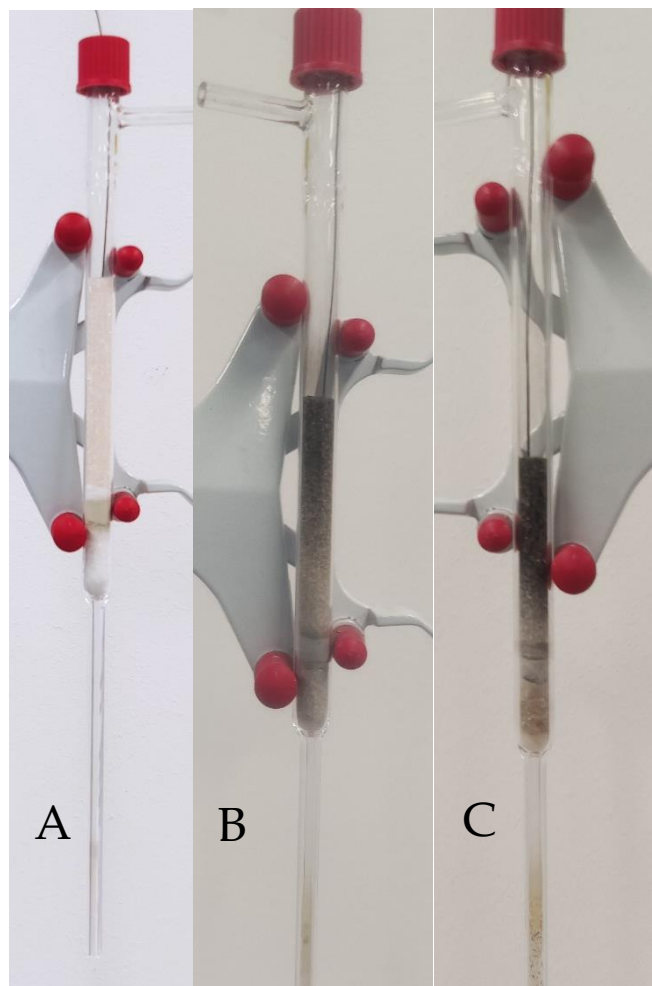


Figure 4.1 – General reactor before experiment (A) and two dirty quartz columns post-experiments (B and C)

From the phenomenon, different questions arose: besides homogeneous reactions, there could have been a chance that re-used quartz grains in catalytic tests could themselves be able to catalyze acetic acid conversion, even if they were subjected to a regeneration procedure to cleanse them. For this reason, the activity of quartz had to be checked. Another possibility could have also been related to the fact that the quartz column length or mesh were not effective in preventing neither secondary reactions neither ketonization itself.

Regarding quartz's regeneration, the procedure was the following:

1. After a substantial amount of dirty quartz was obtained, a reactor completely filled with it was created, with quartz wool only at the shrinkage section
2. Once the reactor was mounted inside the oven, temperature was set at 600°C and a sufficient amount of air (e.g. 50 Nml/min) was injected into the reactor for at least 3 hours, so that complete combustion of carbon molecules was achieved
3. Lastly, a cooldown of the oven was done without stopping the air flow rate into the reactor, until room temperature was reached

After this thermal treatment, the quartz grains were seen recovering the original color since black-deposits were effectively burnt.

Table 4.1 reports the set of reactors used during the Blank tests, grouping them by the effects that were analysed (set of data). The inlet composition of standard acetic acid ketonization tests (3% Acetic acid, 10% N<sub>2</sub> in He) was employed for blank tests, for a correct comparison with catalytic tests.

Reactors summary			
Set of data	Quartz Type	Mass [mg]	Feed composition
#1 – Regeneration effect	Thermally Regenerated Quartz	300	100 Nml/min, 3% Acetic Acid, 20%H <sub>2</sub> , 15% N <sub>2</sub> in He
	Fresh Quartz	305,8	100Nml/min of 3% Acetic acid, 20% H <sub>2</sub> , 15% N <sub>2</sub> in He
#2 – H <sub>2</sub> effect	Fresh Quartz	301,3	66 Nml/min of 3% Acetic acid, 10%N <sub>2</sub> in He
	Fresh Quartz	301,3	66Nml/min 3%HAc, 20%H <sub>2</sub> , 10%N <sub>2</sub> in He
#3 – Flow rate effect	Fresh Quartz	305,8	100Nml/min of 3% Acetic acid, 20% H <sub>2</sub> , 15% N <sub>2</sub> in He
	Fresh Quartz	305,8	150Nml/min of 20% H <sub>2</sub> , 15% N <sub>2</sub> in He

Table 4.1 – Reactors' summary for blank tests

### 4.1.1. Regeneration effect

To check the effectiveness of the regeneration procedure for the quartz that was used during catalytic activity tests, a comparison with batch-new fresh quartz was done. Figure 4.2 and Figure 4.3 reports the results obtained, showed in terms of molar fraction of products, conversion and C-balance over temperature. The term “re-used” refers to a quartz that had gone through a previous catalytic experiment and was thermally regenerated (combustion in pure air at 600°C for at least 3h), while “fresh” indicates a new batch quartz never tested with TiO<sub>2</sub>.

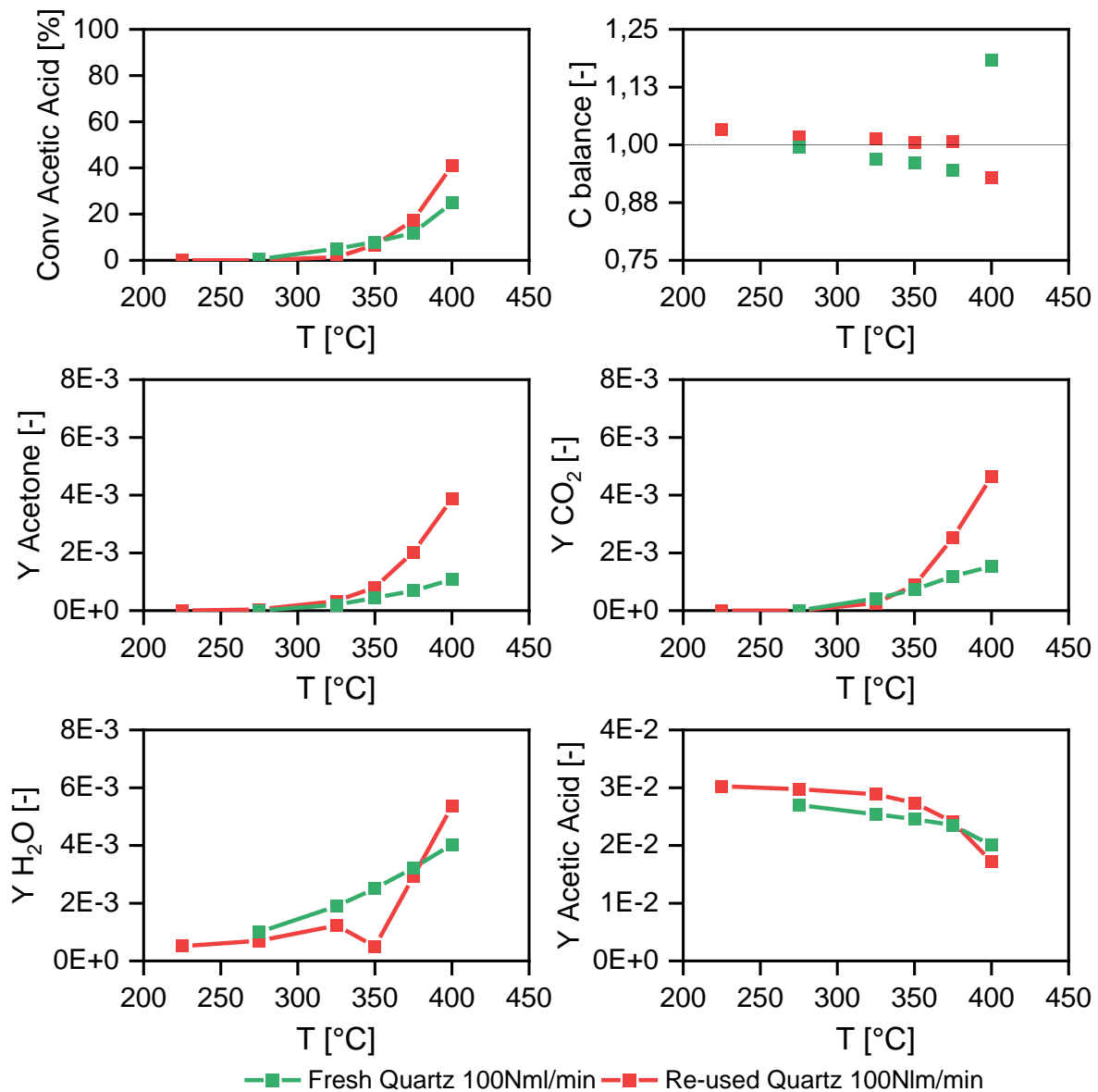


Figure 4.2– Effect of regeneration on quartz reactivity. Flux: 100 Nml/min of 3% Acetic acid, 20% H<sub>2</sub>, 15% N<sub>2</sub> in He (Part 1)

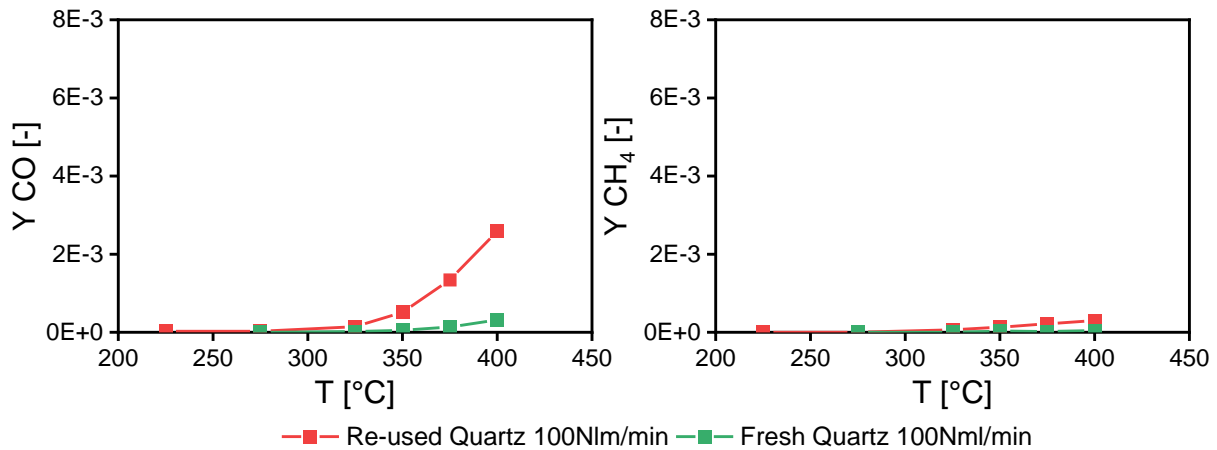


Figure 4.3 – Effect of regeneration on quartz reactivity. Flux: 100 Nml/min of 3% Acetic acid, 20% H<sub>2</sub>, 15% N<sub>2</sub> in He (Part 2)

The comparison clearly shows that acetic acid conversion and products molar fraction were higher in the case of re-used quartz when temperature reached the 300°C threshold.

This means that acetic acid that flows through a fresh quartz column is less reactive than when its fed into a re-used one. This means that the quartz that was employed during catalytic activity tests is not sufficiently cleaned with the regeneration procedure, even if its color is visually restored. For this reason, in this thesis work only fresh quartz grains were employed in tests performed in “risky” conditions ( $T > 300^{\circ}\text{C}$ ).

#### 4.1.2. H<sub>2</sub> co-feed effect

As previously stated in Paragraph 3.2, H<sub>2</sub> positive effects were proven. For this reason, and since H<sub>2</sub> was also co-fed in catalytic reactors, Blank tests with standard acetic acid ketonization inlet mixture with and without H<sub>2</sub> co-feed were performed. This was done with reactor AL22, where the first test had a 20% H<sub>2</sub> co-feed, while the second one had none of it. The results are presented in Figure 4.4, always in terms of molar fractions, conversion and C-balance over temperature.

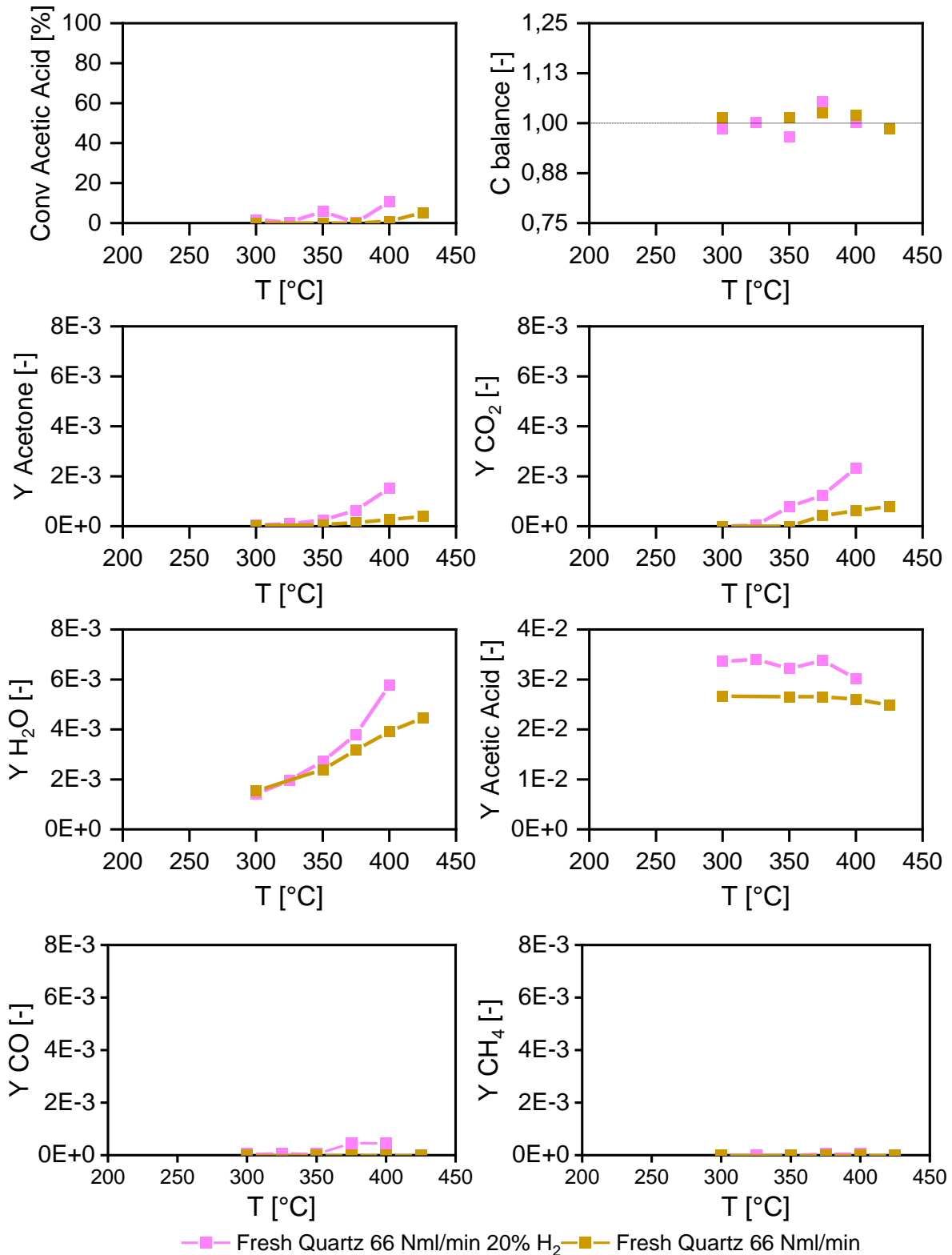


Figure 4.4 – Effect of H<sub>2</sub> co-feed on 66Nml/min of 3% Acetic acid, 20% H<sub>2</sub> (if co-fed), 10% N<sub>2</sub> in He

What emerges from those graphs is that the case without H<sub>2</sub> has a heavy reduction of both acetone and CO<sub>2</sub>, while also other products reduce in their molar fractions. The

overall result is a very low conversion, that reaches 5% only at very high temperature. This means that H<sub>2</sub> plays a very important role in the conversion of acetic acid in blank tests, implying that as temperature increase, acetic acid is more prone to convert in presence of H<sub>2</sub>.

### 4.1.3. Flow rate effect

An inlet flow rate for the catalytic tests had to be chosen. However, a flow rate effect investigation had to be performed, because it is known that a higher flux usually reduces secondary reactions, because the mixture has a lower residence time inside the reactor (i.e. less reaction time). For this reason, total inlet flow rate was increased from 100 Nml/min to 150 Nml/min, while everything else was kept constant (3% Acetic acid, 20% H<sub>2</sub>, 15% N<sub>2</sub> in He). Figure 4.5 and Figure 4.6 report the results obtained, comparing the two tests on AL6.

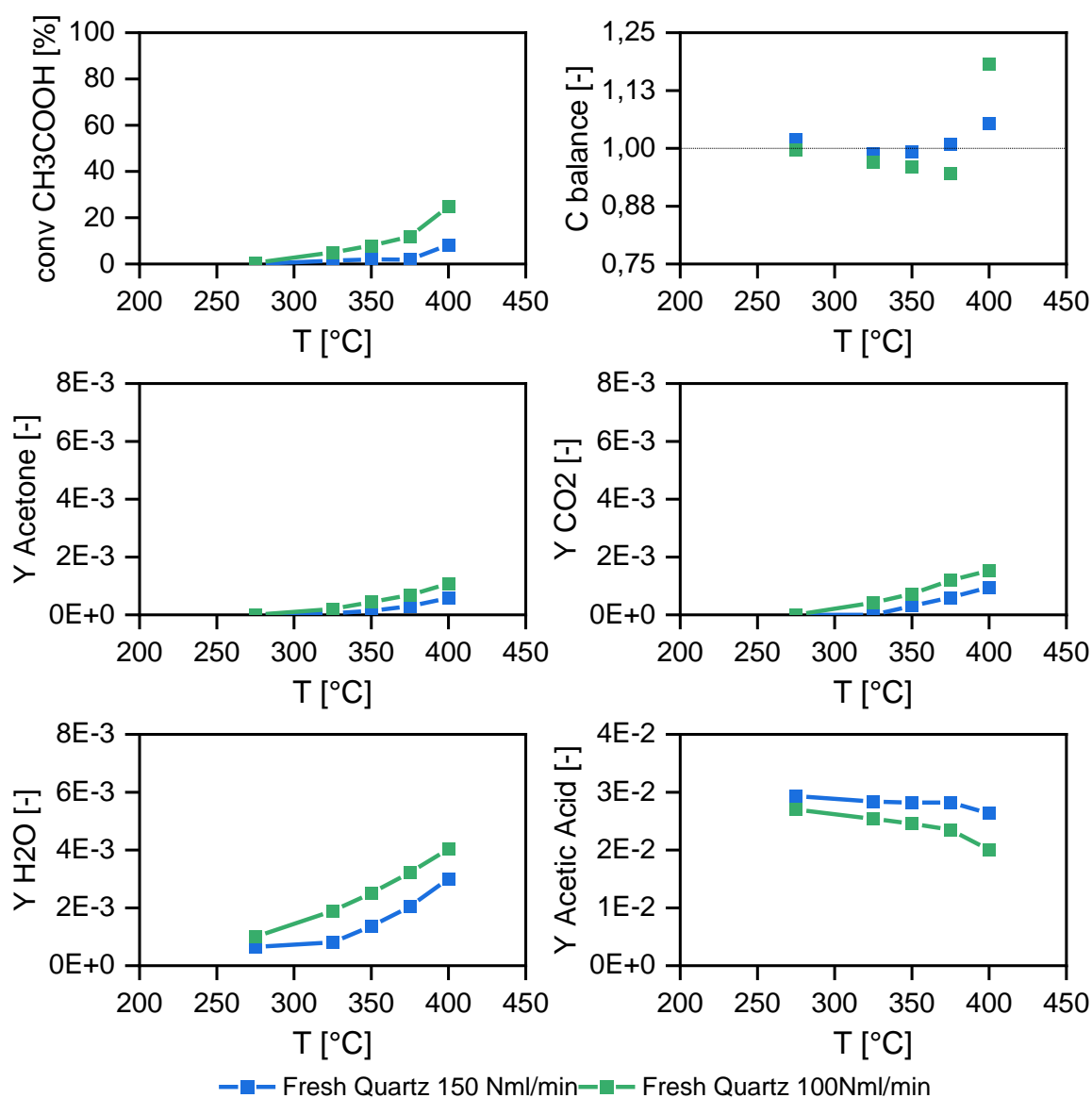


Figure 4.5 - Flow rate effect on quartz reactivity. Flux: 100-150 Nml/min of 3% Acetic acid, 20% H<sub>2</sub> 15% N<sub>2</sub> in He (Part 1)

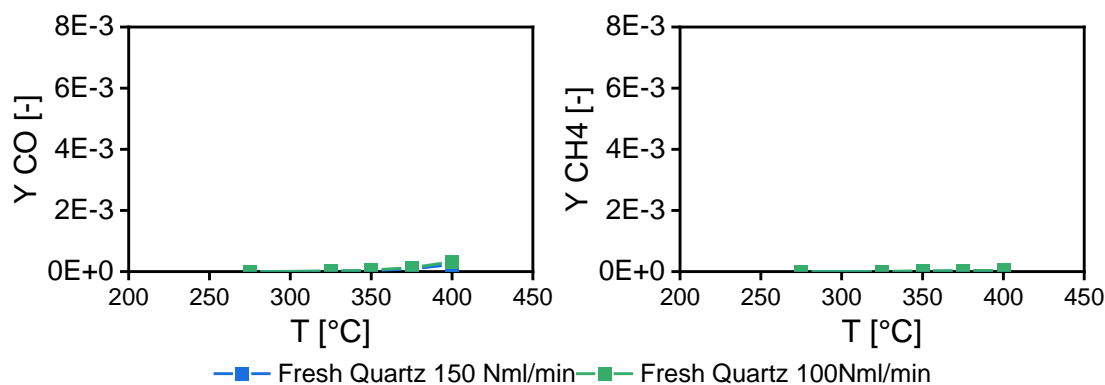


Figure 4.6 – Flow rate effect on quartz reactivity. Flux: 100-150 Nml/min of 3% Acetic acid, 20% H<sub>2</sub> 15% N<sub>2</sub> in He (Part 2)

In the figure, all products are always in lower amount in the higher flow rate case.

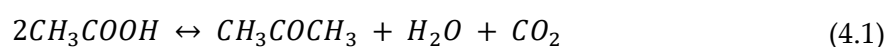
The hypothesis presented before is then correct: as expected, as flow rate increases homogeneous reactions decrease. This behavior suggest that they are responsible for the incipient conversion of acetic acid in the presence of quartz. In particular, conversion goes from a value of 30% (100 Nml/min) to mere 10%, mostly corroborated by the reduction of both acetone, CO<sub>2</sub> and water, that are exactly the main products of ketonization.

Based on these results the operating conditions for heterogeneous experiments were tuned. However, choosing 150 Nml/min as inlet feed presented a more critical problem: pressure drops in the reactor increased. As pressure drops are more critical (i.e. null test) than the positive effect from using bigger flow rates, a set of 100 Nml/min was used for ketonization tests in the low temperature range (T = 200-300°C), since it was also shown that homogeneous reactions did not impact significantly.

The same thing should have been done on the high temperature region; however, as pressure drops increase with temperature, more problems occurred. For this reason, high temperature region inlet feed was set at 66 Nml/min, as further reduction of flow rate was the only feasible solution.

## 4.2. Acetic acid ketonization in the low-temperature range

The first analyses consist of an investigation of the reactivity in the low temperature range, up to 300°C; in these conditions acetic acid ketonization reaction represents the only active reaction pathway with stoichiometry:



Several different catalyst formulation, pre-treatment and operating conditions were explored, as shown by Table 4.2.



Reactors Summary Table			
Set of data	Catalyst Type	Treatment before test	Mass [mg]
#1 – Pre-reduction effect	TiO <sub>2</sub>	Fresh	300,2
#1 – Pre-reduction effect	TiO <sub>2</sub>	Pre-reduction after ketonization	300,2
#1 – Pre-reduction effect	TiO <sub>2</sub>	Pre-reduction on fresh	269,5
#1 – Pre-reduction effect	1,2 wt% Ru/TiO <sub>2</sub> (Cl)	Fresh	185,8
#1 – Pre-reduction effect	1,2 wt% Ru/TiO <sub>2</sub> (Cl)	Pre-reduction after ketonization_1 on fresh	185,8
#1 – Pre-reduction effect	1,2 wt% Ru/TiO <sub>2</sub> (Cl)	Pre-reduction after ketonization_3	185,8
#1 – Pre-reduction effect	1,2 wt% Ru/TiO <sub>2</sub> (Cl)	Pre-reduction after ketonization_3	185,8
#1 – Ru addition effect	1,2 wt% Ru/TiO <sub>2</sub> (Cl)	Pre-reduction on fresh	300
#2 – Ru addition effect	1,2 wt% Ru/TiO <sub>2</sub> (Cl)	Pre-reduction after ketonization_1	185,8
#2 – Ru addition effect	TiO <sub>2</sub>	Pre-reduction	300,3
#2 – Ru addition effect	TiO <sub>2</sub>	Pre-reduction on fresh	TiO <sub>2</sub>
#3 – Precursor effect	1,2 wt% Ru/TiO <sub>2</sub> (Ni)	Pre-reduction on fresh	305,8
#3 – Precursor effect	1,2 wt% Ru/TiO <sub>2</sub> (Cl)	Pre-reduction after ketonization_1	185,8
#3 – Precursor effect	1,2 wt% Ru/TiO <sub>2</sub> (Cl)	Pre-reduction on fresh	300

Table 4.2 – Reactors' conditions summary for ketonization tests

All the experiments presented were made in such a way that the maximum conversion achieved was around 50%. In this way the presence of side reactions was reduced, and catalyst stability was preserved.

All experiments condition are reported in the corresponding section of chapter 2; standard test conditions were:

- GHSV: 20000 NL/h/kg<sub>cat</sub>;
- Feed composition: 3% Acetic acid, 10% N<sub>2</sub> in He

The results of catalytic experiments will be now presented; in particular, effect of pre-reduction, Ru addition and Ru precursor were investigated.

#### 4.2.1. Pre-reduction effect

As previously said in paragraph 2.3.5, the standard procedure for TiO<sub>2</sub> activation involved a reduction pre-treatment in pure H<sub>2</sub> up to 400°C, in line with the literature indications; in fact, Pham et al. in [19], propose a reduction pre-treatment on TiO<sub>2</sub> catalyst to increase the effectiveness of ketonization. This may be explained by the surface reduction by H<sub>2</sub> leading to the formation of Ti<sup>3+</sup> ions that highly enhance the ketonization due to an easier formation of the β-keto acid. Moreover, tests reported in Paragraph 3.2 demonstrated that hydrogen is the key element in removing impurities present on the catalyst (e.g. sulphur is removed in the form of H<sub>2</sub>S). This is further confirmed by the works of Tosoni et al. [19][20], who did a more thorough research on the topic.

Results are reported in Figure 4.7 and Figure 4.8 in terms of conversion, C-balance and outlet molar fraction of products over temperature. For the sake of clarity, “TiO<sub>2</sub> fresh” refers to a non-pre-treated catalyst; “TiO<sub>2</sub> reduced” defines a fresh catalyst that had been reduced prior to the test, while “TiO<sub>2</sub> reduced after ket” means that a previous ketonization test was carried out and a subsequent reduction on the spent was performed. Same classification is adopted for the Ru/TiO<sub>2</sub> cases.

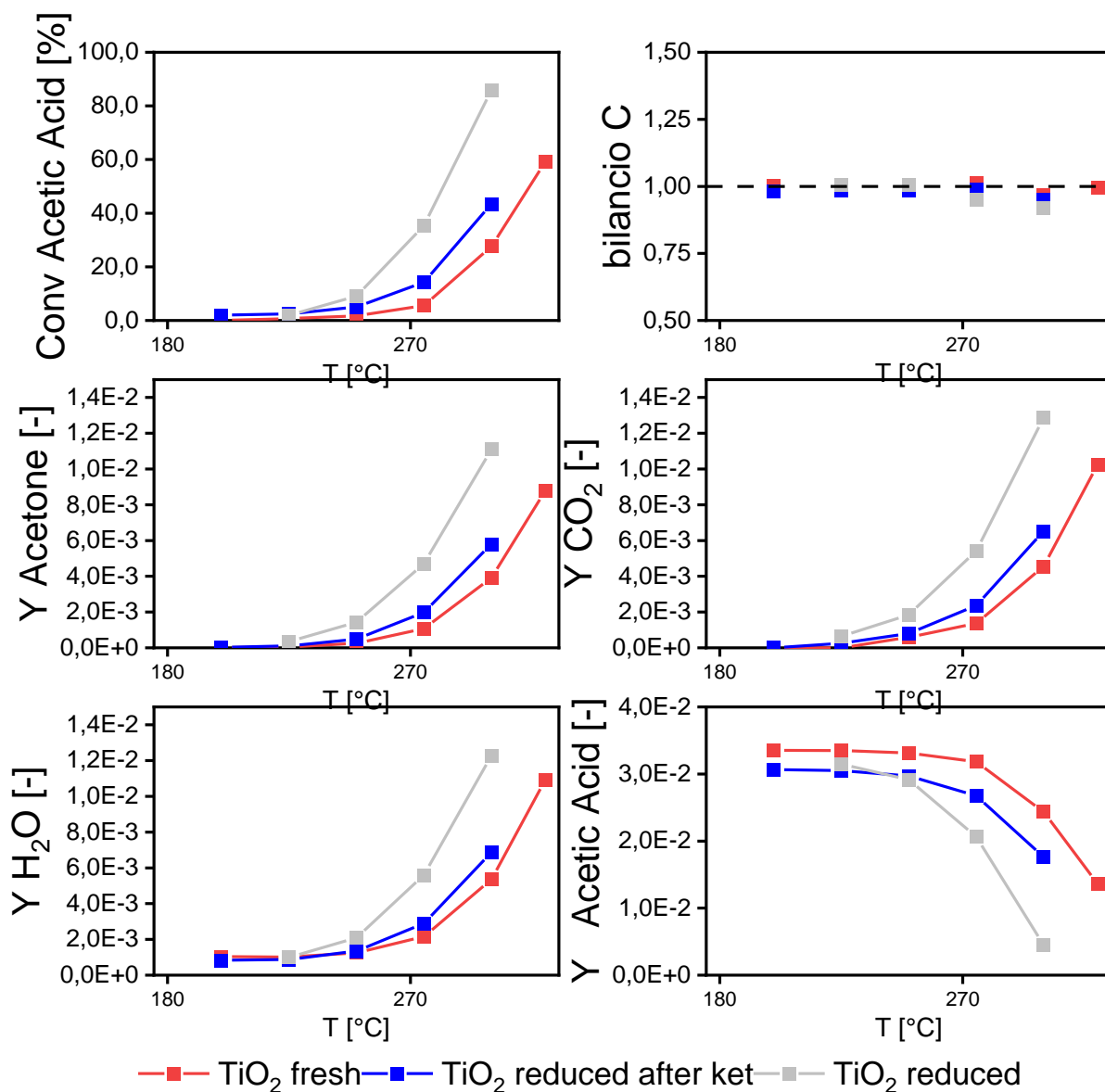


Figure 4.7 – Effect of H<sub>2</sub> pre-treatment on composition for TiO<sub>2</sub> oxidated, reduced after ketonization and reduced. GHSV: 20000 NL/h/kg<sub>cat</sub>; Flux: 3%Acetic acid, 10% N<sub>2</sub> in He

From the graph, it can be observed that the ketonization test over the TiO<sub>2</sub> fresh gives the lowest amount of products output and conversion; the best performing instead is the TiO<sub>2</sub> reduced in H<sub>2</sub> prior to the present ketonization test. An intermediate performance is obtained by reducing the catalyst after the first ketonization test (TiO<sub>2</sub> reduced after ket).

Also based on the characterization results, it is believed that the H<sub>2</sub>-prereduction allowed not only to expose Ti<sup>3+</sup> sites, but it also favored the complete removal of S-species more efficiently than the simple sequence of ketonization tests, as the lower performance of TiO<sub>2\_reduced\_after\_ket</sub> could have possibly been hindered by C-deposition during the ketonization test, not allowing H<sub>2</sub> to effectively reach S-species during reduction.

Figure 4.8 is instead focused on 1,2% Ru/TiO<sub>2</sub> from a RuCl<sub>3</sub> precursor. All tests except Ru/TiO<sub>2</sub>\_reduced were conducted on the same reactor, meaning that it was exposed to multiple subsequent reduction and ketonization tests.

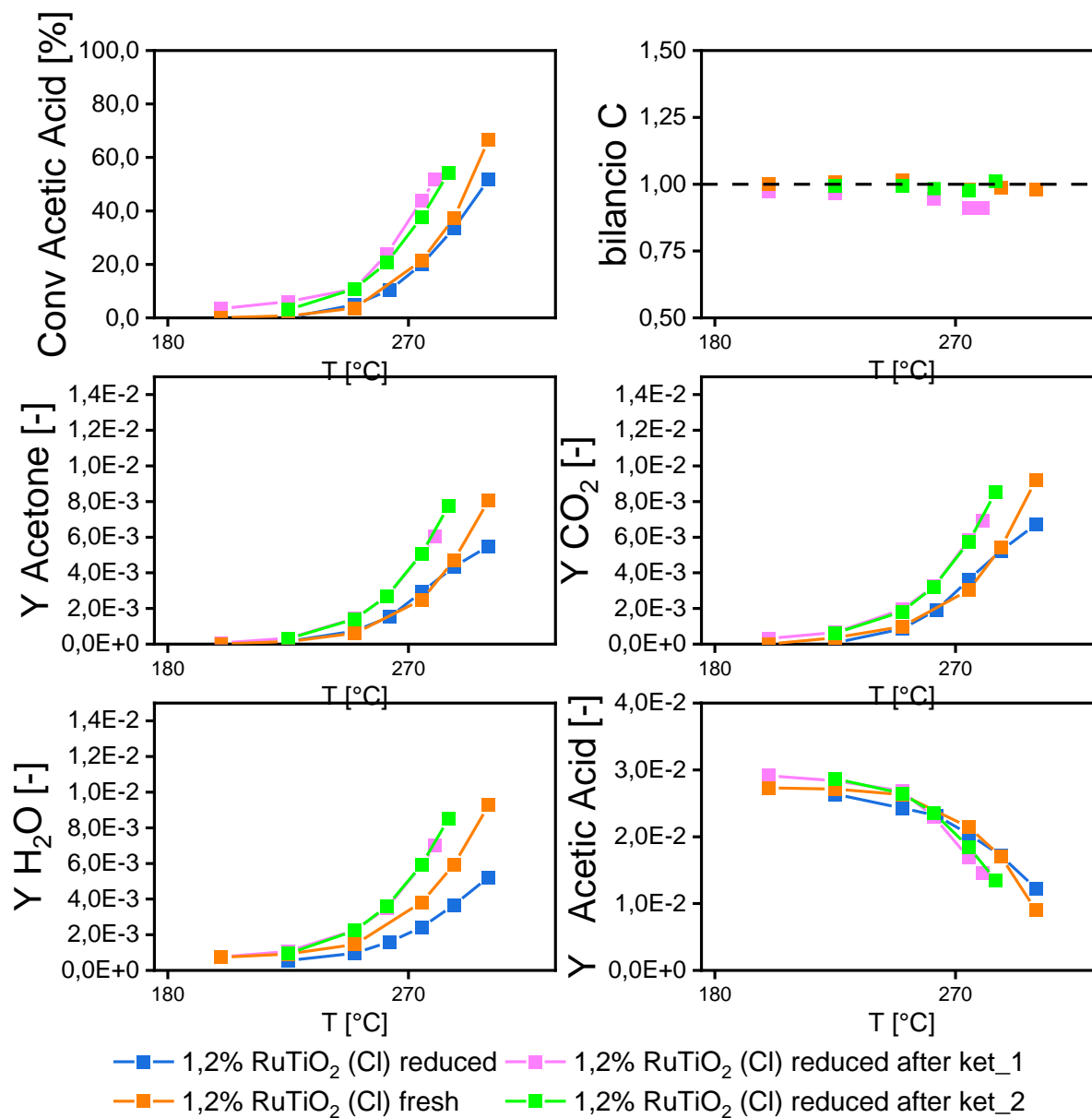


Figure 4.8 - Effect of H<sub>2</sub> pre-treatment on composition for 1,2% Ru/TiO<sub>2</sub> oxidated, reduced after ketonization and reduced. GHSV: 20000 NL/h/kg<sub>cat</sub>; Flux: 3%Acetic acid, 10% N<sub>2</sub> in He

Over this catalyst, the fresh unreduced sample shows the lowest activity, comparable the one obtained after H<sub>2</sub> pretreatment on fresh. Instead, improvements were observed by introducing H<sub>2</sub> treatments in between successive ketonization tests. Indeed, products and conversion increase when hydrogen is added before the experiment: every “reduced” curve is shifted upwards respect to the “fresh” ones. Moreover, a similar positive effect was observed also on TiO<sub>2</sub>.

However, since the promotion of conversion was very important, we cannot exclude that other factors were involved. In particular, it is believed that the series of tests and H<sub>2</sub> reduction contributed to the complete elimination of Cl, from RuCl<sub>3</sub> impregnation. The elimination of Cl is known to be difficult and the calcination treatment up to 400°C might have been insufficient to eliminate it from the catalytic powders (hence, the Ru/TiO<sub>2\_reduced</sub> had poor performance). On the contrary, it is known that H<sub>2</sub>O promotes Cl elimination by forming HCl; since H<sub>2</sub>O is a product of the acetic acid ketonization reaction, it is believed that the first ketonization test (performed on the fresh catalyst) contributed to "wash" Cl from the surface.

Notably the repetition of the ketonization experiments showed that the performance of Ru/TiO<sub>2</sub> was stable.

It is thus concluded that optimal catalytic performances are obtained on:

- TiO<sub>2</sub> after pre-reduction on fresh (6000 NL/h/kg<sub>cat</sub> in pure H<sub>2</sub>, with a T-ramp of 10°C/min at 400°C, 1 h hold and then cooldown at the same rate)
- Ru/TiO<sub>2</sub> after a sequence of ketonization and reduction tests (same condition as TiO<sub>2</sub>)

#### 4.2.2. Ru addition addition

From literature [21], it is known that metal oxides catalyst's doping is a common procedure to enhance the performance of the catalyst itself: the support may lack, from a quantitative point of view, certain properties that could be improved, and this is a possible solution as shown with for example Ce, Ti, Pt, Al, Fe... doping.

This means that Ru addition in fresh catalysts could help the ketonization process.

However, conflicting opinions emerge from the literature: in some cases, when Ru was added, no positive effects were found, as shown in the work by Wang et al.[13]; in this case, it was supposed that either reduced centres did not form during the treatment or that they did not play a role in the reaction. In other cases instead, the addition of ruthenium led to an increase of catalyst activity, as shown by Pham et al.[12], and Chen et al. [22]; for this ones, Ruthenium was chosen on the basis that it should have highly enhanced the creation of oxygen vacancies by promoting reverse oxygen spill-over from the lattice to the metal particle, so that ketonization was substantially improved.

In a previous thesis work [14], the investigation on the topic led instead to the experience of even worse conditions in the case of Ru addition, as products and conversion were lower respect to TiO<sub>2</sub>.

However, in this thesis the optimization of the pre-treatment has shown that Ru catalysts require a specific procedure to disclose the full performance.

Regarding this conclusion, TiO<sub>2</sub> and Ru/TiO<sub>2</sub> results previously obtained were then compared, as shown in Figure 4.9.

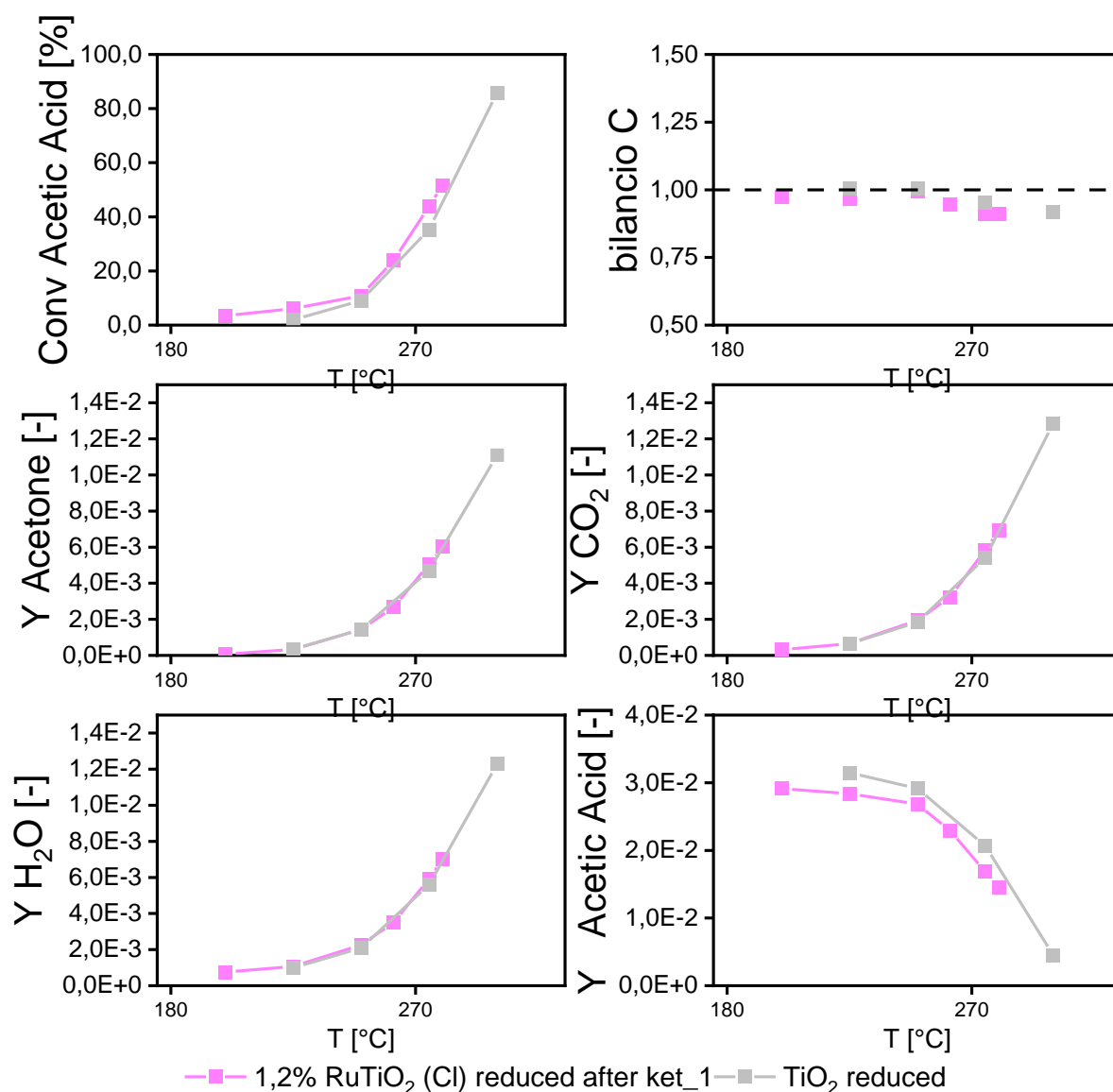


Figure 4.9 – Ru effect on reduced catalysts. GHSV: 20000 NL/h/kg<sub>cat</sub>; Flux: 3%Acetic acid, 10% N<sub>2</sub> in He

In this case the Ru/TiO<sub>2</sub> curve almost completely coincides with the TiO<sub>2</sub> one, with a smaller higher conversion on acetic acid.

The figure shows that that Ru addition in catalyst formulation did not significantly impact on acetic acid conversion (and hence to products evolution) when reduction was considered as pre-treatment.

Further investigation on this reported that the active sites for ketonization are acid-base Ti-O pairs, where the kinetically relevant step is the C-C coupling between an intermediate hydroxy enolate and an acid molecule co-adsorbed in a vicinal acid-base pair [13]. This suggested that maybe, the activating element for ketonization (TiO<sub>2</sub>) was not influenced by the metal addition, but only by its characteristics.

To test this this out, an additional on a different TiO<sub>2</sub> type (Fluka) was done, and it is reported in Figure 4.10

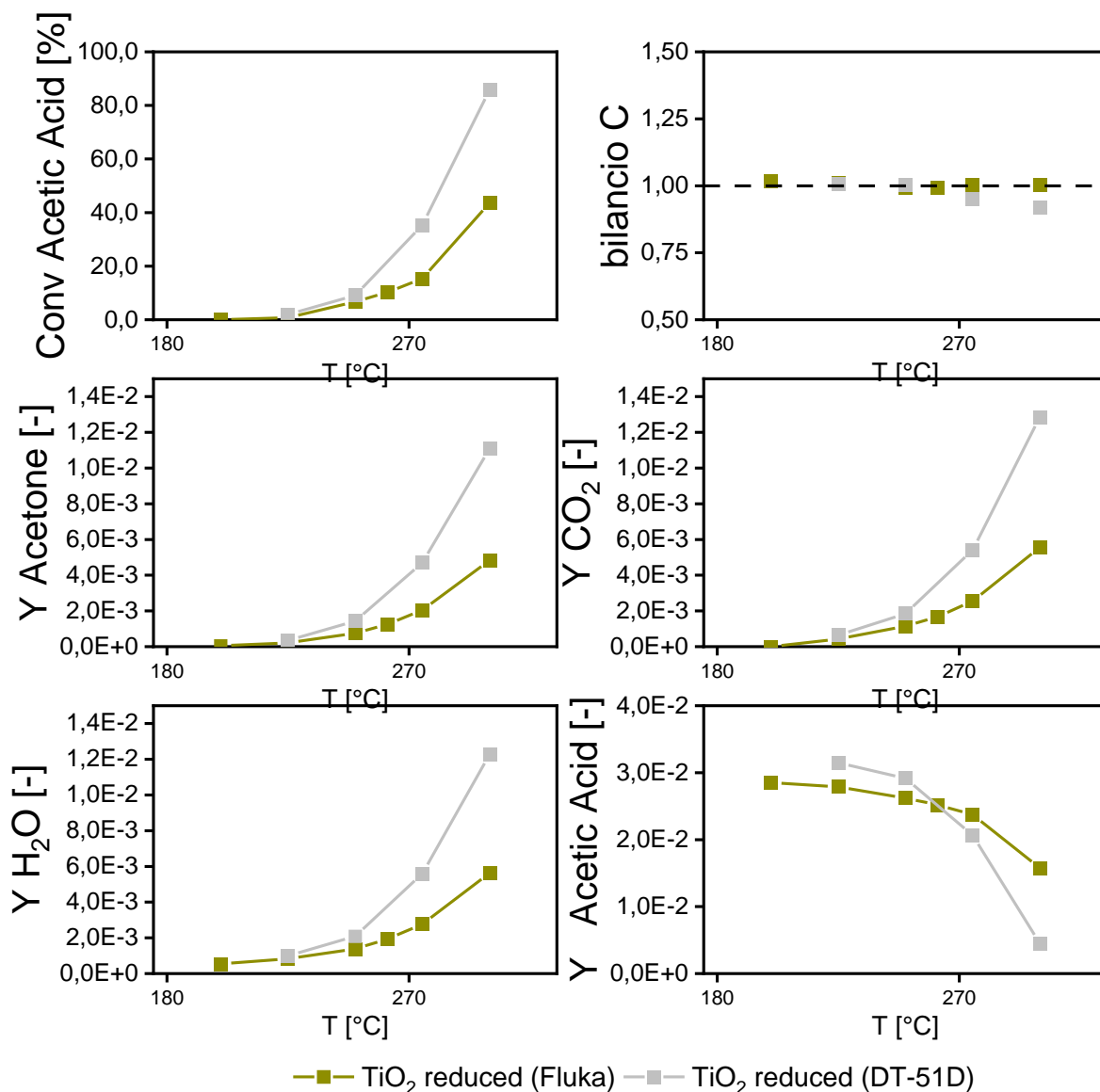


Figure 4.10 – Different TiO<sub>2</sub> (Fluka vs. DT-51D) activity on reduced catalysts. GHSV: 20000 NL/h/kg<sub>cat</sub>; Flux: 3%Acetic acid, 10% N<sub>2</sub> in He

In this case, even if both TiO<sub>2</sub> were pre-reduced, Fluka resulted less performing, as conversion and products substantially reduced. The reason for this is believed to be the different surface area between the two types: BET analyses revealed a 8 m<sup>2</sup>/g<sub>cat</sub> for Fluka, while DT-51D reported 80 m<sup>2</sup>/g<sub>cat</sub>. The factor of 10 difference could further explain that active sites are really on the TiO<sub>2</sub> itself.

From the results obtained, it is then concluded that the addition of the noble metal Ru did not impact on catalyst performance in activating ketonization reaction.

### 4.2.3. Ru precursor effect: Chloride vs Nitrate

Two different Ru precursor were utilized for catalyst preparation (Paragraph 2.2.3):  $\text{Ru}(\text{Cl})_3$  salt (named  $\text{Ru}/\text{TiO}_2(\text{Cl})$  in Table 4.2) and Ru nitrosyl nitrate (named  $\text{Ru}/\text{TiO}_2(\text{N})$  in Table 4.2). Even if Ru addition was already proved negligible for ketonization increase, it might be possible that other properties (e.g. stability) are improved at more severe conditions. For this, a comparison between the two precursors is needed. The behaviours of these two catalytic powders in low temperature ketonization are shown in Figure 4.11. It must be specified that  $\text{Ru}/\text{TiO}_2(\text{Cl})$  and  $\text{Ru}/\text{TiO}_2(\text{N})$  were both subjected to the same standard reduction pre-treatment (Paragraph 2.3.5).

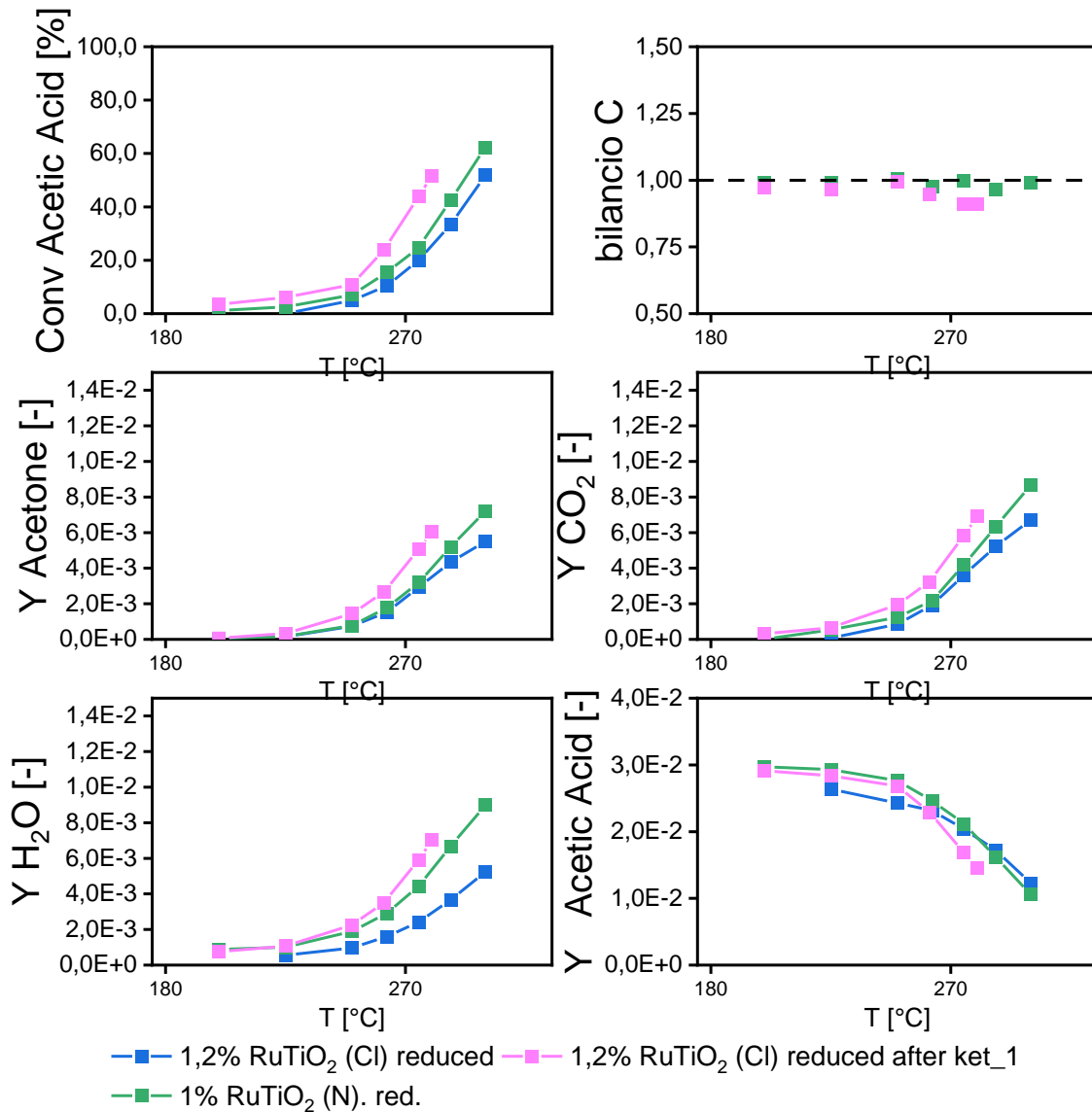


Figure 4.11 – Results comparison between  $\text{Ru}(\text{Cl})$  and  $\text{Ru}(\text{N})$ . GHSV: 20000 NL/h/kg<sub>cat</sub>; Flux: 3%Acetic acid, 10%  $\text{N}_2$  in He



As seen in Fig., the lowest values of acetic acid conversion and products molar fractions are obtained with pre-reduced Ru/TiO<sub>2</sub> (Cl); as already said, this is likely related to the Cl impurities remaining on the catalyst surface. Instead, when the correct pre-reduction procedure on Ru(Cl) is considered (Ru/TiO<sub>2</sub>\_reduced\_after\_ket), it is found that Ru(Cl) is better performing than Ru(N), as it reaches higher conversion values.

### 4.3. Acetic acid ketonization: high temperature analyses

As anticipated in the paragraph above, the last part of the experimental campaign was conducted in the high temperature region ( $T > 300^{\circ}\text{C}$ ).

In a previous thesis work [14], it was observed that carbon-balance to ketonization products (i.e., considering acetone and CO<sub>2</sub> only) declined above 275°C, and this indicates that ketonization alone could not explain high temperature conversion of acetic acid. Figure 4.12 shows Acetic acid conversion coupled with acetone flow rate and C-balance all respect to temperature increase.

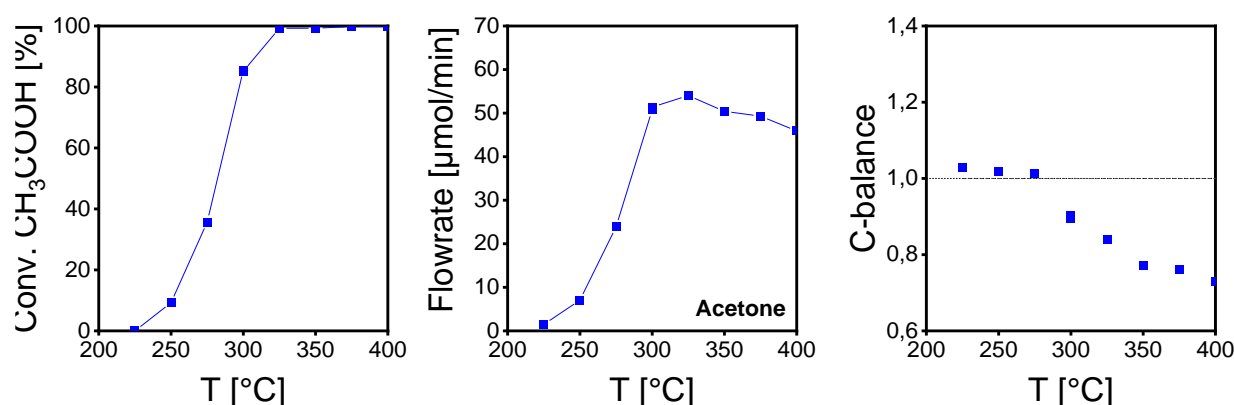


Figure 4.12 – C balance drop on ketonization at high temperature. GHSV = 20,000 NL/h/kg<sub>cat</sub> (total flowrate = 4470 μmol/min). Feed composition: CH<sub>3</sub>COOH=3%, N<sub>2</sub>=10% in He, H<sub>2</sub>=20% in He.

The reason for this was that, despite the registered conversion, not all products were correctly identified: even if ketonization was the dominant reaction for the entire T-range, secondary reactions were activated at sufficiently high temperature and other species were found among products. The complexity of outlet products' composition and the high number of species found required a better composition analysis.

For this purpose, the GC-MS introduced in paragraph 2.1.3 was used. During the tests, each analysis in the online GC-TCD was associated to a sampling of the same gas mixture with injection into the offline GC-MS almost at the same time (the only difference relying in the time required to reach the new instrument). GC-MS analysis were used for species identification and GC-TCD for species identification. After both analyses completed, a comparison of the two chromatograms was made, associating every major peak on the GC-TCD to the corresponding one on the GC-MS. It was

possible to assume that the same order of retention times was maintained for the two GC columns.

An example of the procedure can be seen in Figure 4.13:

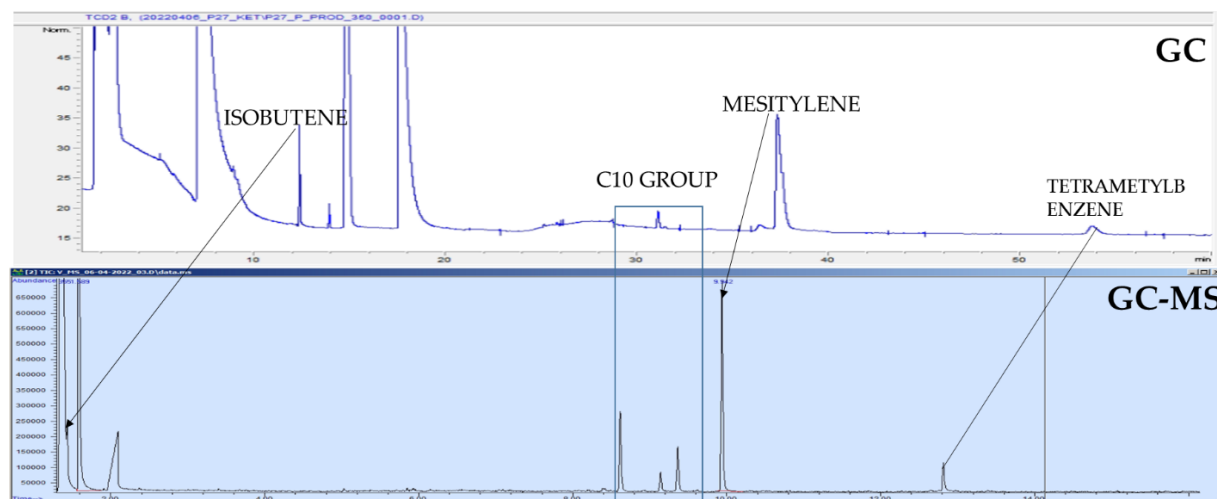


Figure 4.13 – Peak association between GC and GC-MS analyses

Although not all of them were identified because of the GC-MS sensitivity (only very small fractions of unknowns), the process allowed to recognize different type of C-species during the reaction at higher temperature, that are reported in Table 4.3, along with the ones already known:

New species summary			
SPECIE	Retention time [min]	Chemical formula	
Macro	0	$N_2+He+H_2+CH_4+CO$	
CO <sub>2</sub>	2,46	CO <sub>2</sub>	
H <sub>2</sub> O	6,86	H <sub>2</sub> O	
Propylene	8,85	C <sub>3</sub> H <sub>6</sub>	$\begin{array}{c} H & & H \\ & \backslash & / \\ & C=C \\ & / & \backslash \\ H & & CH_3 \end{array}$
Isobutene	12,35	C <sub>4</sub> H <sub>8</sub>	$\begin{array}{c} H_3C \\ & \backslash \\ & C=CH_2 \\ & / \\ H_3C \end{array}$

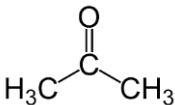
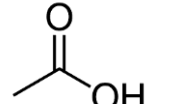
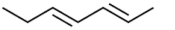
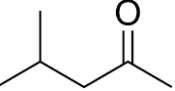
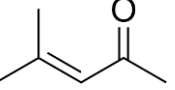
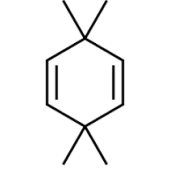
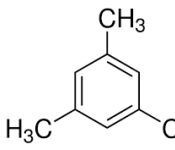
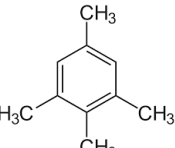
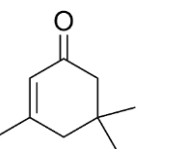
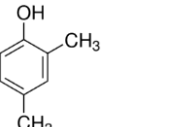
<b>Acetone</b>	14,35	$C_3H_6O$	
<b>CH<sub>3</sub>COOH</b>	17,43	$C_2H_4O_2$	
<b>C<sub>7</sub> group</b>	17-20	$C_7H_{12}$	
<b>Mesityl isobutyl ketone</b>	27,8	$C_6H_{12}O$	
<b>Mesityl oxide</b>	28,9	$C_6H_{10}O$	
<b>Cyclohexadiene Tetramethyl &amp; isomers</b>	30-->35,5	$C_{10}H_{16}$	
<b>Mesitylene</b>	37	$C_9H_{12}$	
<b>Tetramethyl Benzene</b>	53	$C_{10}H_{14}$	
<b>Isophorone</b>	56,71	$C_9H_{14}O$	
<b>Dimethylphenol</b>	64	$C_8H_{10}O$	

Table 4.3 – New species recognized with GC/GC-MS coupling

All prepared reactors were subjected to prolonged ketonization for a total of 4.5h each at fixed temperature. Acetic acid conversion and products molar fractions were monitored at increasing Time on Stream (ToS).

Tests performed are reported here in Table 4.4.

Set of data	Catalyst	Mass [mg]	Feed composition	T [°C]
#1 – T effect	TiO <sub>2</sub>	200,2	66 Nml/min of 3% Acetic acid, 10% N <sub>2</sub> in He	300
	TiO <sub>2</sub>	200,7	66 Nml/min of 3% Acetic acid, 10% N <sub>2</sub> in He	350
	TiO <sub>2</sub>	200,7	66 Nml/min of 3% Acetic acid, 10% N <sub>2</sub> in He	400
#2 – H <sub>2</sub> effect	TiO <sub>2</sub>	200	66 Nml/min of 3% Acetic acid, 20%H <sub>2</sub> , 10% N <sub>2</sub> in He	300
	TiO <sub>2</sub>	200,1	66 Nml/min of 3% Acetic acid, 20%H <sub>2</sub> , 10% N <sub>2</sub> in He	400
#3 – Ru effect	3 wt% Ru/TiO <sub>2</sub> (Cl)	199	66 Nml/min of 3% Acetic acid, 20%H <sub>2</sub> , 10% N <sub>2</sub> in He	400
	TiO <sub>2</sub>	200,1	100 Nml/min of 3% Acetic acid, 20%H <sub>2</sub> , 10% N <sub>2</sub> in He	400
	3 wt% Ru/TiO <sub>2</sub> (Cl)	200,3	100 Nml/min of 3% Acetic acid, 20%H <sub>2</sub> , 10% N <sub>2</sub> in He	400

Table 4.4 – Reactors tested with prolonged ketonization

### 4.3.1. Temperature effect

The first thing that was investigated was the temperature effect. A set of three different testing temperature was chosen:

1. 300°C: maximum temperature at which the low region tests were stopped to avoid losing selectivity to ketonization
2. 400°C: maximum temperature that the catalyst could withstand, as it was the one used for the calcination procedure
3. 350°C: intermediate temperature between the two

Results are reported in Figure 4.14 in terms of molar fraction of products, conversion and C-balance, plotted against time on stream. Ketonization analyses were carried out on three different TiO<sub>2</sub> reactors, after a standard reduction pre-treatment.

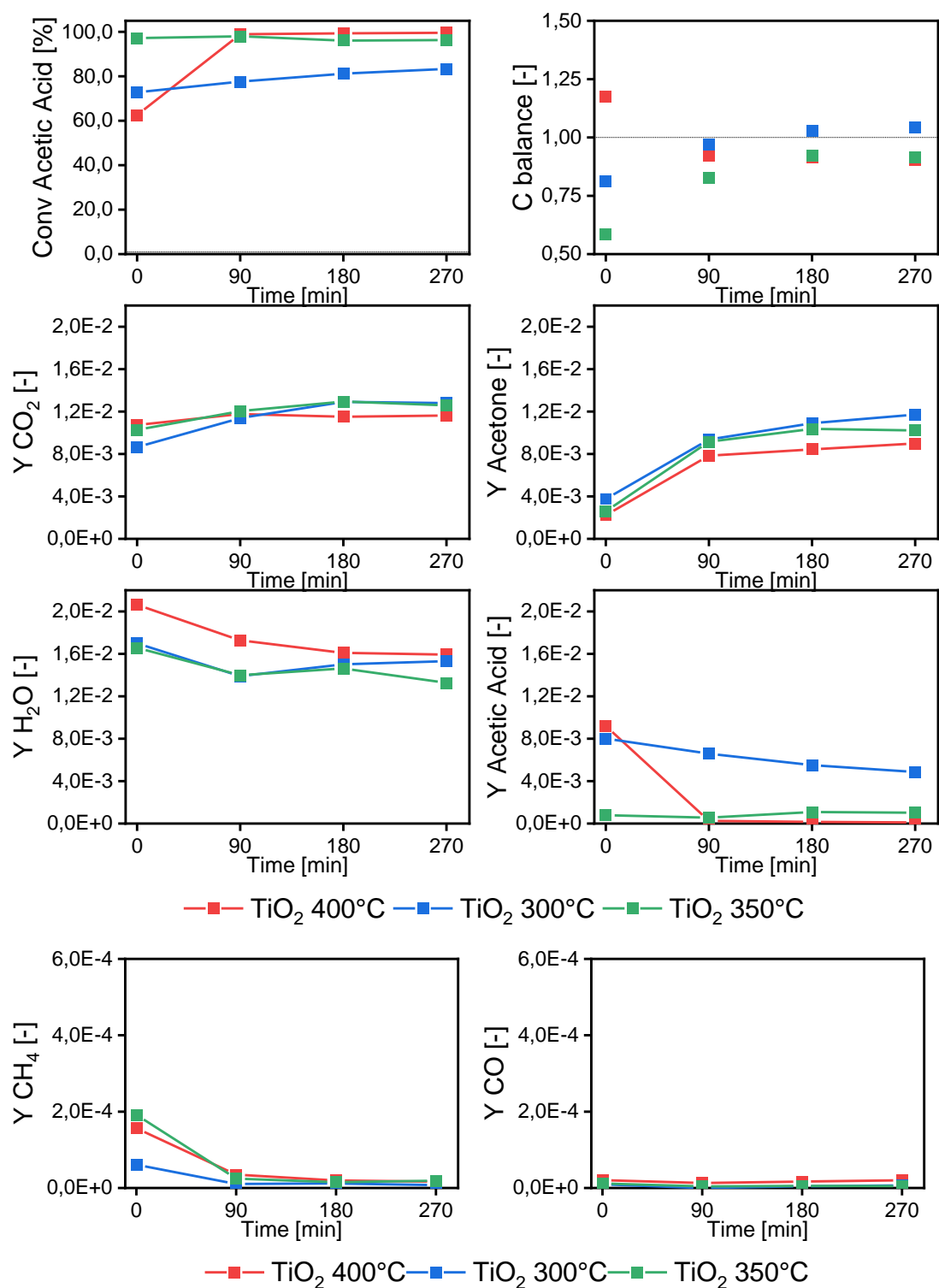


Figure 4.14 – Effect of temperature on conversion, C-balance and molar fraction of ketonization reaction products. GHSV: 20000 NI/h/kg<sub>cat</sub>; Flux: 3% Acetic acid, 10% N<sub>2</sub> in He

Starting from the main products, Acetone, and  $\text{CO}_2$  have the same increasing trend in time, while  $\text{H}_2\text{O}$  stabilizes after an initial decrease; moreover, their order of magnitude is the same (although acetone is a bit smaller in quantity, and the opposite happens for  $\text{H}_2\text{O}$ ), confirming the stoichiometry of the ketonization process for acetic acid. Conversion instead appears to be complete at  $350^\circ\text{C}$  and  $400^\circ\text{C}$ , while for  $300^\circ\text{C}$  it increases but remains below total.

Along with the main ketonization products, additional components were found in the outlet mixture composition, and they are reported in Figure 4.15:

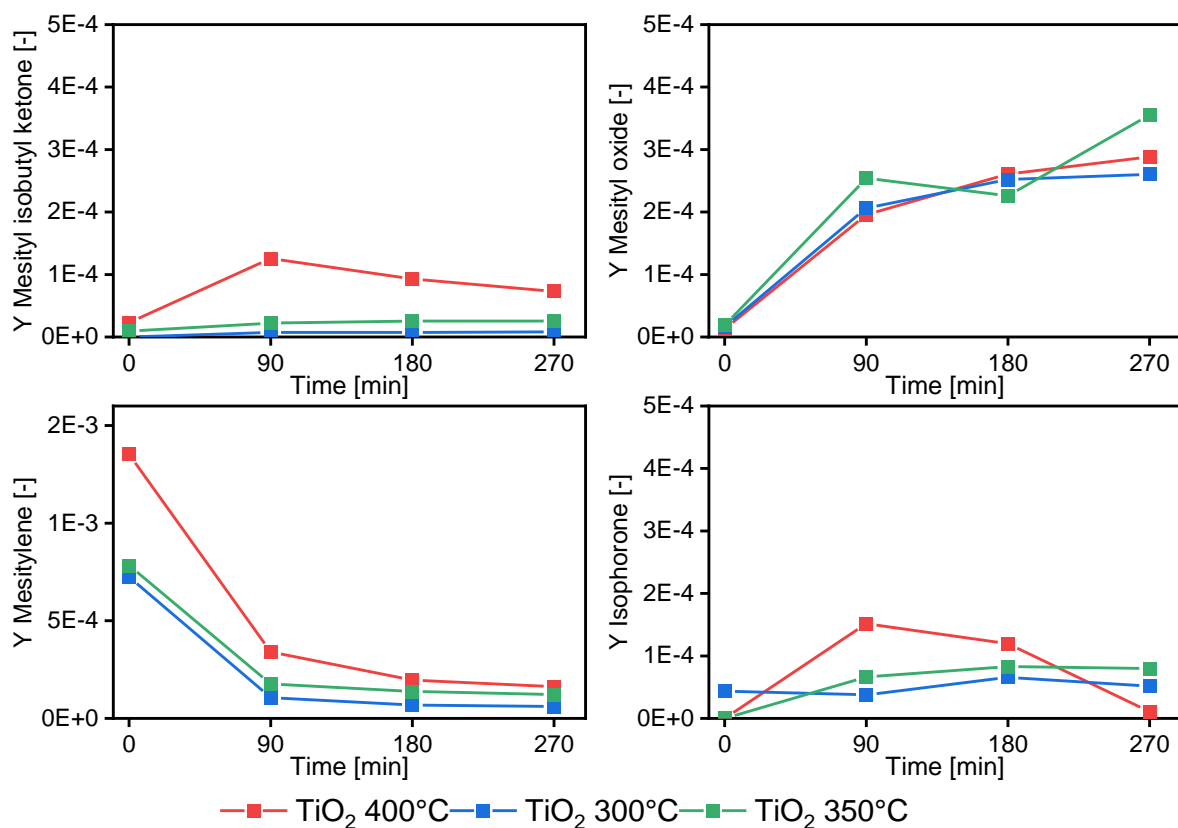


Figure 4.15 – Effect of temperature on condensation products. GHSV: 20000  $\text{NI}/\text{h}/\text{kg}_{\text{cat}}$ ; Flux: 3% Acetic acid, 10%  $\text{N}_2$  in He

Regarding the products, it is immediate to notice that mesitylene is the biggest among them, following a decreasing trend like  $\text{C}_7$ ,  $\text{C}_{10}$  (Cyclo. and Tetramethyl.), isobutene and propylene. Instead, both the  $\text{C}_6$  (mesi ox. and mesi-but-ket.) report an increasing trend in time.

Regarding the trends, the discovery is quite interesting: if we consider the reaction mechanisms, we have to remember that after acetic acid has converted into acetone,

the latter goes through a process of aldol condensation to form higher C-chained elements, as shown in Figure 4.16.

### Consecutive self and cross condensation reactions of acetone

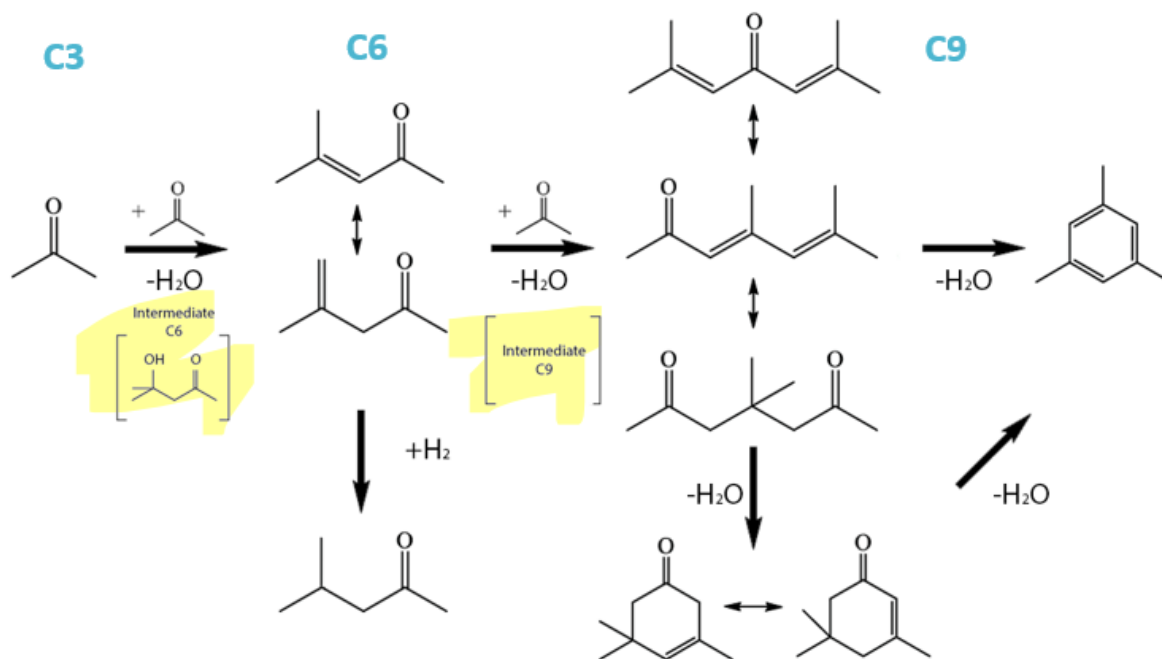


Figure 4.16 – Condensation reactions of acetone

From the Fig. it is explained how two acetone molecules react to form an intermediate C<sub>6</sub> (mesityl isobutyl ketone and mesityl oxide) and a molecule of water. A subsequent reaction of this intermediate C<sub>6</sub> with another acetone molecule forms a C<sub>9</sub> and again a molecule of water. If another water molecule is extracted, the compound transforms from a linear C<sub>9</sub> into a cyclic one (mesitylene and isophorone). This is a very important discovery, as this longer C-chain species are all very good for increasing both biofuels and chemicals properties: blending and other processes becomes very interesting from this point of view.

However, condensation products were not the only other ones found, as propylene, isobutene, C<sub>7</sub>, Cyclohexadiene tetramethyl (and isomers), tetramethyl benzene and dimethylphenol were detected. Figure 4.17 reports those species over time on stream:

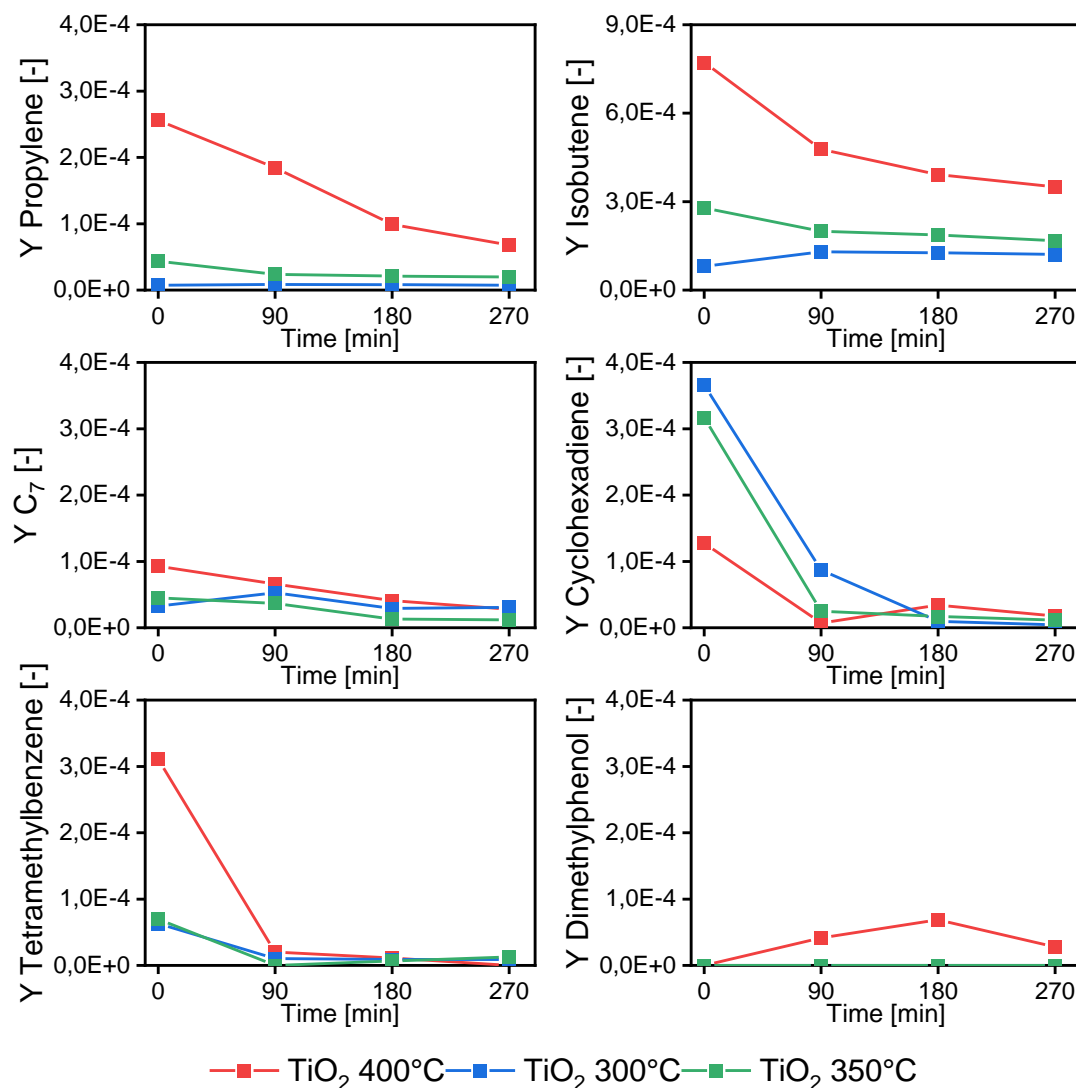


Figure 4.17 – Effect of temperature on olefinic and other products. GHSV: 20000 NI/h/kg<sub>cat</sub>;  
Flux: 3% Acetic acid, 10% N<sub>2</sub> in He

From the analyses, it can be observed that all products found besides dimethylphenol decrease over time, and increasing temperature leads to higher amounts of the same product at the corresponding time.



The origin of all these secondary products comes from other reactions such as the cracking of the bigger condensated products, that also formed intermediate components. The pathway reactions are reported in Figure 4.18.

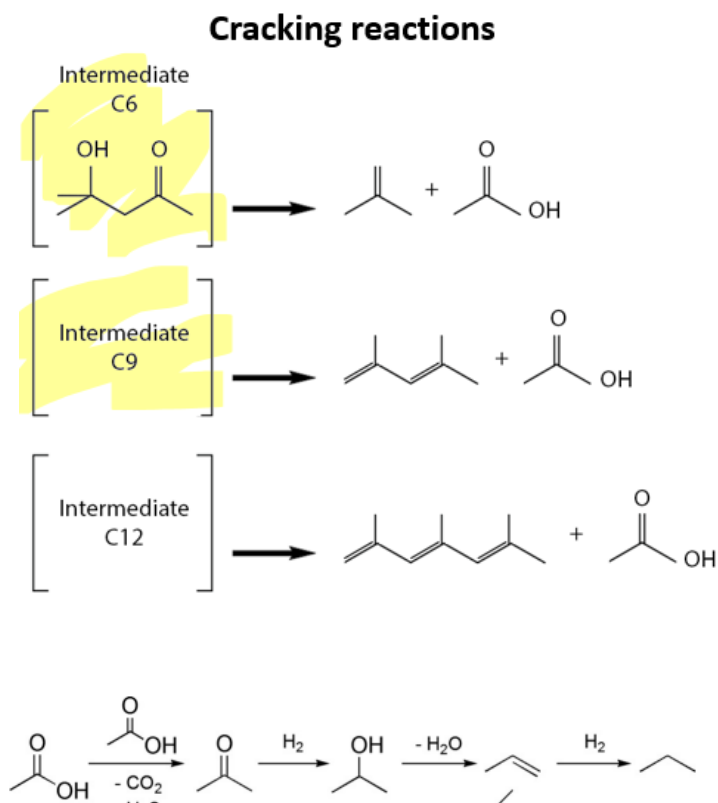


Figure 4.18 – Other secondary reactions of intermediate products

In the Fig., it is shown how from an intermediate component, a cracked species plus an acetic acid molecule is always produced; for C<sub>6</sub> isobutene and acetic acid are formed; from the C<sub>9</sub> instead, a linear C<sub>7</sub> and acetic acid are produced; lastly, from an intermediate C<sub>12</sub>, a linear C<sub>9</sub> and acetic acid are formed. Keto-hydro-deoxygenation (KHDO) is instead believed to be responsible for the propylene production.

The discovery of these reaction has both positive and negative effects; the acetic acid production means that we are partially hindering the conversion of oxygenates into heavier and better C-species (acetic acid converts into acetone, then into intermediates, but at this point it is produced again); however, good products are also being produced, because linear C<sub>7</sub> and C<sub>9</sub> emerge, with also the production of isobutene and propylene.

The identification of the reaction pathways was based on the product distribution observed at the very start of the experiments. However, the production of condensation or cracking species decreases over time, indicating that catalyst behavior is not stable: thus at the beginning the acetone molar fraction is much lower than CO<sub>2</sub>, because of the important contribution of consecutive reactions, but with time, the

acetone content increases. With the increase of ToS, also the  $C_6$  species from acetone condensation increase while  $C_9$  and cracked products ( $C_7$ ,  $C_{10}$ ,  $C_4$ ,  $C_3$ ) collapse abruptly, possibly indicating that the pathways leading to further C-length increase is hindered.

Another important contribution in understanding the reactions' evolution is given by plot of carbon selectivity at increasing temperatures, reported below in Figure 4.19, Figure 4.20 and Figure 4.21 for the three cases considered.

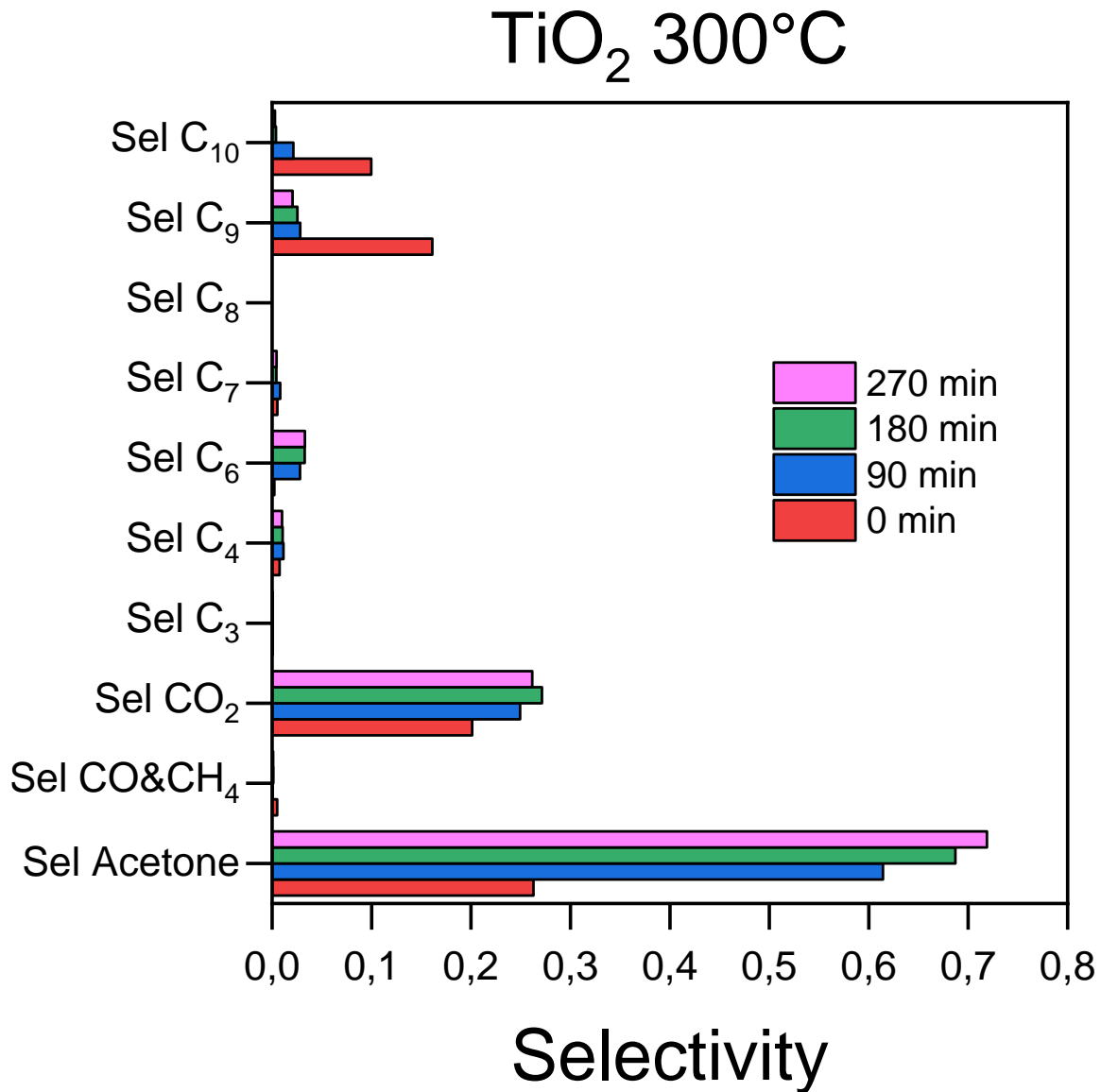


Figure 4.19 - C-selectivity of  $C_i$  products at 300°C over time

The Fig. shows that Acetone selectivity grows from a mere 25% to 72% over time, followed by  $CO_2$  (20 to 25%) and  $C_6$  (3 to 5%); instead, heavier products like  $C_9$  and  $C_{10}$  experience an opposite behaviour, as their selectivity goes from 20% down almost zero; other species like  $C_7$  and  $C_4$  seems to remain almost stable.

This shows more clearly how the reaction pathways that lead to higher C-length elements are hindered over time, as the selectivity of acetone starts low and highly increases after the first analysis, at the expense of the heavier ones that decrease.

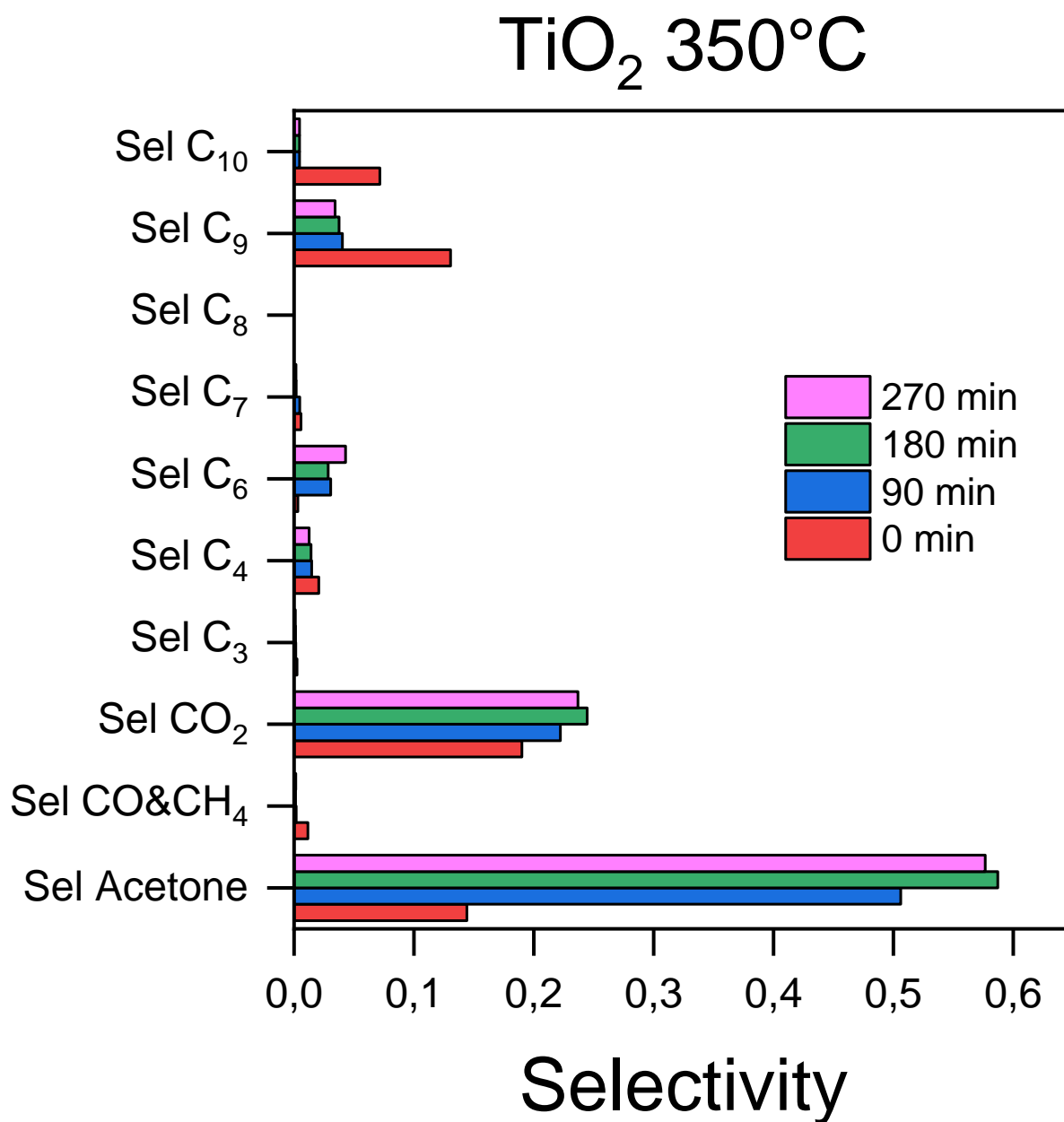


Figure 4.20 - C-selectivity of C<sub>i</sub> products at 350°C over time

The Fig. shows the same trends obtained at 300°C, obtaining the same conclusion as before.

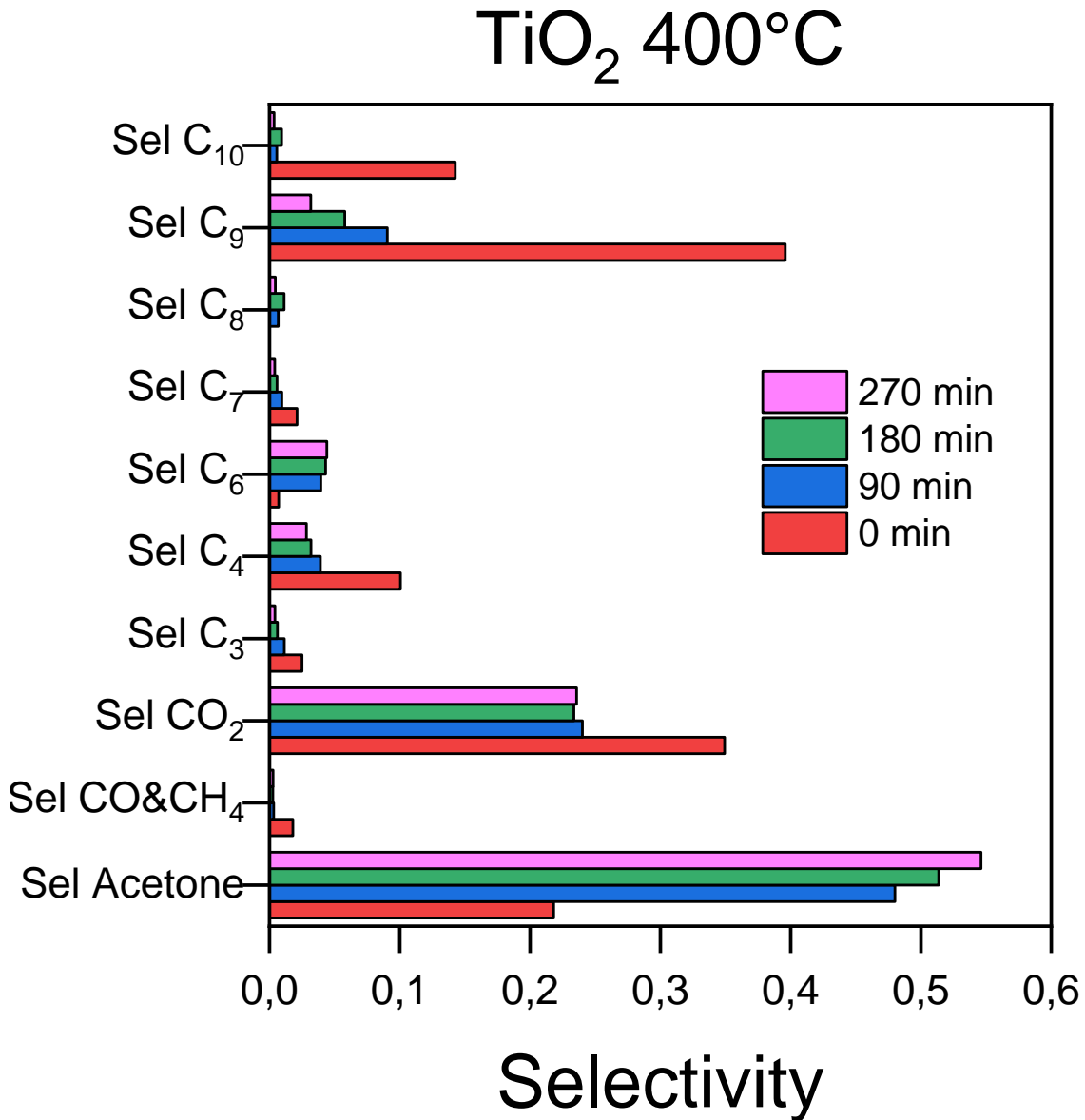


Figure 4.21 – C-selectivity of C<sub>i</sub> products at 400°C over time

Also in this case, a similar trend is obtained; however, initial selectivity of heavier products is much higher, reaching an overall amount of 66,3% in the first analysis, that is quite impressive. However, a more marked reduction is experienced, as for example mesitylene drops from 39% to just 3% after 4.5h, while C<sub>10</sub> goes from 14% to almost zero.

Concerning the effect of temperature, dynamics were more pronounced consistently increasing reaction rates and increasing deactivation rates. At increasing temperature, higher conversion for all the products are observed at the start, however products are subject to a more rapid blockage: for example, the productivity of mesitylene found at 400°C is much higher than the that at 300°C in the first analysis, but after 90 minutes the amount found in the product mixture at 400°C is lower than the one found at 300°C.

### 4.3.2. H<sub>2</sub> co-feed effect

The second effect investigated was the presence of H<sub>2</sub> cofeed during the reaction; in particular, a 20% H<sub>2</sub> flux was considered, while all other conditions were kept the same as before.

Figure 4.22 and Figure 4.23 reports the results obtained for the tests done at 300°C:

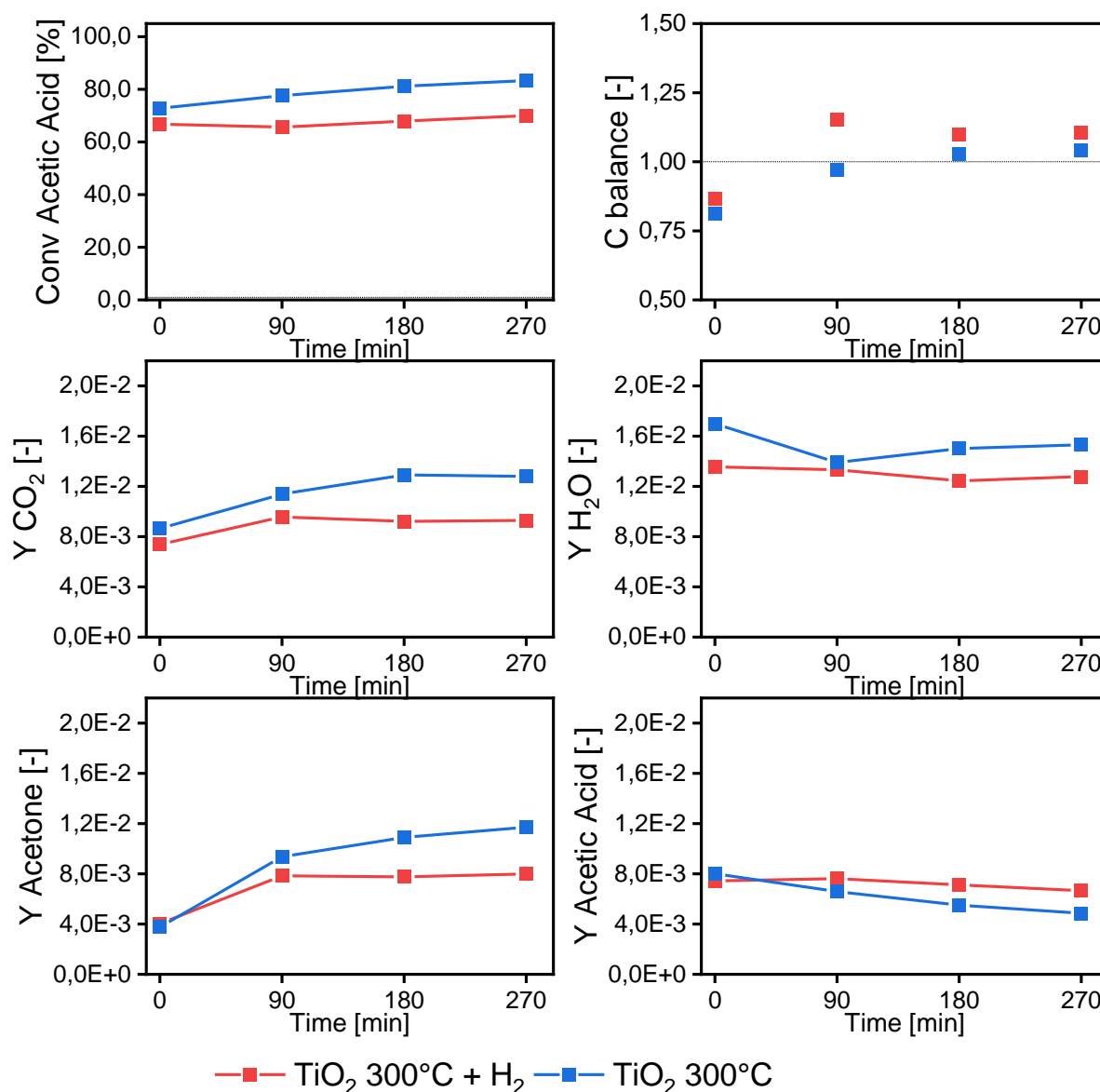


Figure 4.22 – H<sub>2</sub> effect at 300°C on main products composition. GHSV: 20000 NI/h/kg<sub>cat</sub>; Flux: 3% Acetic acid, 20% H<sub>2</sub> (if co-fed), 10% N<sub>2</sub> in He (Part 1)

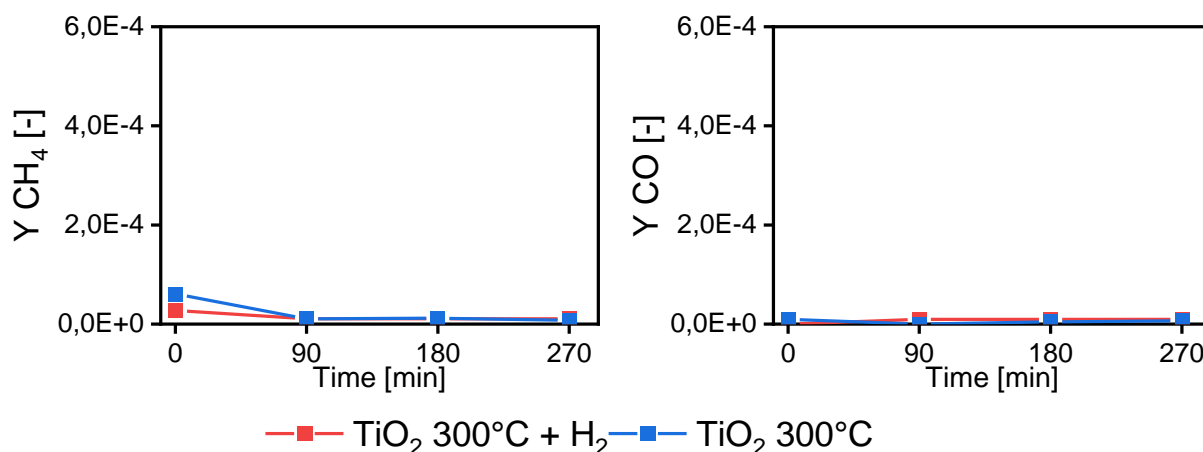


Figure 4.23 - H<sub>2</sub> effect at 300°C on cracking products composition. GHSV: 20000 NI/h/kg<sub>cat</sub>;  
Flux: 3% Acetic acid, 20% H<sub>2</sub> (if co-fed), 10% N<sub>2</sub> in He (Part 2)

In this case what can be seen by the graphs is that conversion is lower when H<sub>2</sub> is co-fed; same conclusion can be said for the products like for example acetone, CO<sub>2</sub>, H<sub>2</sub>O (as conversion is lower, it is expected) but they also seem to remain more constant with time respect to the TiO<sub>2</sub> only case. This behavior can be tentatively associated with a competitive adsorption of H<sub>2</sub> on the catalyst surface that reduces the number of active sites.

As for the condensate products, they are shown in Figure 4.24:

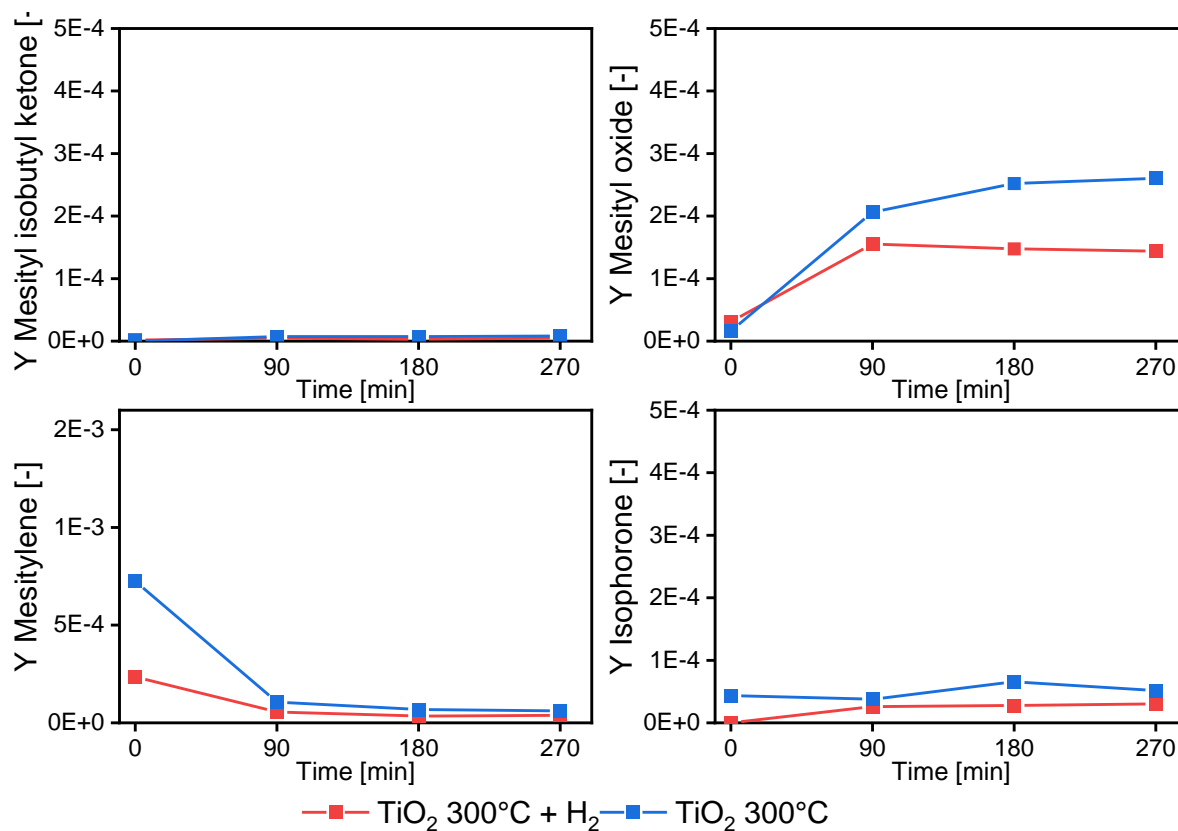


Figure 4.24 - H<sub>2</sub> effect at 300°C on condensate products composition. GHSV: 20000 NI/h/kg<sub>cat</sub>;  
Flux: 3% Acetic acid, 20% H<sub>2</sub> (if co-fed), 10% N<sub>2</sub> in He

Consistently with the decrease of acetone content, also the production of longer chain compounds decrease.

Lastly, olefins and other products are reported in Figure 4.25.

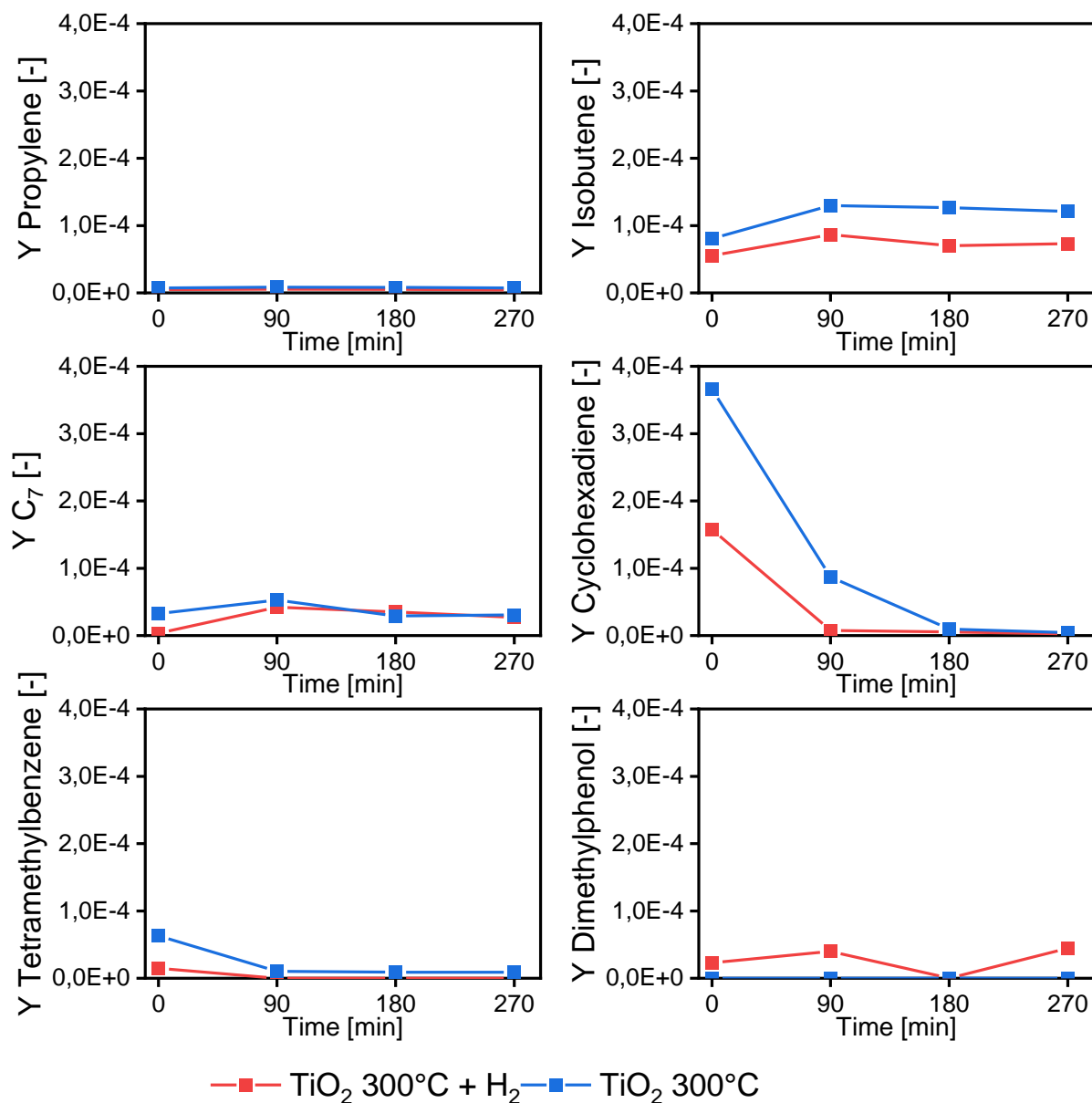


Figure 4.25 - H<sub>2</sub> effect at 300°C on other products composition. GHSV: 20000 NI/h/kg<sub>cat</sub>; Flux: 3% Acetic acid, 20% H<sub>2</sub> (if co-fed), 10% N<sub>2</sub> in He

Also in these cases, a decrease of productivity was observed for each species. Which confirms the consecutive nature of such products with respect to acetone.

In conclusion, it can be observed that globally H<sub>2</sub> co-feed at 300°C lowers the activity.

The effect of H<sub>2</sub> co-feed was analyzed also at 400°C, as shown in Figure 4.26 and Figure 4.27 in the same scheme as before:

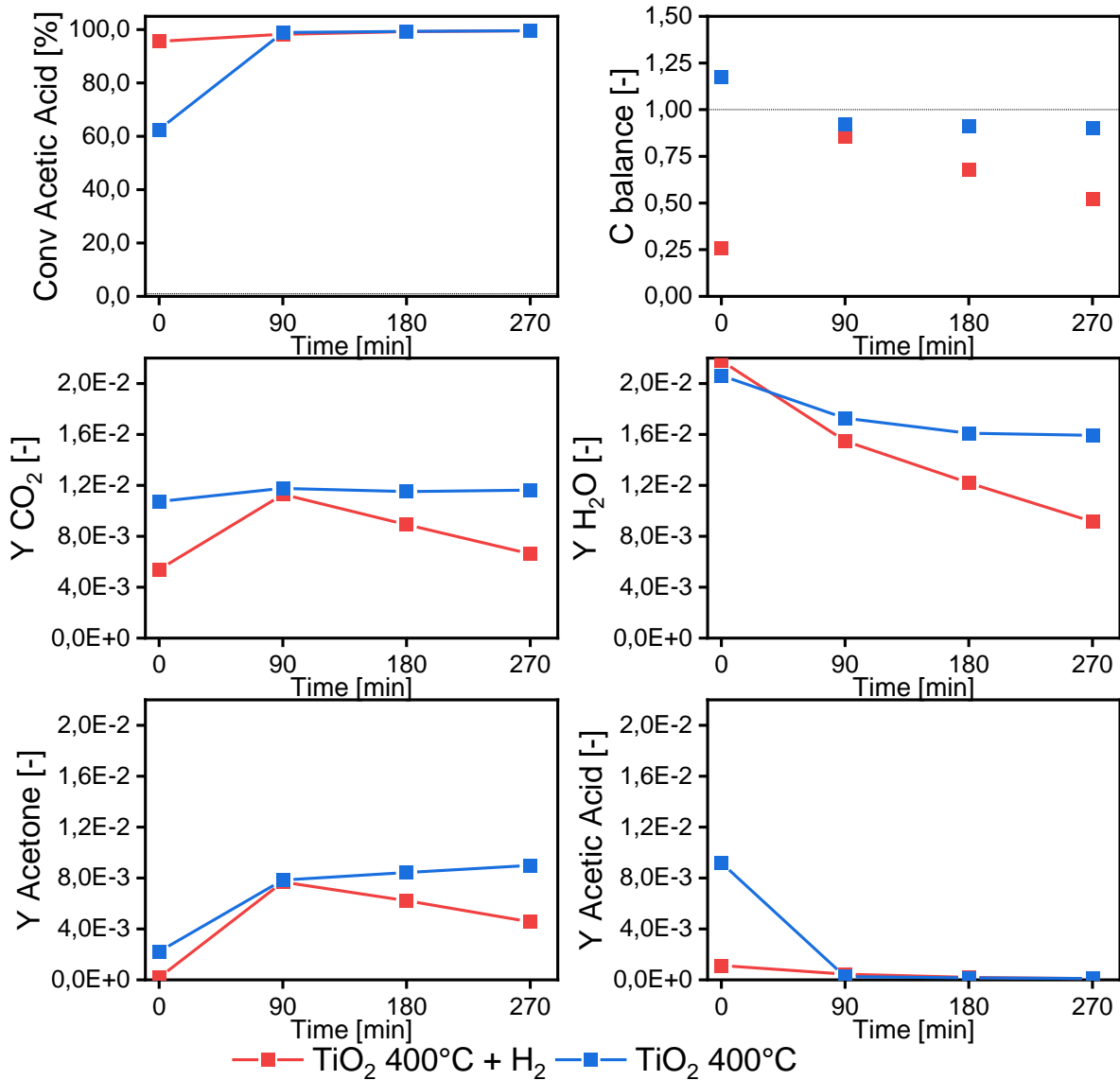


Figure 4.26 - H<sub>2</sub> effect at 400°C on main products composition. GHSV: 20000 NI/h/kg<sub>cat</sub>; Flux: 3% Acetic acid, 20% H<sub>2</sub> (if co-fed), 10% N<sub>2</sub> in He

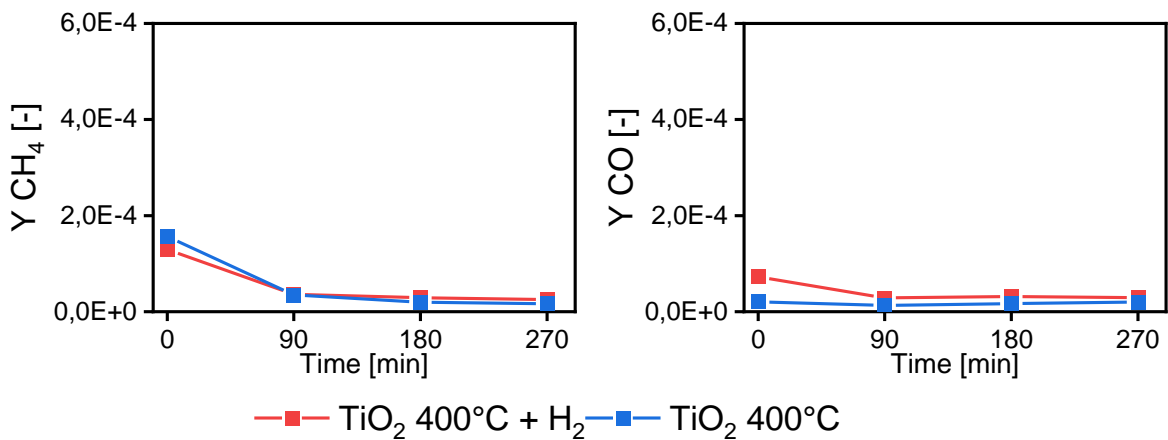


Figure 4.27 - H<sub>2</sub> effect at 400°C on main products composition. GHSV: 20000 NI/h/kg<sub>cat</sub>; Flux: 3% Acetic acid, 20% H<sub>2</sub> (if co-fed), 10% N<sub>2</sub> in He (Part 2)



The conversion of acetic acid was higher with H<sub>2</sub>-cofed at the very start of the experiment; however the initial C-balance was very poor, which suggests the importance of adsorption/desorption slow dynamics that might be involved in the “storage” of the reactant in the reactor volume.

At 90 minutes, the C-balance of the experiment was settled, but then it decays progressively likely due to the onset of deactivation phenomena that might explain the general decline of the productivity.

Condensation products are reported in Figure 4.28.

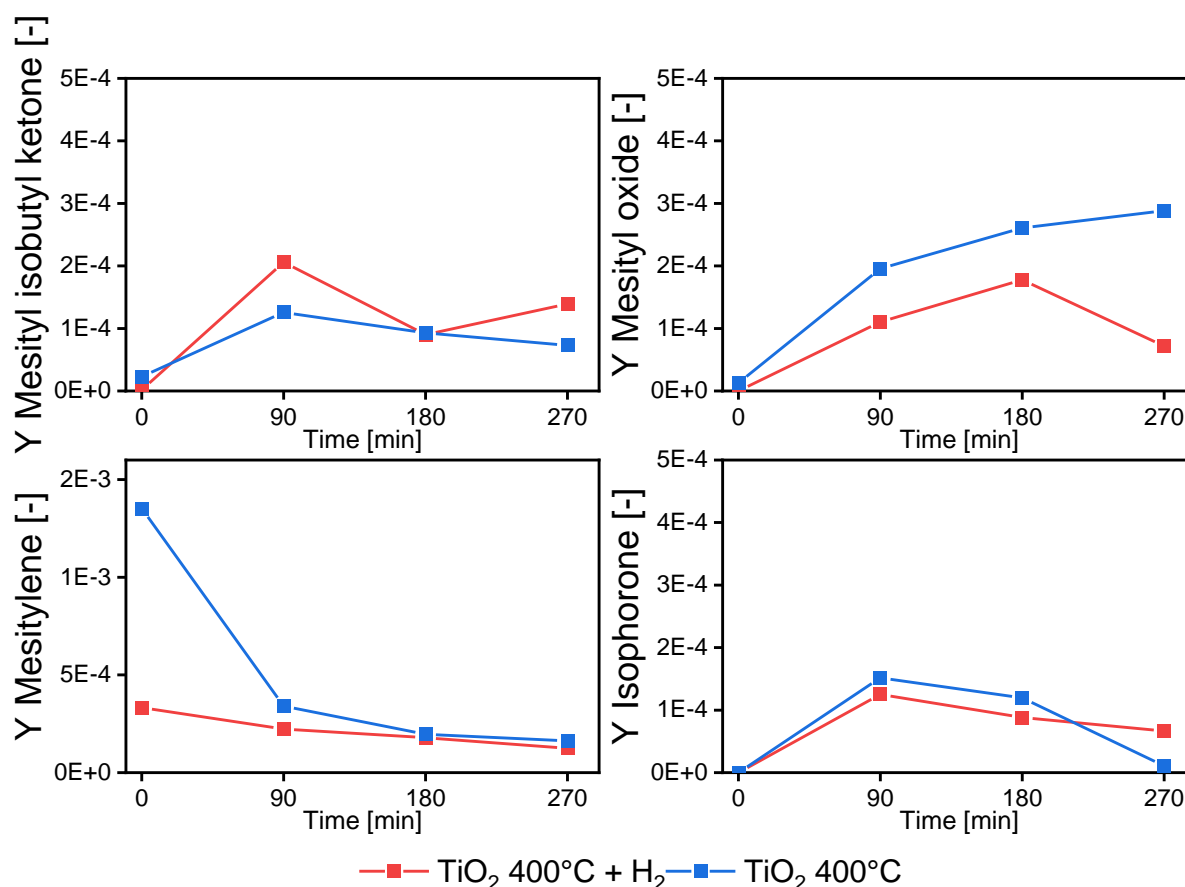


Figure 4.28 - H<sub>2</sub> effect at 400°C on condensation products composition. GHSV: 20000  
 NI/h/kg<sub>cat</sub>; Flux: 3% Acetic acid, 20% H<sub>2</sub> (if co-fed), 10% N<sub>2</sub> in He

Here products have all decreasing trends like before, except for mesityl-iso-ket that increase.

Lastly, other secondary products are shown in Figure 4.29.

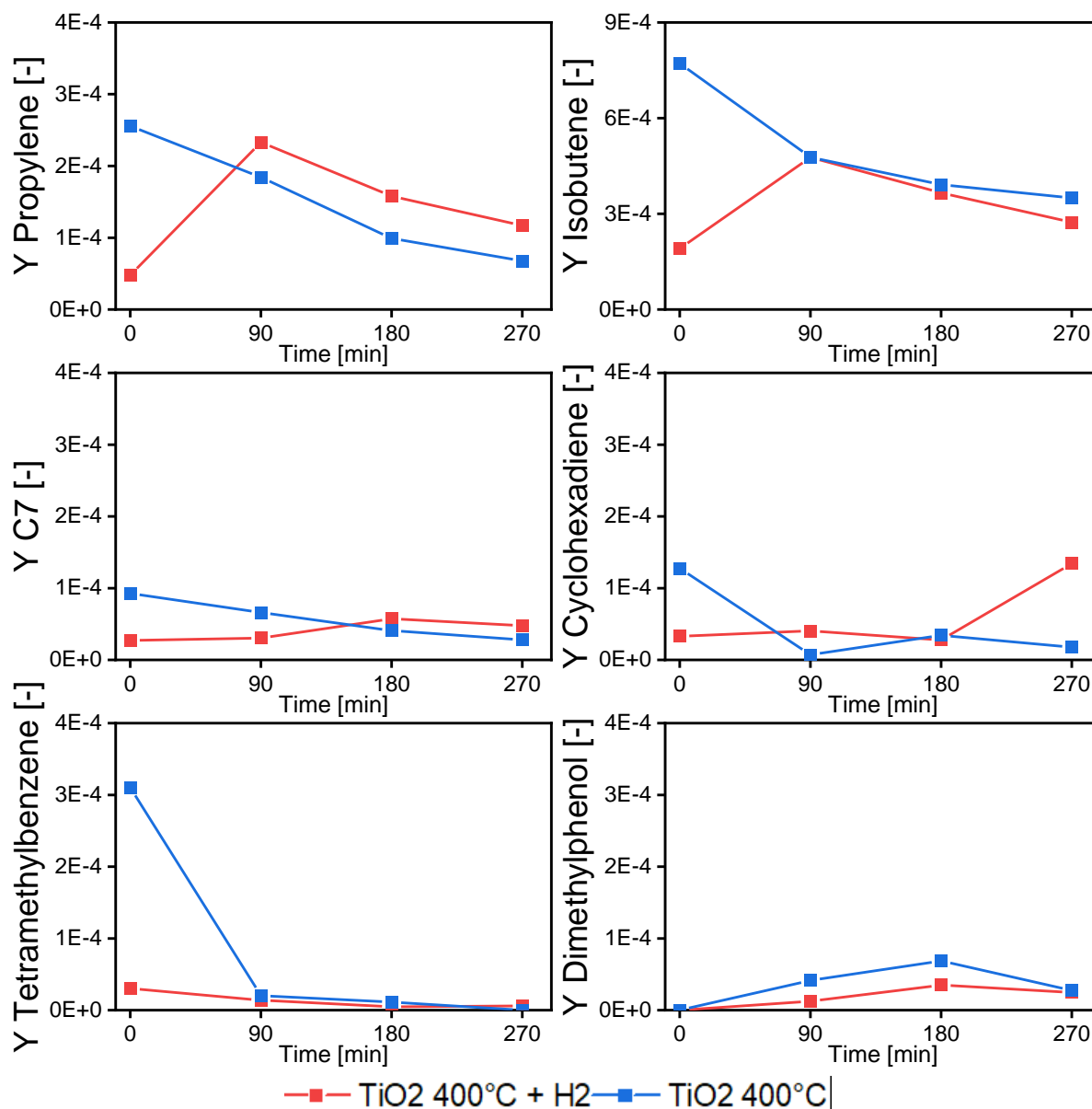


Figure 4.29 - H<sub>2</sub> effect at 400°C on secondary products composition. GHSV: 20000 NI/h/kg<sub>cat</sub>;  
Flux: 3% Acetic acid, 20% H<sub>2</sub> (if co-fed), 10% N<sub>2</sub> in He

Again, different trends can be seen: isobutene, tetra-benz and phenol are lower, while C<sub>7</sub>, propylene and cyclo increase.

The reason for the C-balance and products trends is not simple to explain; with TiO<sub>2</sub> at lower temperatures (only at 400°C the first point had a low C-balance) this did not happen, meaning that here either a transient in the reaction could be happening, or either something was blocking mainly acetone, as it was the main lacking product. After the first point, the balance is partially recovered, but then it starts decreasing again: the problem this time could be related to condensation of products in liquid phase, that accumulated mainly on the reactor tail. The effect was seen visually after the reactor was dismantled from the oven (Figure 4.30); further investigation of the species condensed showed very heavy C-species.

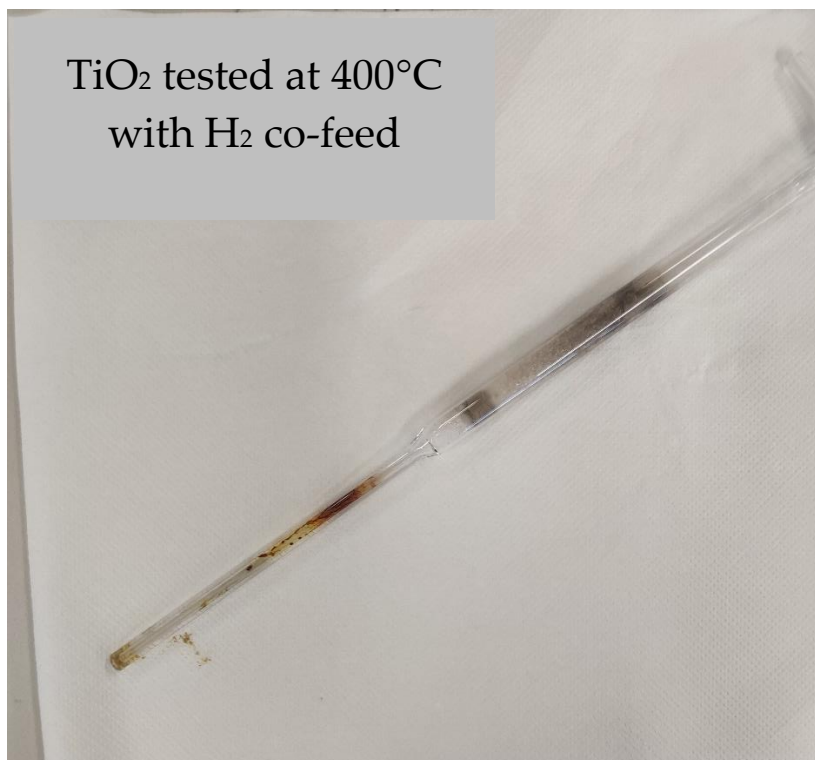


Figure 4.30 – Condensation of C-species on the reactor tail for tests on TiO<sub>2</sub> at 400°C

#### 4.3.3. Ru/TiO<sub>2</sub> vs TiO<sub>2</sub>

The last effect investigated was the addition of Ruthenium. From the previous test Ru proved to not change or improve the performances of ketonization on the low T range, so an evaluation of its effects for higher temperatures was needed.

The tests compared the two different catalysts in the case of H<sub>2</sub> cofeed at 400°C, and the results are shown in Figure 4.31 and Figure 4.32.

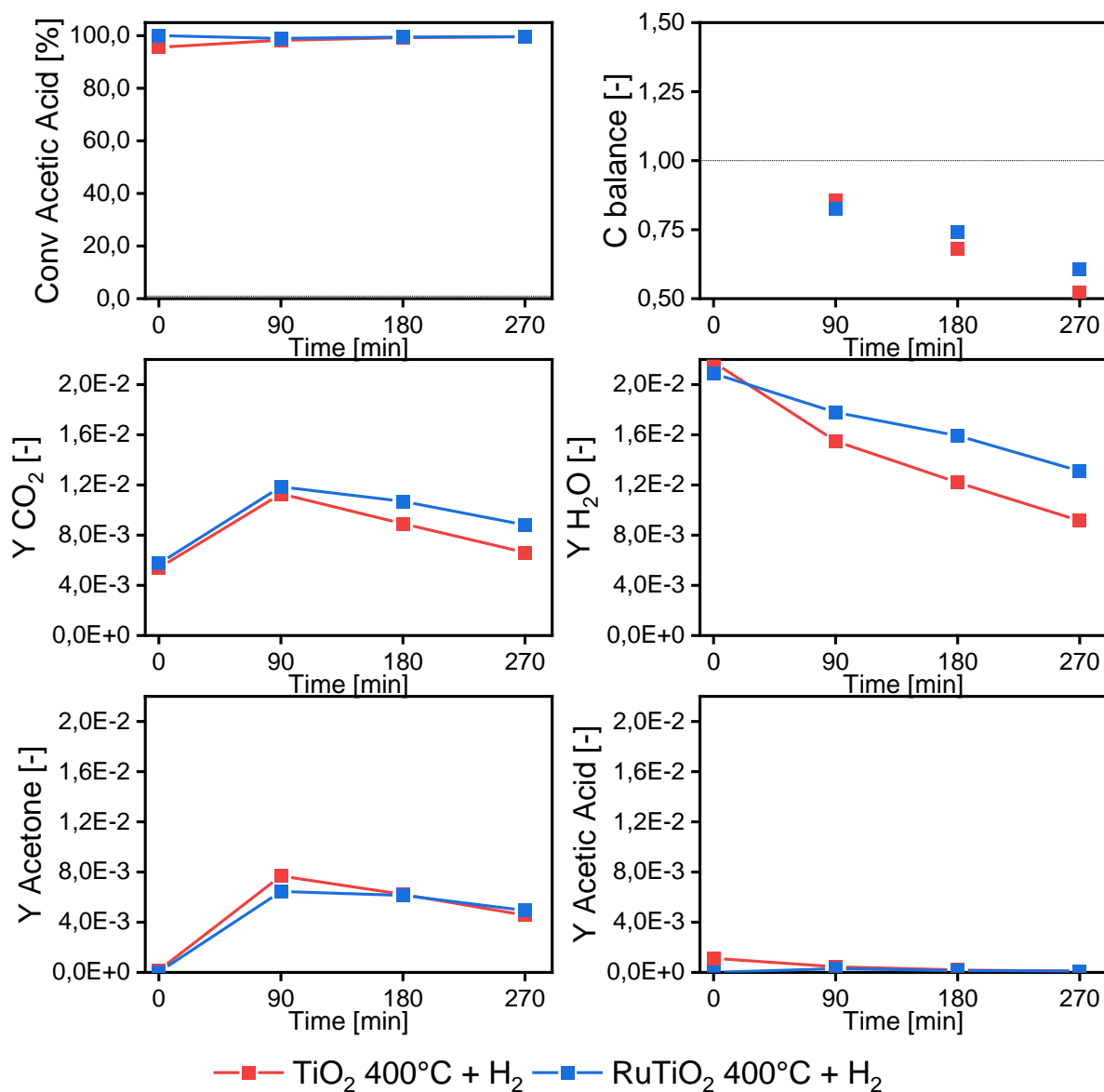


Figure 4.31 – Ru addition effect at 400°C on main products composition. GHSV: 20000  $\text{Nl/h/kg}_{\text{cat}}$ ; Flux: 3% Acetic acid, 20%  $\text{H}_2$ , 10%  $\text{N}_2$  in He (Part 1)

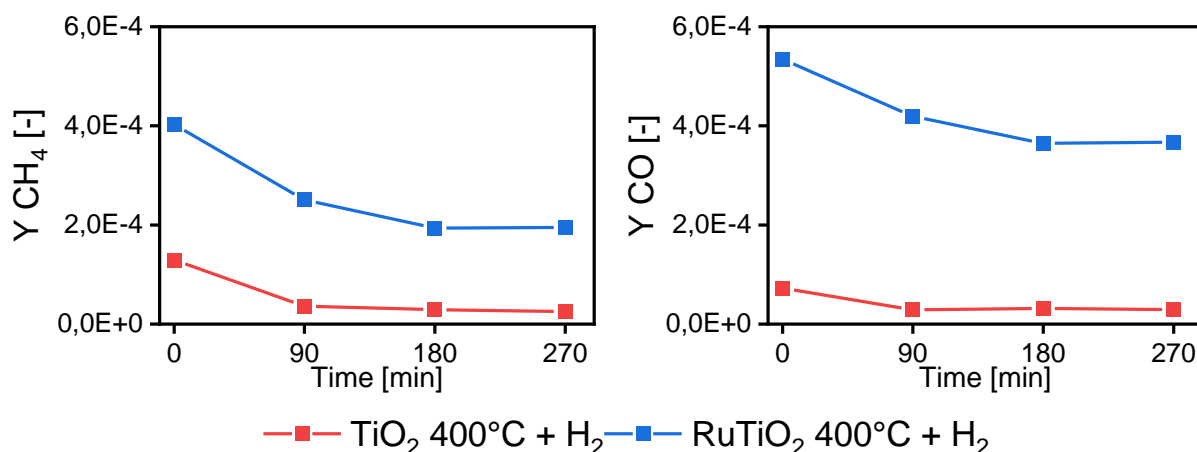


Figure 4.32 - Ru addition effect at 400°C on main products composition. GHSV: 20000 NI/h/kg<sub>cat</sub>; Flux: 3% Acetic acid, 20% H<sub>2</sub> (if co-fed), 10% N<sub>2</sub> in He (Part 2)

In both experiments, C-balances were in large defect at the reaction start, and improved with time on stream up to 90 minutes. This confirms the importance of the slow dynamics of equilibration of adsorption/desorption steps such that the reactor behaved as buffer for the accumulation of reactant and/or products. In particular, since acetone concentration also grew with time, the dynamics suggest a strong adsorption of ketone on the catalyst surface. At longer time on steam, the C-balance decreased again together with the productivity of several higher molecular species products; this instead suggests the onset of deactivation or self-inhibition phenomena due to the strong adsorption of the condensation products.

The main product output is very similar, with Ru case producing a bit more CO<sub>2</sub> and H<sub>2</sub>O, and far more CH<sub>4</sub> and CO.

Condensation products are reported in Figure 4.33.

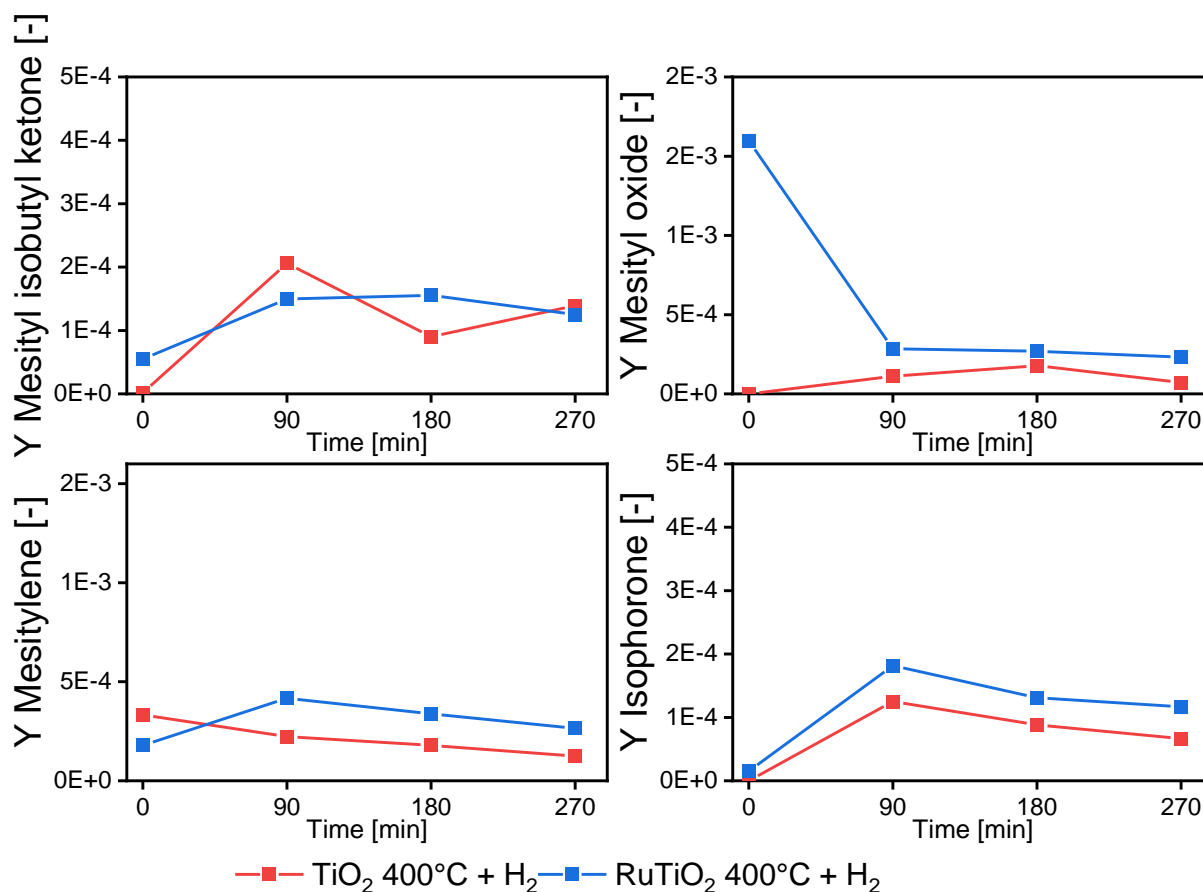


Figure 4.33 - Ru addition effect at 400°C on condensation products composition. GHSV: 20000 NI/h/kg<sub>cat</sub>; Flux: 3% Acetic acid, 20% H<sub>2</sub>, 10% N<sub>2</sub> in He

Ru/TiO<sub>2</sub> seems to perform better than TiO<sub>2</sub> when considering products coming from condensation reactions, as they all increase respect to the TiO<sub>2</sub> case.

Concerning the other products, data are reported in Figure 4.34.

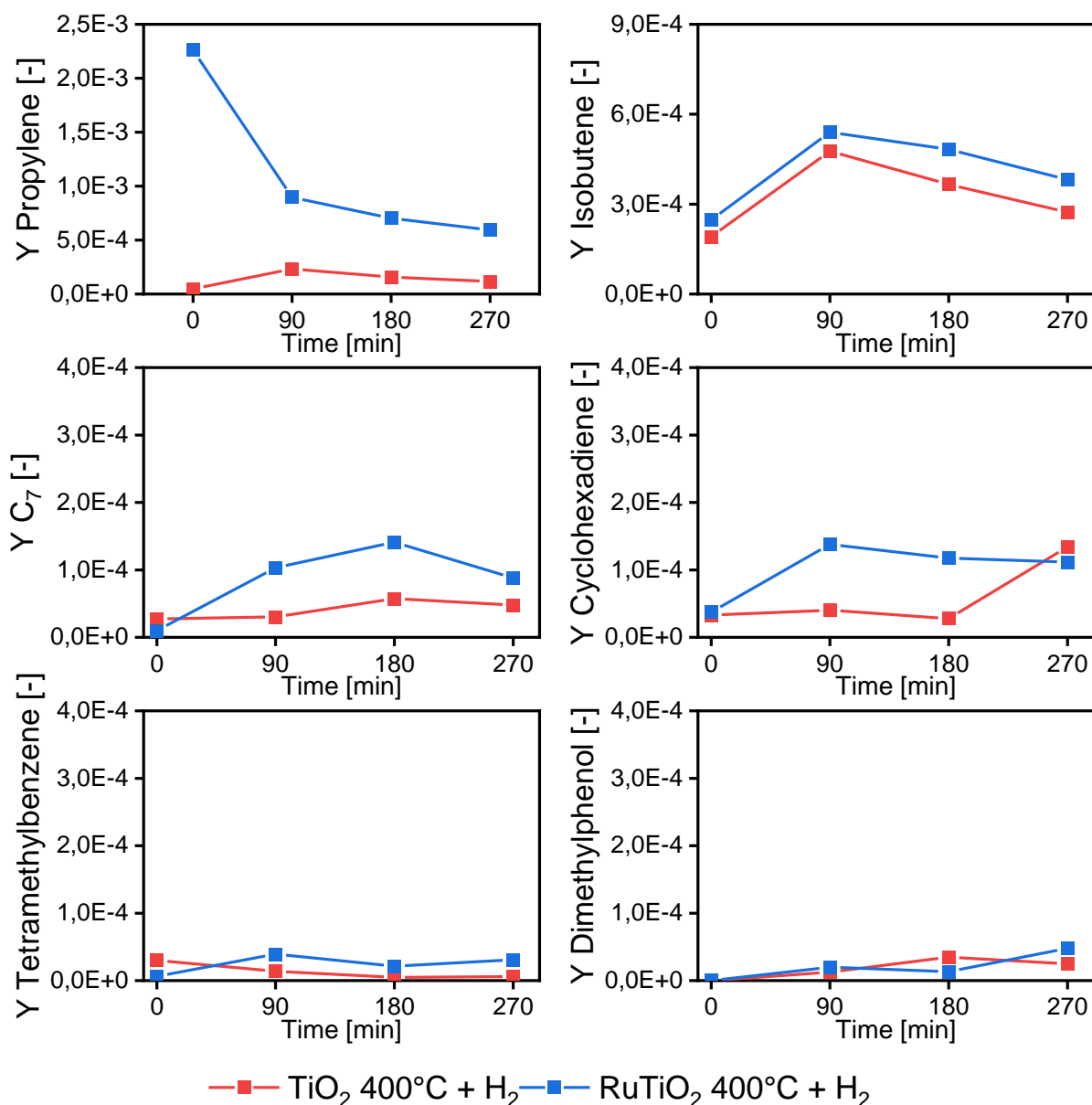


Figure 4.34 - Ru addition effect at 400°C on other secondary products composition. GHSV: 20000 NI/h/kg<sub>cat</sub>; Flux: 3% Acetic acid, 20% H<sub>2</sub>, 10% N<sub>2</sub> in He

A significantly larger amount of propylene was observed as well as a general promotion of the olefinic species.

However, a decay was also experienced on Ru, which confirms that the phenomena of irreversible adsorption and/or condensation could not be prevented by the metal phase..

A possible solution to the problem could have been increasing the flow rate of the inlet feed: allowing less reaction time (i.e. the reactants stay less time inside the catalytic bed), the product would not have had the time to either adsorb or condensate into heavier ones.

This particular condition was tested increasing the flow rate from 66 Nml/min to 100 Nml/min for the tests done at 400°C with H<sub>2</sub> co-feed. Figure 4.35 and Figure 4.36 reports the results at 100Nml/min compared to the TiO<sub>2</sub> tested at 400°C in the previous paragraph, that was the last one where no sudden C-drops were observed.

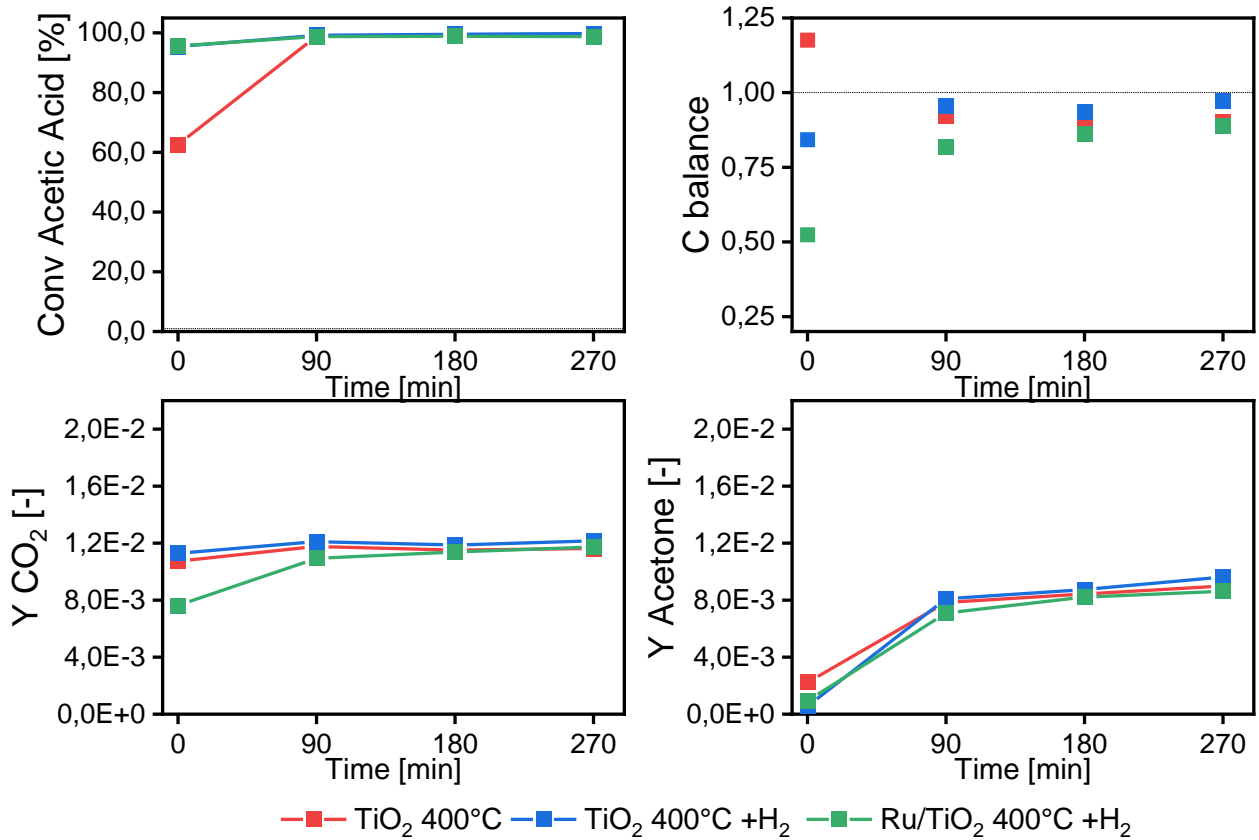


Figure 4.35 - H<sub>2</sub> effect at 400°C and 100 Nml/min on main products composition. GHSV: 20000 NI/h/kg<sub>cat</sub>; Flux: 3% Acetic acid, 20% H<sub>2</sub> (if co-fed), 10% N<sub>2</sub> in He



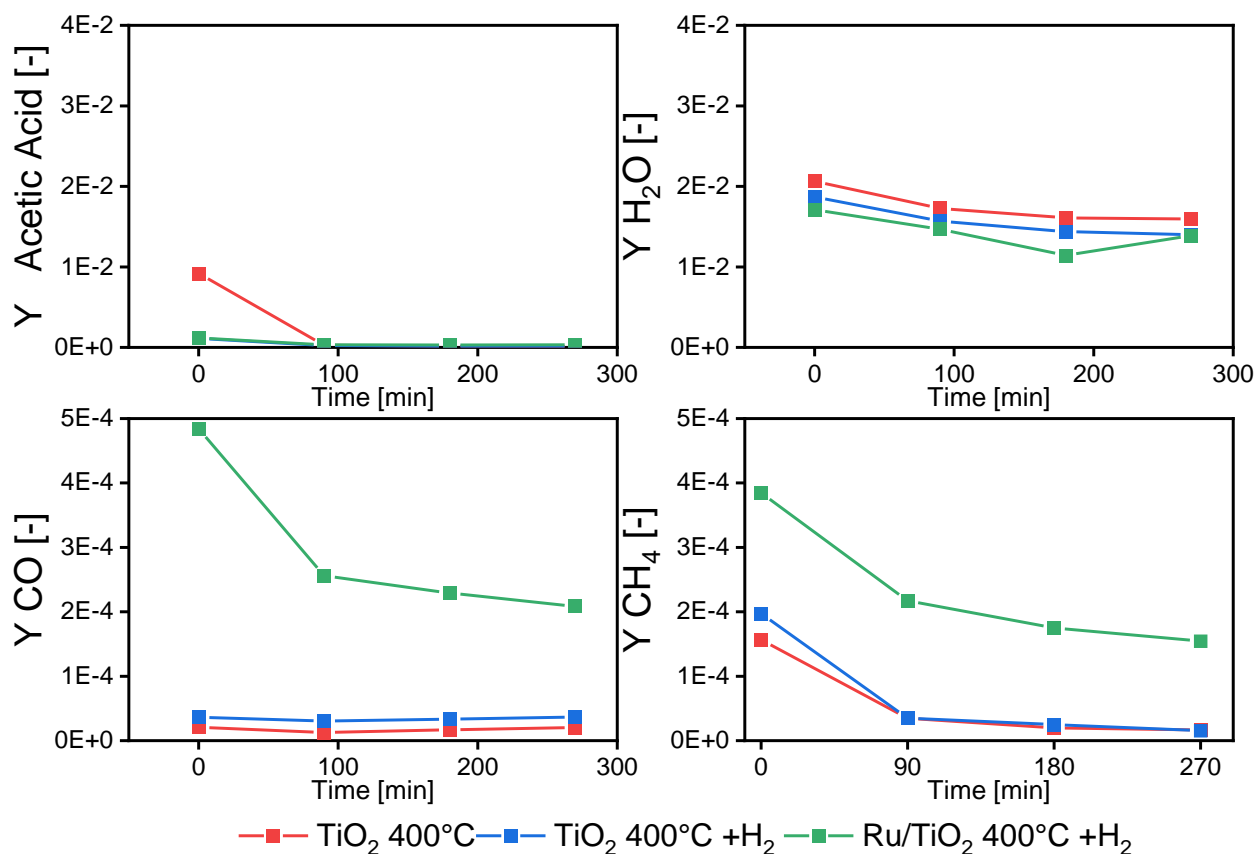


Figure 4.36 -  $\text{H}_2$  effect at 400°C and 100 Nml/min on main products composition. GHSV: 20000 NI/h/kg<sub>cat</sub>; Flux: 3% Acetic acid, 20%  $\text{H}_2$  (if co-fed), 10%  $\text{N}_2$  in He

From the Fig., it can be observed that this time, conversion is again maxed out, but C-balance do not drop anymore: instead, it seems to recover with time, as we go from 75 to 95% ( $\text{TiO}_2+\text{H}_2$ ) and from 50% to 90% ( $\text{Ru/TiO}_2$ ). The same trend is followed by acetone, while  $\text{CO}_2$  seems to be more stable. An important note is observed for  $\text{CH}_4$  and CO in the case of  $\text{Ru/TiO}_2$ , that are much higher than the other two cases.

Condensation products are reported with the same scheme in Figure 4.37.

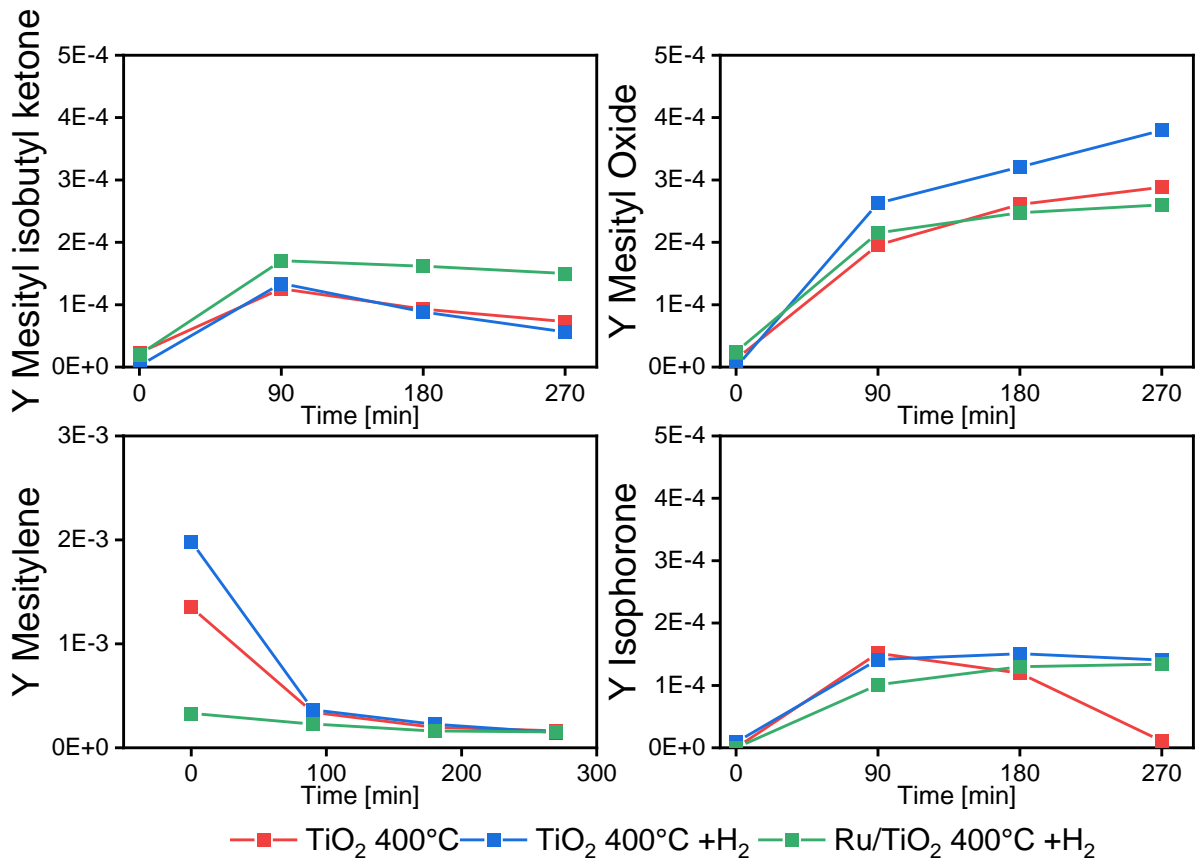


Figure 4.37 -  $\text{H}_2$  effect at 400°C and 100 Nml/min on condensation products composition.

GHSV: 20000  $\text{Nl/h/kg}_{\text{cat}}$ ; Flux: 3% Acetic acid, 20%  $\text{H}_2$  (if co-fed), 10%  $\text{N}_2$  in He

Here the same trend observed before is maintained, as  $\text{C}_6$  and isophorone follow the trend of acetone. Unfortunately, mesitylene is quite lower in the  $\text{Ru/TiO}_2$  case, while it increases for  $\text{TiO}_2$  with  $\text{H}_2$  co-feed.

As for cracking products, data are reported in Figure 4.38.

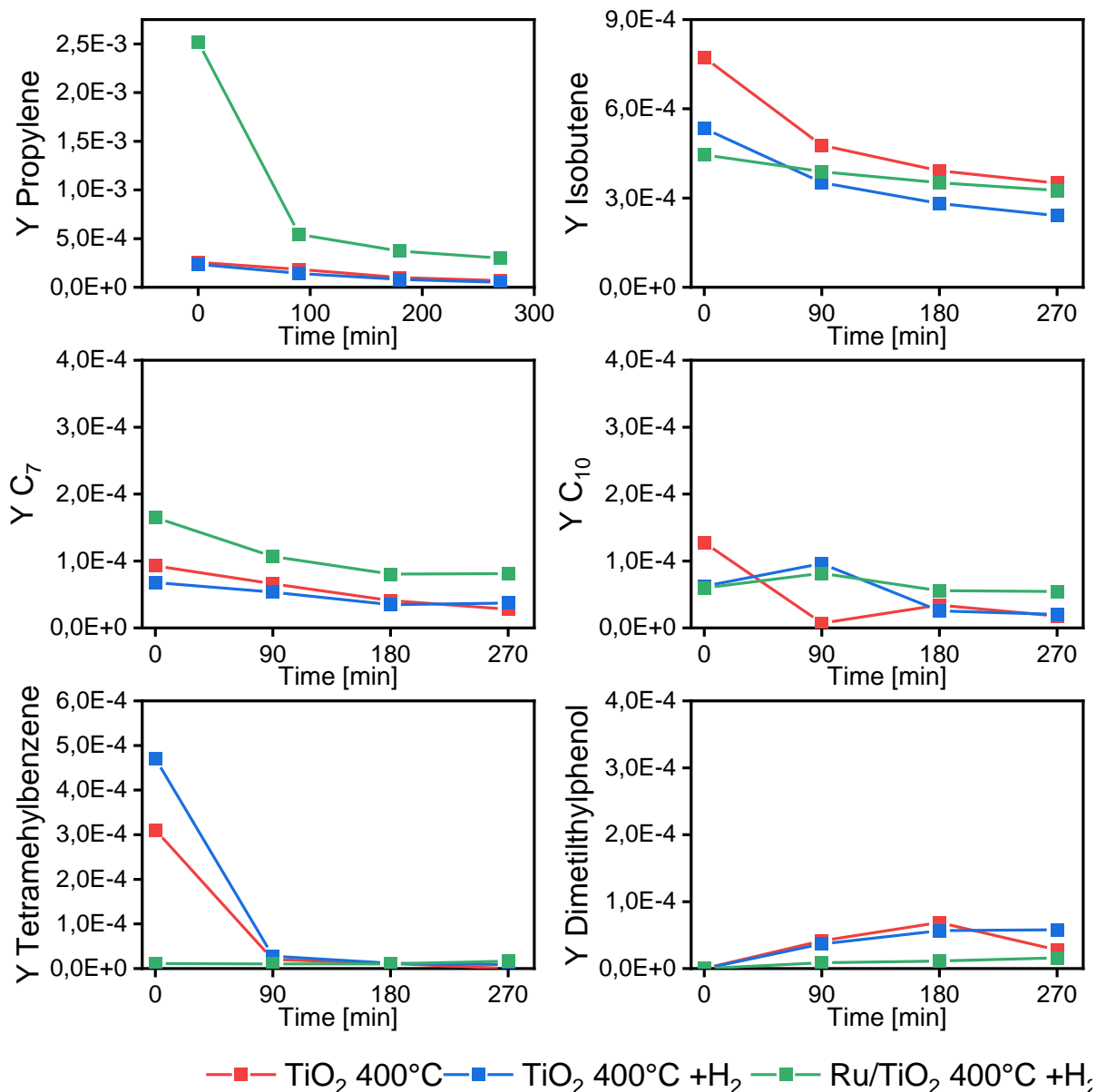


Figure 4.38 -  $\text{H}_2$  effect at 400°C and 100 Nml/min on cracking products composition. GHSV: 20000  $\text{Nl/h/kg}_{\text{cat}}$ ; Flux: 3% Acetic acid, 20%  $\text{H}_2$  (if co-fed), 10%  $\text{N}_2$  in He

$\text{H}_2$ -co-feed does not improve the  $\text{TiO}_2$ , as all products have similar trends, while Ru addition seems to favor the cracking reactions into mostly propylene (one order of magnitude higher) and  $\text{C}_7$  (slightly higher).

In conclusion, it is observed that  $\text{H}_2$  co-feed into the higher temperature region seems to promote slow dynamics of equilibration of adsorption/desorption steps such that the reactor behaved as buffer for the accumulation of reactant and/or products, as the trend was experienced in all cases tested.

Low flow rate also seems to promote strong adsorption of condensation products, confirmed by the C-balance drops after 90 minutes. Instead, when inlet feed is

increased, the phenomena is believed to be dampened, as C-balance recovers (not immediately, but over time).

A decreasing trend of the heavier products is still observed, meaning that reaction pathways' blocking is happening in all cases, prompting interesting challenges in terms of catalyst stability. Lastly, it is noted that Ru addition in the presence of H<sub>2</sub> at higher T highly favors the formation of both CH<sub>4</sub> and propylene, suggesting that these cracking reactions are more active.

#### 4.4. TPO

TPO tests were performed on spent catalytic powder aiming to analyse possible carbon deposits formation during ketonization experiments. In particular, after every 4.5 h-long ketonization experiment, a TPO test was performed the influence of ketonization temperature, H<sub>2</sub> co-feed, and catalyst composition on the accumulation of C were investigated. Figure 4.39 shows an example of reactor post-ketonization, with an important darkening of the reactor packing (both quartz and cat particles) and the reactor walls.

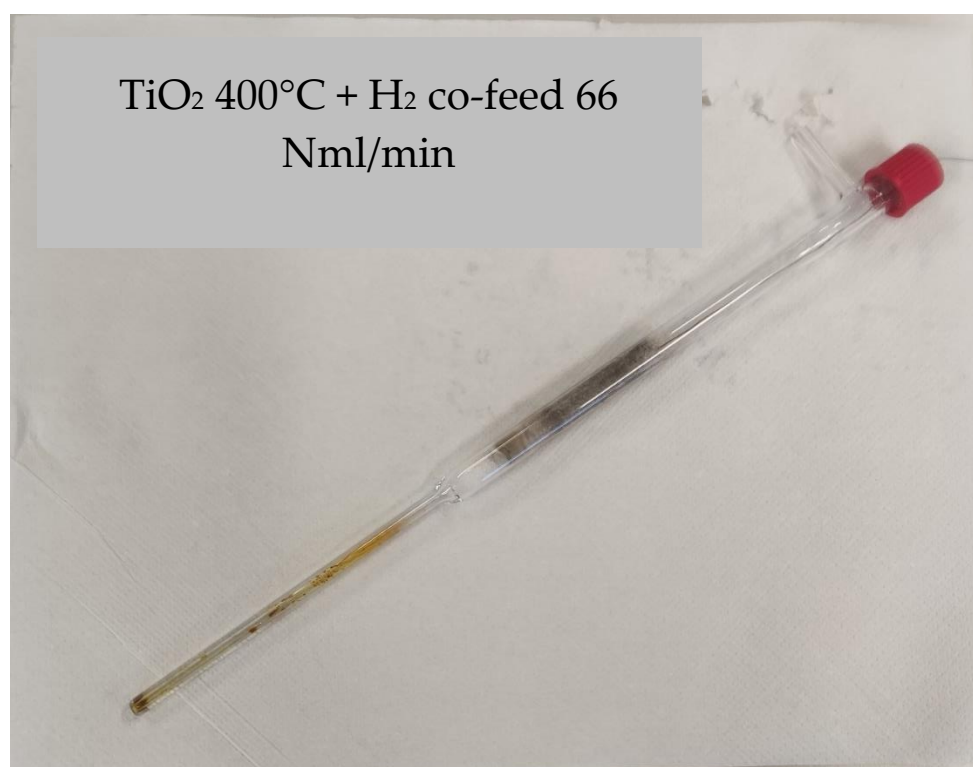


Figure 4.39 – Reactor view post-experiment with prolonged ketonization of TiO<sub>2</sub> at 400°C with H<sub>2</sub> co-feed

Each test was carried out using 25 Nml/min of air and a temperature ramp rate of 2°C/min from room temperature up to 600°C. Analyses composition with the use of the Micro-GC were performed. Moreover, all the species observed were normalized to the catalyst mass, so a comparison between the tests could be done.

The summary of reactors used was already provided in Table 4.4, as they were subsequently tested after ketonization.

#### 4.4.1. Temperature effect

The effect of ketonization temperature on C-formation was firstly studied: since three ketonization set points were chosen (300°C, 350°C and 400°C), an investigation on how much T influenced the carbon deposition on the catalyst had to be performed.

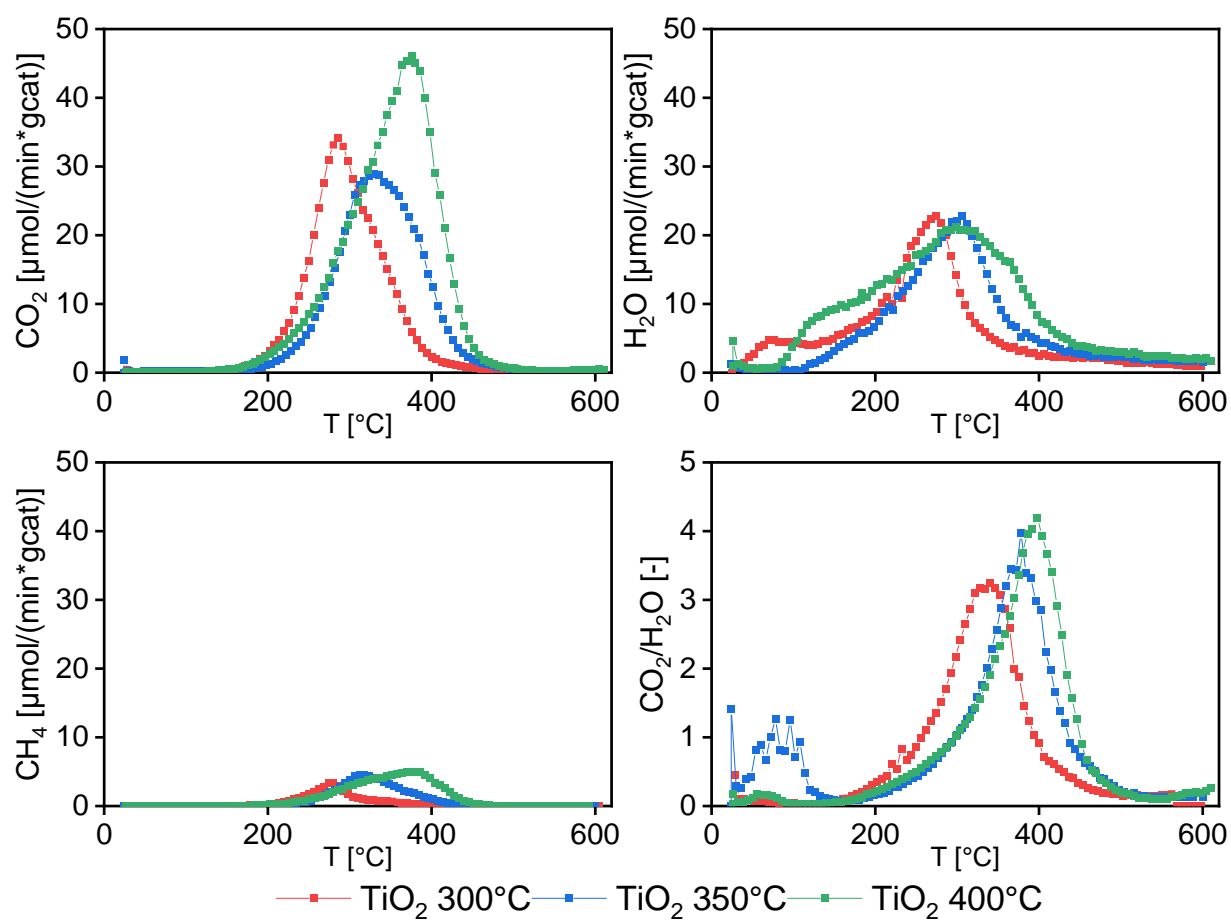


Figure 4.40 shows the products composition (normalized to the catalyst mass) and  $\text{CO}_2/\text{H}_2\text{O}$  ratio over temperature for the three different temperatures chosen during ketonization.

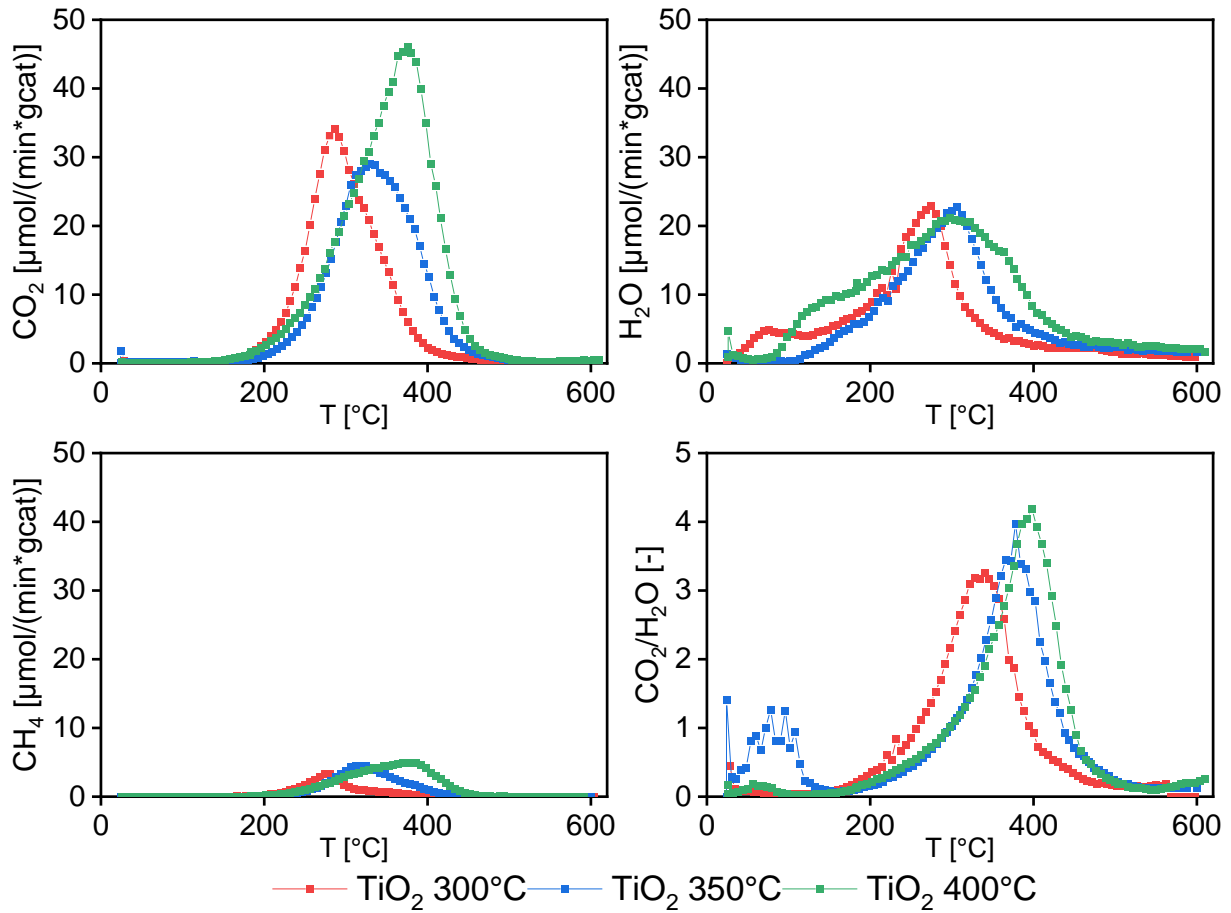
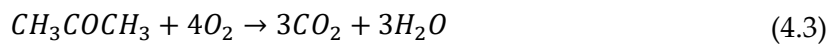
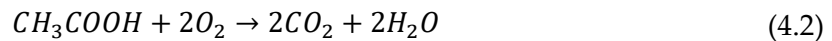


Figure 4.40 – Products composition over Temperature on TPO analyses for TiO<sub>2</sub> tested at the three different ketonization temperatures. Flux: 25 Nml/min of air.

In every TPO, CO<sub>2</sub>, CH<sub>4</sub> and H<sub>2</sub>O were observed. CO<sub>2</sub> and H<sub>2</sub>O came from the combustion reaction of C species with oxygen, as shown in Equation (4.2) for acetic acid and Equation (4.3) for acetone:



However, those are only an example of two possible reactions, as from TPD on acetic acid it was demonstrated that higher C-species deposits on the catalyst surface. In particular, if we consider a generic higher C-species, the combustion reaction is shown in Equation (4.4):



However, since H<sub>2</sub>O is also found, this means that hydrogenated species are present, and only the combustion of graphitic C deposits cannot be considered alone.

As for CH<sub>4</sub>, its origin could possibly be from cracking reactions previously mentioned, as a methanation is unlikely happening.

For the sake of clarity, TPO tests will be named with a reference to the previous ketonization temperature (e.g. TiO<sub>2\_300</sub> stands for the one subjected to ketonization at 300°C)

Regarding CO<sub>2</sub> trends observed in TPO, maximum peak height is found at increasing temperature for the three cases: TiO<sub>2\_300</sub> has a peak at 270°C, the one tested at 350°C has it at 330°C while the TiO<sub>2\_400</sub> is around 380°C. Moreover, it can be observed that the CO<sub>2</sub> peak of TiO<sub>2\_350</sub>, shifted towards higher temperatures, has a maximum value lower than TiO<sub>2\_300</sub>. TiO<sub>2\_400</sub> instead reports an increase of both maximum peak temperature and amount.

A similar observation can be done for the CH<sub>4</sub> curves: all TiO<sub>2</sub> show an increase of maximum peak temperature and maximum quantity that increases as the ketonization temperature at which they were tested increase.

The same conclusion however cannot be said for H<sub>2</sub>O. here the differences reside in the fact that the TiO<sub>2\_300</sub> and TiO<sub>2\_350</sub> show a different behavior on the lower temperature range (30-150°C) while for higher ones they are very similar (TiO<sub>2\_350</sub> slightly shifted towards higher temperatures, but plotted curve is comparable). Instead, TiO<sub>2\_400</sub> shows a much higher quantity in the lower region, while a 2-peak contribution can be observed when T reaches the 300-350°C range.

Lastly, the CO<sub>2</sub>/H<sub>2</sub>O graph shows that a peak amount of 3.5 moles of CO<sub>2</sub> were produced for every mole of water for TiO<sub>2\_300</sub>, while for TiO<sub>2\_350</sub> and TiO<sub>2\_400</sub> the value reached a maximum of 4.5.

All the quantities found were integrated in time to find the total quantities deposited. Results are reported into Table 4.5.

Integration results for TPO tests on TiO <sub>2</sub>			
Species	TiO <sub>2_300</sub>	TiO <sub>2_350</sub>	TiO <sub>2_400</sub>
CO <sub>2</sub> [mmol/g <sub>cat</sub> ]	8.27	9.12	13.78
H <sub>2</sub> O [mmol/g <sub>cat</sub> ]	7.02	6.63	10.47
CH <sub>4</sub> [mmol/g <sub>cat</sub> ]	0.61	1.11	1.65
<b>Total C [mmol/g<sub>cat</sub>]</b>	<b>8.88</b>	<b>10.23</b>	<b>15.43</b>

Table 4.5 - Integration results for TPO tests on TiO<sub>2</sub> at 300-350-400°C

From all the graphs and table, quite a few remarkable conclusions can be derived.

Firstly, C-deposits increase as the ketonization temperature at which every TiO<sub>2</sub> was tested increases. In particular, while between 300 and 350°C the difference is not so high, the trend is systematic and the 400°C case shows a doubled C-deposition from the 300°C case.

Moreover, if we consider that all tests were subjected to 66 Nml/min of 3% acetic acid for 4.5 hours, the percentage of C deposited can be derived with Equation (4.5) and (4.6).

$$n_{C \text{ converted}} = \frac{n_{C \text{ acetic acid}} * F_{\text{acetic acid converted}}}{m_{\text{cat}}} * 60[\text{min}] * 4.5 [\text{h}] \quad (4.5)$$

$$\%_{C \text{ dep}} = \frac{n_{C \text{ TPO}}}{n_{C \text{ converted tot}}} \quad (4.6)$$

Where  $F_{\text{acetic acid converted}}$  and  $m_{\text{cat}}$  are expressed in terms of  $\left[\frac{\text{mmol}}{\text{min} * \text{g}_{\text{cat}}}\right]$  and  $[\text{g}_{\text{cat}}]$ , while  $n_i$  is in terms of  $[\text{mmol}]$ .

The total amount of C-moles obtained is around 230-240 mmol/g<sub>cat</sub> (depending on experimental errors on mass and flow rate measurements). Finally, the % of C that deposited is computed and reported in Table 4.6.

Percentage of C-moles deposited during ketonization			
	TiO <sub>2_300</sub>	TiO <sub>2_350</sub>	TiO <sub>2_400</sub>
% <sub>C</sub> deposited	3,7	4,3	6,5

Table 4.6 – Percentage of C deposited during ketonization of TiO<sub>2</sub> at 300-350-400°C

The values obtained demonstrates a very important conclusion: 6.5% of total C-deposited respect to the one that has converted does not justify the C-balances drop after 90 minutes. Even if TiO<sub>2</sub> goes through an intensive deposition at higher T (6.5% is still relevant), the amount is not enough. This could possibly indicate two scenarios:

1. Products in gaseous phase went missing/were not detected for some reason
2. C-balances drop are all connected to the condensation phenomena occurring downstream of the catalytic bed, specifically in the tail of the reactor

However, since it was also visually seen, it cannot be excluded that the lacking C deposited also in the quartz column, while another part condensed in the reactor tail.



Another important thing to remember is that after the TPO, the reactor regained its clean color, but the darkened region on the tail was not fully removed, as visible traces remained. For this reason, the estimation done could also be imprecise.

The increasing percentage is also a proof of what was visually seen on the reactors, as shown in Figure 4.41.

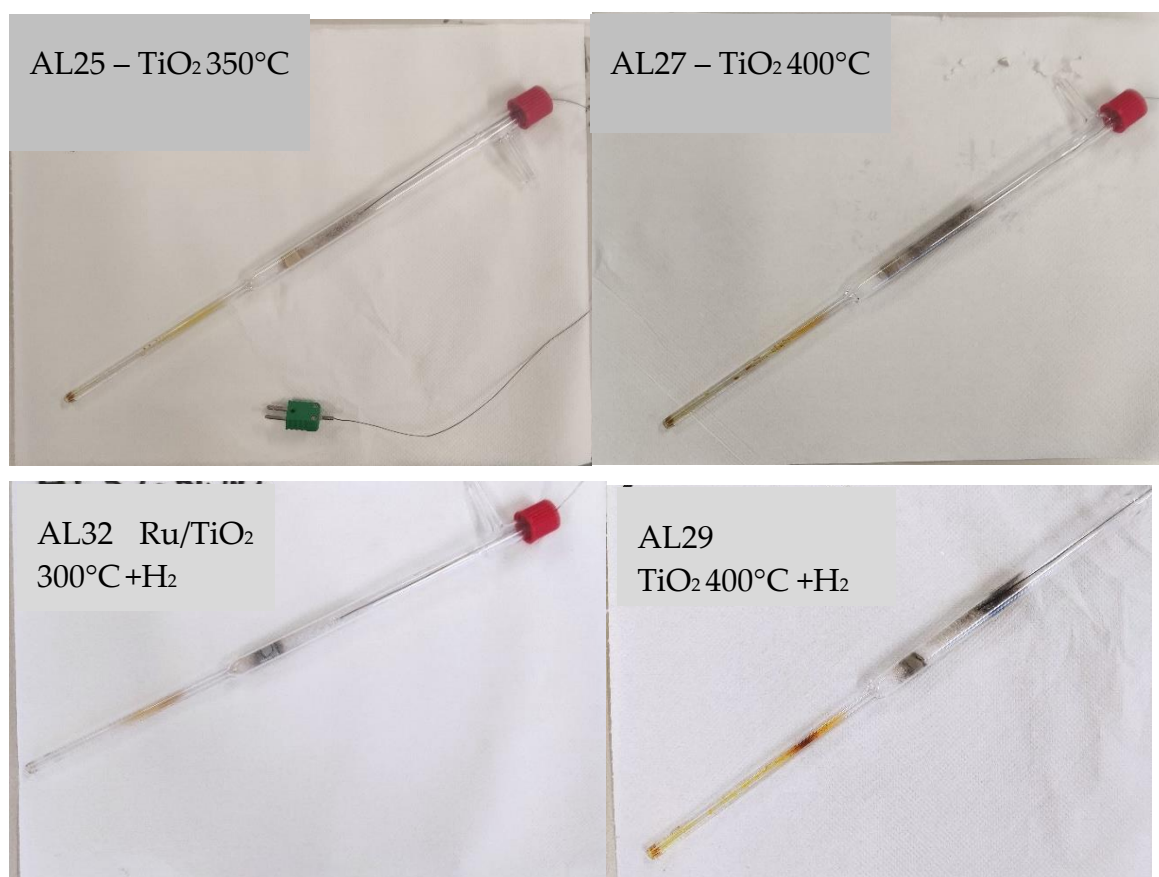


Figure 4.41 – Reactor view at two different temperatures (300 and 400°C) for TiO<sub>2</sub> and Ru/TiO<sub>2</sub> post-keronization

It is immediate to notice that as temperature increase, the dirtiness of the reactor increases, meaning that more C had deposited.

Secondly, from the CO<sub>2</sub>/H<sub>2</sub>O ratio curve it is immediately understood that the combustion of C-species interested either unsaturated compounds or multiple C-bonds species like aromatics. It is however reminded that finding the combustion reactions' stoichiometry only from this type of curve is very difficult, meaning that also the nature of those species is not clear enough.

Lastly, the H<sub>2</sub>O obtained could not be coming only from combustion, as it is the only one that does not show a very different behavior as experienced with CO<sub>2</sub> and CH<sub>4</sub>.

The reason behind this could be attributed to the nature of  $\text{TiO}_2$ , meaning that it absorbed a good quantity of water during catalyst preparation.

#### 4.4.2. $\text{H}_2$ co-feed effect

TPO analyses were performed also over the samples of  $\text{TiO}_2$  tested at 300 and 400°C with and without  $\text{H}_2$  co-feed.

Figure 4.42 reports the composition of  $\text{CO}_2$ ,  $\text{H}_2\text{O}$  and  $\text{CH}_4$  over temperature for the comparison of ketonization temperature of 400°C.

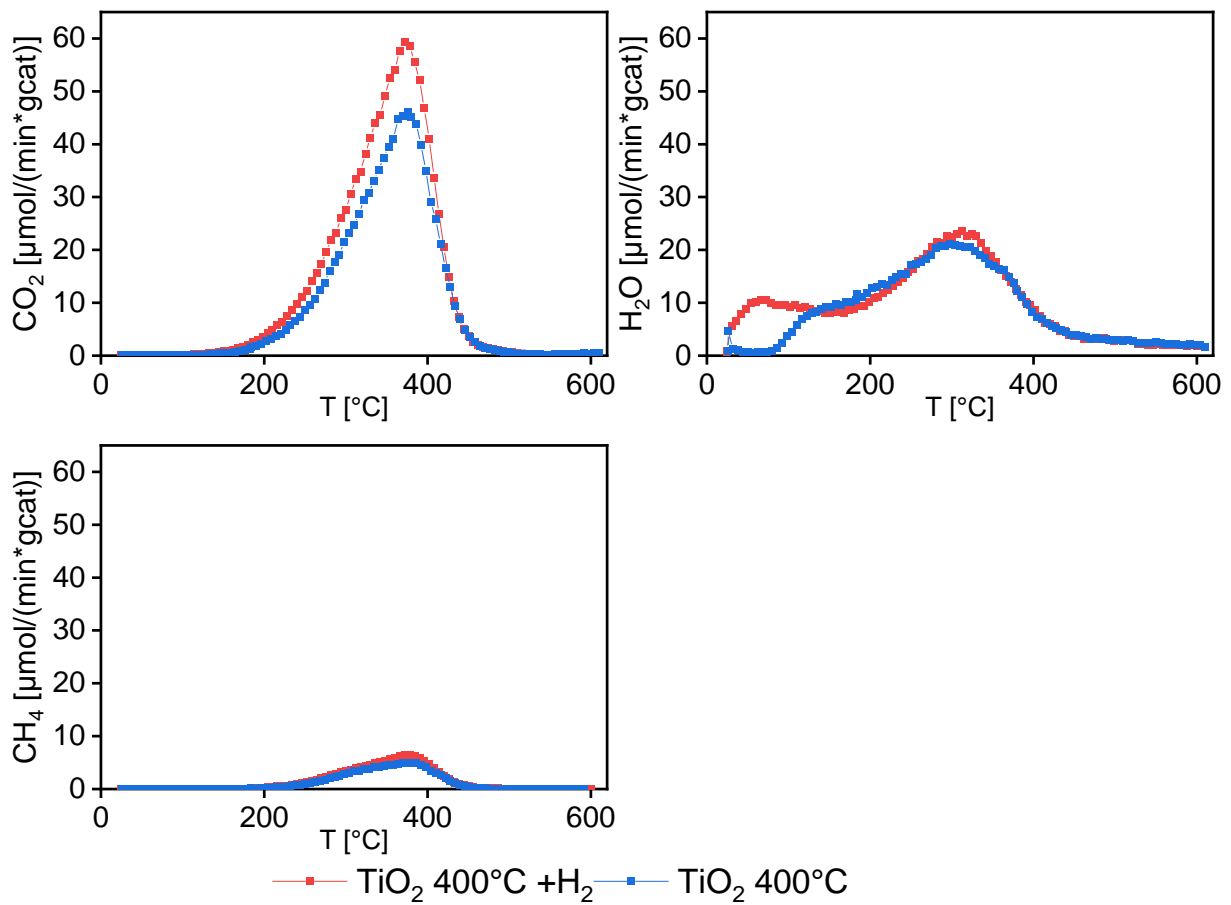


Figure 4.42 –  $\text{CO}_2$ ,  $\text{H}_2\text{O}$  and  $\text{CH}_4$  composition over temperature for TPO tests on  $\text{TiO}_2$ <sub>400</sub> and  $\text{TiO}_2$ <sub>400\_H2</sub>

Figure 4.43 reports the same graph scheme, but this time for the two  $\text{TiO}_2$  previously tested at 300°C.

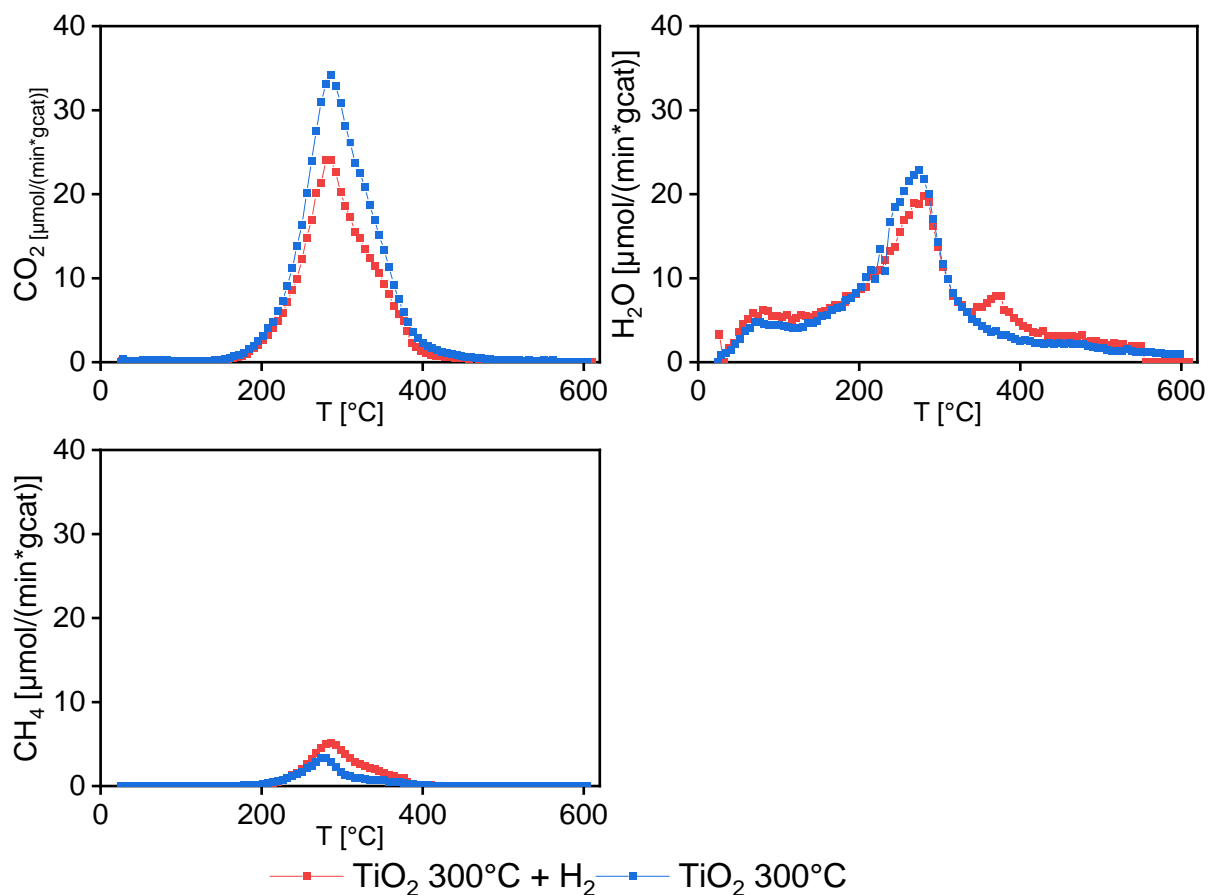


Figure 4.43 - CO<sub>2</sub>, H<sub>2</sub>O and CH<sub>4</sub> composition over temperature for TPO tests on TiO<sub>2</sub><sub>300</sub> and TiO<sub>2</sub><sub>300</sub>+H<sub>2</sub>

Regarding the 400°C case, the first thing that can be noticed is about CO<sub>2</sub>: the one tested with H<sub>2</sub> shows an increased amount respect to the one tested without it; however, the trend of the curve is not modified, as it maintain the same shape and does not change also the maximum peak temperature (around 380°C). Same conclusion is obtained for CH<sub>4</sub>. However, this time the increase is very small, and the two curves are very similar. Lastly, water shows the same trend only after 100°C, with again a small increase in the higher temperature region (300-350°C).

The integration of results is reported in Table 4.7.

Integration results for TPO on TiO <sub>2_400</sub> and TiO <sub>2_400_H2</sub>		
Species	TiO <sub>2_400</sub>	TiO <sub>2_400_H2</sub>
CO <sub>2</sub> [mmol/g <sub>cat</sub> ]	13.78	18.14
H <sub>2</sub> O [mmol/g <sub>cat</sub> ]	10.47	13.56
CH <sub>4</sub> [mmol/g <sub>cat</sub> ]	1.65	2.11
Total C [mmol/g <sub>cat</sub> ]	15.43	20.25

Table 4.7 - Integration results for TPO on TiO<sub>2\_400</sub> and TiO<sub>2\_400\_H2</sub>

As for percentage of C deposited, data are showed in Table 4.8.

Percentage of C-moles deposited		
	TiO <sub>2_400_H2</sub>	TiO <sub>2_400</sub>
% <sub>C</sub> deposited	8,5	6,5

Table 4.8 – Percentage of C deposited for TiO<sub>2</sub> at 400°C

Results shows that H<sub>2</sub> addition as a reactant favors the C-deposition of the catalyst surface, as reported both from graphical analysis (CO<sub>2</sub> and CH<sub>4</sub> increase) and the integrations. This was however expected, as in the case with H<sub>2</sub> a more aggressive conversion of higher C-species was observed, coupled with the possibility of important products condensation and accumulation in the tail of the reactor.

For the 300°C case instead, the observations are opposite to the ones done before: all components experience a reduction of amount deposited. In particular the same curve behavior is maintained as before, with the only exception being water at higher temperature (400°C mark) that shows a small second peak and an initial slightly higher concentration. The integrations are reported in Table 4.9.

Integration results for TPO on TiO <sub>2_300</sub> and TiO <sub>2_300_H2</sub>		
Species	TiO <sub>2_300</sub>	TiO <sub>2_300_H2</sub>
CO <sub>2</sub> [mmol/g <sub>cat</sub> ]	8.27	6.02
H <sub>2</sub> O [mmol/g <sub>cat</sub> ]	7.02	9.01
CH <sub>4</sub> [mmol/g <sub>cat</sub> ]	0.61	1.06
Total C [mmol/g <sub>cat</sub> ]	8.88	7.08

Table 4.9 - Integration results for TPO on TiO<sub>2\_300</sub> and TiO<sub>2\_300\_H2</sub>

As for the total C deposited on the surface, data are reported in Table 4.10.

Percentage of C-moles deposited		
	TiO <sub>2_300_H2</sub>	TiO <sub>2_300</sub>
%c deposited	2,98	3,7

Table 4.10 – Percentage of C-moles for TiO<sub>2</sub> at 300°C

The results confirm what was graphically observed: less CO<sub>2</sub> and CH<sub>4</sub> deposited on the surface of the TiO<sub>2</sub> that was subjected to hydrogen, while water increased.

The decrease of C-deposition can be partially explained by the blank tests performed before ketonization: in them, the reactivity of quartz exposed to H<sub>2</sub> increased only when temperature reached at least 350°C, with a maximum at 400°C. This could mean that, since at 300°C almost no conversion happened, H<sub>2</sub> played its more common and known role of anti-coking element. Another important contribution is that hydrogen addition at 300°C did not show the same effects of when it was done at 400°C.

This is a very important conclusion because, as reported from literature [23], an important H<sub>2</sub> pre-treatment before calcination in air of metal oxides obtained a very stable performance and high coke resistance of the catalyst, showing also a more distributed and interactive metal with the support. A further investigation on this matter could be very interesting, because of the doubled nature of H<sub>2</sub> presence at different temperatures, and for the fact that the pre-treatment could also increase the performance of Ru addition.

#### 4.4.3. Ru/TiO<sub>2</sub> vs TiO<sub>2</sub>

The second effect investigated was the presence of ruthenium, to understand if it could possibly increase or reduce C-deposition.

For the comparison, TiO<sub>2</sub><sub>400\_H2</sub> (H<sub>2</sub> as cofeed) and Ru/TiO<sub>2</sub><sub>400\_H2</sub> (Cl) were considered. Results are reported in Figure 4.44 in the same scheme as before.

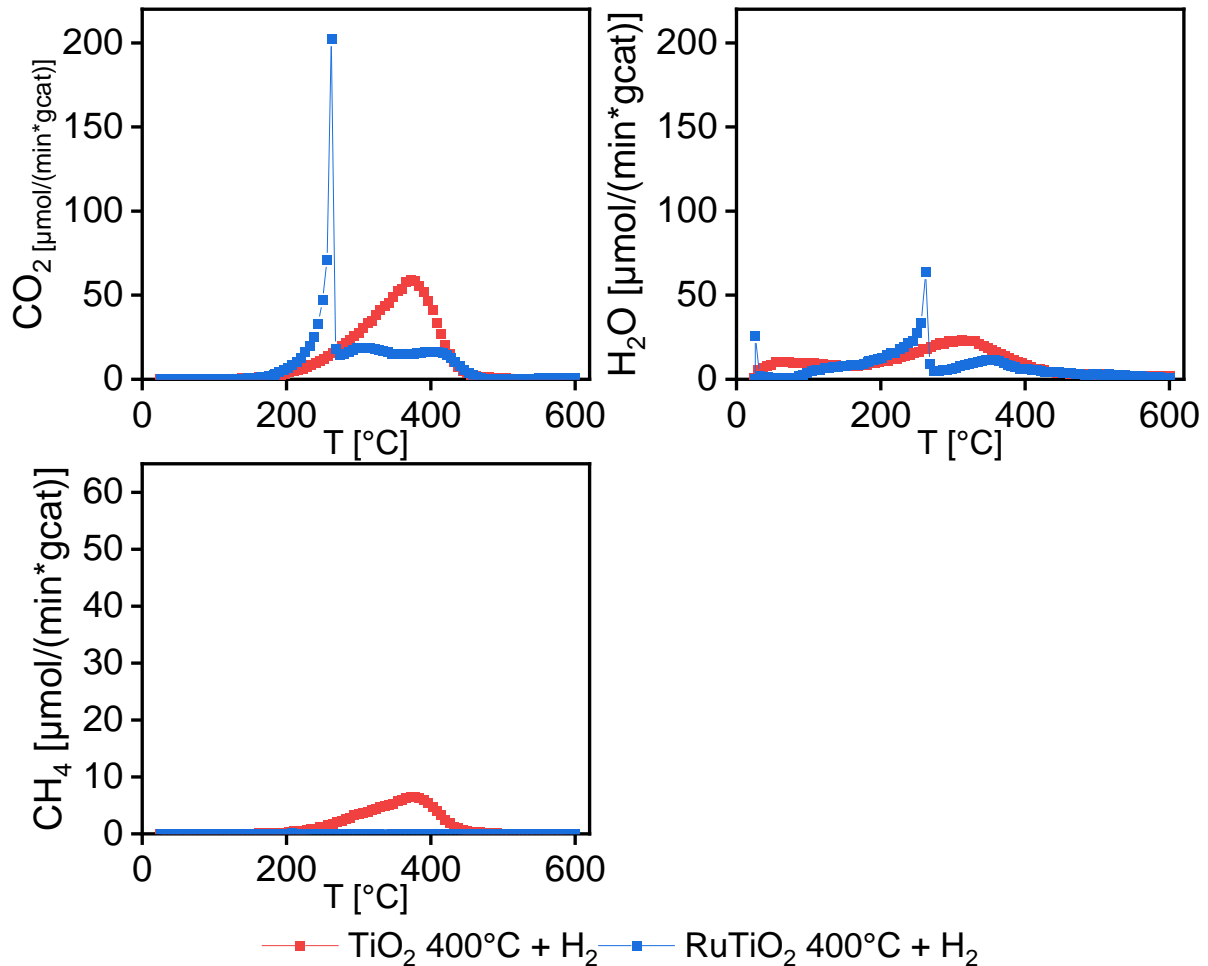


Figure 4.44 – Composition results over temperature for TiO<sub>2</sub> and Ru/TiO<sub>2</sub> (Cl) ketonized at 400°C with H<sub>2</sub>

From the graphs, three main differences can be seen: firstly, the CO<sub>2</sub> peak of Ru/TiO<sub>2</sub> at the same temperature range of 280-450°C is many times smaller both for CO<sub>2</sub> and H<sub>2</sub>O; secondly, with Ru addition a sharp peak emerges; lastly, any trace of CH<sub>4</sub> is not found for the case with ruthenium. All quantities have been integrated as before, and are reported in Table 4.11.

Integration results for TPO on Ru effect		
Species	Ru/TiO <sub>2_400_H2</sub>	TiO <sub>2_400_H2</sub>
CO <sub>2</sub> [mmol/g <sub>cat</sub> ]	14.77	18.14
H <sub>2</sub> O [mmol/g <sub>cat</sub> ]	11.31	13.56
CH <sub>4</sub> [mmol/g <sub>cat</sub> ]	0.0089	2.11
<b>Total C desorbed [mmol/g<sub>cat</sub>]</b>	<b>14.78</b>	<b>20.25</b>

Table 4.11 – Integration results for Ru effect on TiO<sub>2\_400\_H2</sub> and Ru/TiO<sub>2\_400\_H2</sub>

As for the percentage of C deposited, data are reported in Table 4.12.

Percentage of C-moles deposited		
	TiO <sub>2_400_H2</sub>	Ru/TiO <sub>2_400_H2</sub>
%C deposited	8,5	6,2

Table 4.12 – C-moles percentage difference between TiO<sub>2</sub> and Ru/TiO<sub>2</sub> at 400°C

In this case, it is noticeable that firstly Ru shifts part of the C-deposits at lower temperature: the reason for this can be attributed to the nature of the metal that activate more easily combustion of the C-species deposited near its clusters. Secondly, Ru addition reduce carbon deposition (around -5 mmol/g<sub>cat</sub>), and that is a very positive contribution to the catalyst stability. Moreover, no methane was found during the oxidation procedure, meaning that no cracking reactions took place.

Lastly, contrary to the expectations, H<sub>2</sub>O amount is just slightly lower, possibly meaning again that H<sub>2</sub>O presence could be related to the hydrophilic nature of TiO<sub>2</sub>.





## 5 Conclusions

Waste biomasses valorisation can support the decarbonization of those sectors of mobility and economy whose short-term evolution requires a green liquid fuel (e.g. aviation and shipping market). Pyrolysis is a promising technology to convert waste lignocellulosic biomass into valuable liquid fuels, but several negative features of bio-oil (poor stability, acidity, coking tendency, high oxygen content) limit both its direct use and its upgrading processes. These negative factors are mainly caused by the presence of C<sub>2</sub>-C<sub>4</sub> oxygenates in bio-oil. A possible solution to improve bio-oil quality is the development of a catalytic upgrading stage of pyrolysis vapors aiming to convert these detrimental light oxygenates into useful products. A possible route involves C-C coupling processes, where light oxygenates are converted to higher species via chain-growth reactions, thus increasing the carbon-chain length while reducing the overall O/C ratio.

In the previous thesis work [14], it was observed that TiO<sub>2</sub> represent a good catalyst in promoting acetic acid ketonization reaction (C<sub>2</sub> acetic acid → C<sub>3</sub> acetone); moreover, TiO<sub>2</sub> proved also to be a promoter of secondary chain-growth reactions from acetone when temperature were sufficiently high (C<sub>3</sub> → C<sub>6</sub> and C<sub>9</sub>). However, significant issues in terms of catalyst stability emerged. Moreover, it was surprisingly observed that the addition of Ru to catalytic formulation lowered the catalysts performance in ketonization. Within this framework, the present thesis work aimed to further comprehend the mechanisms behind chain-elongation reactions on TiO<sub>2</sub> and to pursue the development of a proper active and stable catalytic system for the production of fuel-like compounds.

An in-depth catalyst characterization study was performed, to better understand the nature of the catalysts. Morphological analyses, TPR, NH<sub>3</sub>/CO<sub>2</sub> TPD tests, acetic acid TPD test and TPO experiments were indeed carried out on several TiO<sub>2</sub> as well as Ru/TiO<sub>2</sub> samples. Morphological analyses carried out on fresh and spent TiO<sub>2</sub> before/after ketonization revealed that the exposure to ketonization reacting mixture at high temperature (400 °C) for 4.5h lead to partial blocking of the catalysts' pores, likely due to C-species accumulation.

CO<sub>2</sub> and NH<sub>3</sub> TPD tests proved the acidic nature of TiO<sub>2</sub> catalysts. However, results showed that H<sub>2</sub> pre-treatment contributed marginally to the increase of basic sites. Moreover, the CO<sub>2</sub> adsorption/desorption test seems to identify the H<sub>2</sub> pre-treated TiO<sub>2</sub> as the surface that is more prone to interact with an acidic and O-rich molecule as CO<sub>2</sub>.

Notably, the carboxylic group of acetic acid is the functional group that is closest to the full oxidation state of CO<sub>2</sub>.

Acetic acid Adsorption and TPD tests were carried out on TiO<sub>2</sub> and Ru/TiO<sub>2</sub> pre-treated catalysts to investigate its own reactivity on their surface. Data showed that ketonization reaction started from 200°C, with a minimal contribution from Ru addition. Acetic acid desorption was followed firstly by acetone formation, and then by isobutene formation, that is likely originated from the cracking of an intermediate C<sub>6</sub> component (from acetone condensation). In the presence of Ru, also CH<sub>4</sub> is observed desorbing at higher temperature, suggesting the onset of cracking reactions.

As in the previous thesis work [14], an experimental study on a model oxygenate and a model reacting system was carried out: acetic acid ketonization on TiO<sub>2</sub> catalyst. The experimental campaign investigated different effects on ketonization in the lower and higher temperature ranges respectively. Standard ketonization test conditions considered an inlet feed with GHSV of 20000 NL/h/kg<sub>cat</sub>, 3% Acetic acid, 10% N<sub>2</sub> in He.

The effect of TiO<sub>2</sub> and Ru/TiO<sub>2</sub> pre-treatment in H<sub>2</sub> on low temperature (200-300°C) acetic acid ketonization were investigated. As a results, an appropriate protocol for catalyst pre-treatment procedure was tuned, both for TiO<sub>2</sub> (6000 NL/h/kg<sub>cat</sub> of pure H<sub>2</sub>, T-ramp of 10°C/min up to 400°C with 1h hold and subsequent cooldown at same rate) and for Ru/TiO<sub>2</sub> (the same reduction treatment performed on TiO<sub>2</sub> must be preceded by a ketonization test). Hence, it was proven that the apparent inhibiting effect of Ru observed in the previous thesis, was due to the ineffective removal of Cl impurities (from catalyst preparation). However, TiO<sub>2</sub> was proven to be the active material promoting ketonization reaction, as Ru addition did not improve ketonization activity.

High temperature performances of TiO<sub>2</sub> were investigated by analysing the catalyst activity at fixed temperature for 4.5 h while monitoring the evolution of product distribution. Effects of temperature (300-350-400°C), H<sub>2</sub> co-feed (0-20%) and Ru addition on the reaction were evaluated. As experienced in the previous thesis, results showed the activation of secondary chain-growth reactions at 400°C, such that species different from ketonization products were detected. In this thesis, the dynamic evolution of products mixture composition was carefully followed, such that it was possible to identify the reaction pathways active in the system. Self- and cross- aldol condensation reactions from acetone are activated, leading to the production of species with six C-atoms (Mesityl isobutyl ketone and Mesityl oxide) and 9 carbon atoms (Mesitylene). The presence of heavy olefins (C<sub>4</sub>-C<sub>7</sub> and C<sub>10</sub>) suggests instead the onset of cracking reactions (of the same surface intermediates produced in acetone condensation route).

These Heavier C-species detected were of particular importance, as some of them are very good contributor in blendings for jet-fuel, which represent the real scope of this catalytic upgrading of bio-oxygenates; among them cyclic hydrocarbons like

mesitylene and tetramethyl benzene fit well into this category, due to the absence of O atoms in the molecules and to the increased C-chain length.

In addition, these secondary condensation and cracking reactions were also observed at 300-350 °C, proving that it is not necessary to reach 400°C and complete acetic acid conversion to see acetone converting.

For all the cases studied, both TiO<sub>2</sub> and Ru/TiO<sub>2</sub> showed an unstable behaviour at increasing ToS, such that the production of C<sub>6+</sub> species extinguished almost completely within the first hour. The phenomena can be directly linked to the previous morphological analyses, where a blocking mechanism was suggested; moreover also C-balance highlights a C-loss in the first hour of the experiments

Challenges in terms of more detailed analyses in the higher temperature range are definitely a way forward, coupled with the possible improvement of TiO<sub>2</sub> properties, as they could lead to more selective reaction pathways for the intended goal pursued. In particular, the acidic nature of TiO<sub>2</sub> can possibly promotes the cracking route to olefins, which are well known coke precursor and that can possibly be the responsible for pores blockage and catalyst activity. Different catalyst formulation can be tested to “kill” the acidic nature of TiO<sub>2</sub>.



## Bibliography

- [1] McKinsey, "Global Energy Perspective 2022 McKinsey ' s Global Energy Perspective is a collaboration between Energy Insights and adjacent practices," no. April, 2022, [Online]. Available: <https://www.mckinsey.com/~media/McKinsey/Industries/Oil and Gas/Our Insights/Global Energy Perspective 2022/Global-Energy-Perspective-2022-Executive-Summary.pdf>
- [2] B. Looney, "Statistical Review of World Energy globally consistent data on world energy markets . and authoritative publications in the field of energy," *Rev. World Energy data*, vol. 70, pp. 8–20, 2021.
- [3] C. Briens, J. Piskorz, and F. Berruti, "Biomass Valorization for Fuel and Chemicals Production -- A Review," *Int. J. Chem. React. Eng.*, vol. 6, no. 1, 2008, doi: 10.2202/1542-6580.1674.
- [4] N. L. Panwar, R. Kothari, and V. V. Tyagi, "Thermo chemical conversion of biomass - Eco friendly energy routes," *Renew. Sustain. Energy Rev.*, vol. 16, no. 4, pp. 1801–1816, 2012, doi: 10.1016/j.rser.2012.01.024.
- [5] S. G. Sahu, N. Chakraborty, and P. Sarkar, "Coal-biomass co-combustion: An overview," *Renew. Sustain. Energy Rev.*, vol. 39, pp. 575–586, 2014, doi: 10.1016/j.rser.2014.07.106.
- [6] C. L. Yiin, S. Yusup, P. Udomsap, B. Yoosuk, and S. Sukkasi, *Stabilization of Empty Fruit Bunch (EFB) derived Bio-oil using Antioxidants*, vol. 33, no. Heinzerling 2010. Elsevier, 2014. doi: 10.1016/B978-0-444-63456-6.50038-7.
- [7] T. N. Pham, D. Shi, and D. E. Resasco, "Kinetics and mechanism of ketonization of acetic acid on Ru/TiO<sub>2</sub> catalyst," *Top. Catal.*, vol. 57, no. 6–9, pp. 706–714, 2013, doi: 10.1007/s11244-013-0227-7.
- [8] E. F. Iliopoulou, K. S. Triantafyllidis, and A. A. Lappas, "Overview of catalytic upgrading of biomass pyrolysis vapors toward the production of fuels and high-value chemicals," *Wiley Interdisciplinary Reviews: Energy and Environment*, vol. 8, no. 1. 2019. doi: 10.1002/wene.322.
- [9] S. Wang and E. Iglesia, "Experimental and theoretical assessment of the

- mechanism and site requirements for ketonization of carboxylic acids on oxides," *J. Catal.*, vol. 345, pp. 183–206, 2017, doi: 10.1016/j.jcat.2016.11.006.
- [10] B. Boekaerts and B. F. Sels, "Catalytic advancements in carboxylic acid ketonization and its perspectives on biomass valorisation," *Appl. Catal. B Environ.*, vol. 283, p. 119607, Apr. 2021, doi: 10.1016/J.APCATB.2020.119607.
- [11] Z. He and X. Wang, "Required catalytic properties for alkane production from carboxylic acids: Hydrodeoxygenation of acetic acid," 2013.
- [12] T. N. Pham, D. Shi, and D. E. Resasco, "Reaction kinetics and mechanism of ketonization of aliphatic carboxylic acids with different carbon chain lengths over Ru/TiO<sub>2</sub> catalyst," *J. Catal.*, vol. 314, pp. 149–158, 2014, doi: 10.1016/j.jcat.2014.04.008.
- [13] S. Wang and E. Iglesia, "Experimental and theoretical assessment of the mechanism and site requirements for ketonization of carboxylic acids on oxides," *J. Catal.*, vol. 345, pp. 183–206, 2017, doi: 10.1016/j.jcat.2016.11.006.
- [14] F. Caremoli, Master thesis in Politecnico di Milano, "Catalytic upgrade of bio-vapours: Experimental analysis of acetic acid ketonization on TiO<sub>2</sub> catalyst," 2021.
- [15] J. H. Shin, G. J. Kim, and S. C. Hong, "Reaction properties of ruthenium over Ru/TiO<sub>2</sub> for selective catalytic oxidation of ammonia to nitrogen," *Appl. Surf. Sci.*, vol. 506, no. November 2019, p. 144906, 2020, doi: 10.1016/j.apsusc.2019.144906.
- [16] S. Chai *et al.*, "Boosting CO<sub>2</sub> methanation activity on Ru/TiO<sub>2</sub> catalysts by exposing (001) facets of anatase TiO<sub>2</sub>," *J. CO<sub>2</sub> Util.*, vol. 33, no. June, pp. 242–252, 2019, doi: 10.1016/j.jcou.2019.05.031.
- [17] R. V. Mikhaylov, K. V. Nikitin, N. I. Glazkova, and V. N. Kuznetsov, "Temperature-programmed desorption of CO<sub>2</sub>, formed by CO photooxidation on TiO<sub>2</sub> surface," *J. Photochem. Photobiol. A Chem.*, vol. 360, no. January, pp. 255–261, 2018, doi: 10.1016/j.jphotochem.2018.04.055.
- [18] L. Faba, J. Gancedo, J. Quesada, E. Diaz, and S. Ordóñez, "One-Pot Conversion of Acetone into Mesitylene over Combinations of Acid and Basic Catalysts," *ACS Catal.*, vol. 11, no. 18, pp. 11650–11662, 2021, doi: 10.1021/acscatal.1c03095.
- [19] S. Tosoni, H. Y. T. Chen, A. R. Puigdollers, and G. Pacchioni, "TiO<sub>2</sub> and ZrO<sub>2</sub> in biomass conversion: Why catalyst reduction helps," *Philosophical Transactions of the Royal Society A: Mathematical, Physical and Engineering Sciences*, vol. 376, no. 2110. Royal Society Publishing, Jan. 13, 2018. doi: 10.1098/rsta.2017.0056.
- [20] S. Tosoni and G. Pacchioni, "Acetic acid ketonization on tetragonal zirconia: Role of surface reduction," *J. Catal.*, vol. 344, pp. 465–473, Dec. 2016, doi: 10.1016/J.JCAT.2016.10.002.

- [21] F. Lu, B. B. Jiang, J. Wang, Z. Huang, Z. Liao, and Y. Yang, "Insights into the improvement effect of Fe doping into the CeO<sub>2</sub> catalyst for vapor phase ketonization of carboxylic acids," *Mol. Catal.*, vol. 444, pp. 22–33, Jan. 2018, doi: 10.1016/J.MCAT.2017.05.022.
- [22] H. Y. T. Chen, S. Tosoni, and G. Pacchioni, "Adsorption of ruthenium atoms and clusters on anatase TiO<sub>2</sub> and tetragonal ZrO<sub>2</sub>(101) surfaces: A comparative DFT study," *J. Phys. Chem. C*, vol. 119, no. 20, pp. 10856–10868, 2015, doi: 10.1021/jp510468f.
- [23] X. Y. Gao, K. Hidajat, and S. Kawi, "Facile synthesis of Ni/SiO<sub>2</sub> catalyst by sequential hydrogen/air treatment: A superior anti-coking catalyst for dry reforming of methane," *J. CO<sub>2</sub> Util.*, vol. 15, pp. 146–153, Sep. 2016, doi: 10.1016/J.JCOU.2016.05.007.





## List of Figures

Figure 1.1 – Liquid bio-fuels projection to 2050.....	4
Figure 1.2 – Ketonization reaction .....	7
Figure 1.3 – Ketonization path of reaction Part. 1 .....	8
Figure 1.4 – Ketonization path of reaction Part. 2 .....	9
Figure 1.5 – Aldol condensation mechanism of aldehydes or ketones .....	10
Figure 2.1 – Picture of the plant.....	14
Figure 2.2 – P&ID of the plant .....	14
Figure 2.3 – Calibration result for air MFC.....	16
Figure 2.4 – Reactor scheme.....	18
Figure 2.5 – Temperature profile of the reactor .....	19
Figure 2.6 – Scheme of the valve positions, A and B.....	20
Figure 2.7 – Example of resulting chromatogram .....	21
Figure 2.8 – Picture of GC-TCD.....	22
Figure 2.9 – Picture of Micro-GC.....	24
Figure 2.10 – Acetic acid recognition from GC-MS analysis.....	25
Figure 2.11 – Picture of GC-MS .....	26
Figure 2.12 – Dry impregnation for Ru/TiO <sub>2</sub> from nitrate solution. TiO <sub>2</sub> (A), Flask with nitrate solution (B), impregnated Ru/TiO <sub>2</sub> (C) .....	28
Figure 2.13 – Catalytic bed reactors: Fixed(A), Fluidized(B) and Moving(C) .....	32
Figure 2.14 – Reactor scheme.....	33
Figure 2.15 - Example of Origin graph.....	45
Figure 3.1 – BET results comparison between TiO <sub>2</sub> fresh and TiO <sub>2</sub> spent .....	48
Figure 3.2 – Hg porosimetry on TiO <sub>2</sub> fresh and TiO <sub>2</sub> .spent.....	50
Figure 3.3 - TPR results on TiO <sub>2</sub> and Ru/TiO <sub>2</sub> .....	51
Figure 3.4 - Analysis of the gas-phase composition during TPR tests over the sample of TiO <sub>2</sub> , Ru/TiO <sub>2</sub> from chloride and nitrate Ru precursors. (Part 1) .....	54

Figure 3.5 – Analysis of the gas-phase composition during TPR tests over the sample of TiO <sub>2</sub> , Ru/TiO <sub>2</sub> from chloride and nitrate Ru precursors. (Part 2) .....	55
Figure 3.6 – CO <sub>2</sub> TPD results for TiO <sub>2</sub> fresh, TiO <sub>2</sub> reduced and TiO <sub>2</sub> reduced after ket .....	57
Figure 3.7 - NH <sub>3</sub> TPD results on TiO <sub>2</sub> fresh, TiO <sub>2</sub> reduced and TiO <sub>2</sub> reduced after ket .....	59
Figure 3.8 - Acetic Acid TPD on TiO <sub>2</sub> , Ru/TiO <sub>2</sub> (Cl) and Ru/TiO <sub>2</sub> all reduced .....	61
Figure 3.9 – Cracking mechanism of intermediate C <sub>6</sub> .....	62
Figure 4.1 – General reactor before experiment (A) and two dirty quartz columns post-experiments (B and C) .....	66
Figure 4.2– Effect of regeneration on quartz reactivity. Flux: 100 Nml/min of 3% Acetic acid, 20% H <sub>2</sub> , 15% N <sub>2</sub> in He (Part 1) .....	68
Figure 4.3 – Effect of regeneration on quartz reactivity. Flux: 100 Nml/min of 3% Acetic acid, 20% H <sub>2</sub> , 15% N <sub>2</sub> in He (Part 2) .....	69
Figure 4.4 – Effect of H <sub>2</sub> co-feed on 66Nml/min of 3% Acetic acid, 20% H <sub>2</sub> (if co-fed), 10% N <sub>2</sub> in He .....	70
Figure 4.5 - Flow rate effect on quartz reactivity. Flux: 100-150 Nml/min of 3% Acetic acid, 20% H <sub>2</sub> 15% N <sub>2</sub> in He (Part 1) .....	71
Figure 4.6 – Flow rate effect on quartz reactivity. Flux: 100-150 Nml/min of 3% Acetic acid, 20% H <sub>2</sub> 15% N <sub>2</sub> in He (Part 2) .....	72
Figure 4.7 – Effect of H <sub>2</sub> pre-treatment on composition for TiO <sub>2</sub> oxidated, reduced after ketonization and reduced. GHSV: 20000 NL/h/kg <sub>cat</sub> ; Flux: 3%Acetic acid, 10% N <sub>2</sub> in He .....	75
Figure 4.8 - Effect of H <sub>2</sub> pre-treatment on composition for 1,2% Ru/TiO <sub>2</sub> oxidated, reduced after ketonization and reduced. GHSV: 20000 NL/h/kg <sub>cat</sub> ; Flux: 3%Acetic acid, 10% N <sub>2</sub> in He .....	76
Figure 4.9 – Ru effect on reduced catalysts. GHSV: 20000 NL/h/kg <sub>cat</sub> ; Flux: 3%Acetic acid, 10% N <sub>2</sub> in He .....	78
Figure 4.10 – Different TiO <sub>2</sub> (Fluka vs. DT-51D) activity on reduced catalysts. GHSV: 20000 NL/h/kg <sub>cat</sub> ; Flux: 3%Acetic acid, 10% N <sub>2</sub> in He.....	79
Figure 4.11 – Results comparison between Ru(Cl) and Ru(N). GHSV: 20000 NL/h/kg <sub>cat</sub> ; Flux: 3%Acetic acid, 10% N <sub>2</sub> in He.....	80
Figure 4.12 – C balance drop on ketonization at high temperature. GHSV = 20,000 NL/h/kg <sub>cat</sub> (total flowrate = 4470 μmol/min). Feed composition: CH <sub>3</sub> COOH=3%, N <sub>2</sub> =10% in He, H <sub>2</sub> =20% in He.....	81
Figure 4.13 – Peak association between GC and GC-MS analyses.....	82

Figure 4.14 – Effect of temperature on conversion, C-balance and molar fraction of ketonization reaction products. GHSV: 20000 NI/h/kg <sub>cat</sub> ; Flux: 3% Acetic acid, 10% N <sub>2</sub> in He .....	85
Figure 4.15 – Effect of temperature on condensation products. GHSV: 20000 NI/h/kg <sub>cat</sub> ; Flux: 3% Acetic acid, 10% N <sub>2</sub> in He.....	86
Figure 4.16 – Condensation reactions of acetone.....	87
Figure 4.17 – Effect of temperature on olefinic and other products. GHSV: 20000 NI/h/kg <sub>cat</sub> ; Flux: 3% Acetic acid, 10% N <sub>2</sub> in He.....	88
Figure 4.18 – Other secondary reactions of intermediate products.....	89
Figure 4.19 - C-selectivity of C <sub>i</sub> products at 300°C over time.....	90
Figure 4.20 - C-selectivity of C <sub>i</sub> products at 350°C over time.....	91
Figure 4.21 – C-selectivity of C <sub>i</sub> products at 400°C over time.....	92
Figure 4.22 – H <sub>2</sub> effect at 300°C on main products composition. GHSV: 20000 NI/h/kg <sub>cat</sub> ; Flux: 3% Acetic acid, 20% H <sub>2</sub> (if co-fed), 10% N <sub>2</sub> in He (Part 1).....	93
Figure 4.23 - H <sub>2</sub> effect at 300°C on cracking products composition. GHSV: 20000 NI/h/kg <sub>cat</sub> ; Flux: 3% Acetic acid, 20% H <sub>2</sub> (if co-fed), 10% N <sub>2</sub> in He (Part 2).....	94
Figure 4.24 - H <sub>2</sub> effect at 300°C on condensate products composition. GHSV: 20000 NI/h/kg <sub>cat</sub> ; Flux: 3% Acetic acid, 20% H <sub>2</sub> (if co-fed), 10% N <sub>2</sub> in He.....	94
Figure 4.25 - H <sub>2</sub> effect at 300°C on other products composition. GHSV: 20000 NI/h/kg <sub>cat</sub> ; Flux: 3% Acetic acid, 20% H <sub>2</sub> (if co-fed), 10% N <sub>2</sub> in He.....	95
Figure 4.26 - H <sub>2</sub> effect at 400°C on main products composition. GHSV: 20000 NI/h/kg <sub>cat</sub> ; Flux: 3% Acetic acid, 20% H <sub>2</sub> (if co-fed), 10% N <sub>2</sub> in He.....	96
Figure 4.27 - H <sub>2</sub> effect at 400°C on main products composition. GHSV: 20000 NI/h/kg <sub>cat</sub> ; Flux: 3% Acetic acid, 20% H <sub>2</sub> (if co-fed), 10% N <sub>2</sub> in He (Part 2).....	96
Figure 4.28 - H <sub>2</sub> effect at 400°C on condensation products composition. GHSV: 20000 NI/h/kg <sub>cat</sub> ; Flux: 3% Acetic acid, 20% H <sub>2</sub> (if co-fed), 10% N <sub>2</sub> in He.....	97
Figure 4.29 - H <sub>2</sub> effect at 400°C on secondary products composition. GHSV: 20000 NI/h/kg <sub>cat</sub> ; Flux: 3% Acetic acid, 20% H <sub>2</sub> (if co-fed), 10% N <sub>2</sub> in He.....	98
Figure 4.30 – Condensation of C-species on the reactor tail for tests on TiO <sub>2</sub> at 400°C .....	99
Figure 4.31 – Ru addition effect at 400°C on main products composition. GHSV: 20000 NI/h/kg <sub>cat</sub> ; Flux: 3% Acetic acid, 20% H <sub>2</sub> , 10% N <sub>2</sub> in He (Part 1).....	100
Figure 4.32 - Ru addition effect at 400°C on main products composition. GHSV: 20000 NI/h/kg <sub>cat</sub> ; Flux: 3% Acetic acid, 20% H <sub>2</sub> (if co-fed), 10% N <sub>2</sub> in He (Part 2).....	101

Figure 4.33 - Ru addition effect at 400°C on condensation products composition. GHSV: 20000 NI/h/kg <sub>cat</sub> ; Flux: 3% Acetic acid, 20% H <sub>2</sub> , 10% N <sub>2</sub> in He.....	102
Figure 4.34 - Ru addition effect at 400°C on other secondary products composition. GHSV: 20000 NI/h/kg <sub>cat</sub> ; Flux: 3% Acetic acid, 20% H <sub>2</sub> , 10% N <sub>2</sub> in He.....	103
Figure 4.35 - H <sub>2</sub> effect at 400°C and 100 Nml/min on main products composition. GHSV: 20000 NI/h/kg <sub>cat</sub> ; Flux: 3% Acetic acid, 20% H <sub>2</sub> (if co-fed), 10% N <sub>2</sub> in He .....	104
Figure 4.36 - H <sub>2</sub> effect at 400°C and 100 Nml/min on main products composition. GHSV: 20000 NI/h/kg <sub>cat</sub> ; Flux: 3% Acetic acid, 20% H <sub>2</sub> (if co-fed), 10% N <sub>2</sub> in He .....	105
Figure 4.37 - H <sub>2</sub> effect at 400°C and 100 Nml/min on condensation products composition. GHSV: 20000 NI/h/kg <sub>cat</sub> ; Flux: 3% Acetic acid, 20% H <sub>2</sub> (if co-fed), 10% N <sub>2</sub> in He .....	106
Figure 4.38 - H <sub>2</sub> effect at 400°C and 100 Nml/min on cracking products composition. GHSV: 20000 NI/h/kg <sub>cat</sub> ; Flux: 3% Acetic acid, 20% H <sub>2</sub> (if co-fed), 10% N <sub>2</sub> in He .....	107
Figure 4.39 – Reactor view post-experiment with prolonged ketonization of TiO <sub>2</sub> at 400°C with H <sub>2</sub> co-feed .....	108
Figure 4.40 – Products composition over Temperature on TPO analyses for TiO <sub>2</sub> tested at the three different ketonization temperatures. Flux: 25 Nml/min of air.....	110
Figure 4.41 – Reactor view at two different temperatures (300 and 400°C) for TiO <sub>2</sub> and Ru/TiO <sub>2</sub> post-keronization.....	113
Figure 4.42 – CO <sub>2</sub> , H <sub>2</sub> O and CH <sub>4</sub> composition over temperature for TPO tests on TiO <sub>2_400</sub> and TiO <sub>2_400_H2</sub> .....	114
Figure 4.43 - CO <sub>2</sub> , H <sub>2</sub> O and CH <sub>4</sub> composition over temperature for TPO tests on TiO <sub>2_300</sub> and TiO <sub>2_300_H2</sub> .....	115
Figure 4.44 – Composition results over temperature for TiO <sub>2</sub> and Ru/TiO <sub>2</sub> (Cl) ketonized at 400°C with H <sub>2</sub> .....	118

## List of Tables

Table 2.1 – Antoine coefficients table .....	17
Table 2.2 – GC columns specifications .....	21
Table 2.3 – Columns characteristics for Micro GC Fusion .....	23
Table 2.4 – GC-MS column characteristics.....	25
Table 2.5 – Reactors summary .....	37
Table 2.6 – Response factors table for GC.....	42
Table 3.1 - BET results test for TiO <sub>2</sub> fresh and TiO <sub>2</sub> spent .....	49
Table 3.2 - Hg porosimetry results on TiO <sub>2</sub> spent and TiO <sub>2</sub> fresh .....	50
Table 3.3 – Catalyst tested with CO <sub>2</sub> TPD.....	56
Table 3.4 - Integration results for CO <sub>2</sub> TPD tests .....	57
Table 3.5 – Integration results of NH <sub>3</sub> TPD .....	59
Table 3.6 – Catalysts tested with Acetic Acid TPD.....	60
Table 3.7 - Integration results for Acetic acid TPD.....	62
Table 4.1 – Reactors’ summary for blank tests .....	67
Table 4.2 – Reactors’ conditions summary for ketonization tests .....	73
Table 4.3 – New species recognized with GC/GC-MS coupling .....	83
Table 4.4 – Reactors tested with prolonged ketonization.....	84
Table 4.5 - Integration results for TPO tests on TiO <sub>2</sub> at 300-350-400°C.....	111
Table 4.6 – Percentage of C deposited during ketonization of TiO <sub>2</sub> at 300-350-400°C .....	112
Table 4.7 - Integration results for TPO on TiO <sub>2_400</sub> and TiO <sub>2_400_H2</sub> .....	116
Table 4.8 – Percentage of C deposited for TiO <sub>2</sub> at 400°C .....	116
Table 4.9 - Integration results for TPO on TiO <sub>2_300</sub> and TiO <sub>2_300_H2</sub> .....	117
Table 4.10 – Percentage of C-moles for TiO <sub>2</sub> at 300°C.....	117
Table 4.11 – Integration results for Ru effect on TiO <sub>2_400_H2</sub> and Ru/TiO <sub>2_400_H2</sub> .....	119
Table 4.12 – C-moles percentage difference between TiO <sub>2</sub> and Ru/TiO <sub>2</sub> at 400°C.....	119



## List of symbols

Variable	Description	SI unit
$F_i$	Flow rate	Nml/min
$N_i$	Flow rate	Nml/min
$a$	MFC curve slope	Nml/min/%opening
$b$	MFC curve intercept	Nml/min
$p$	Pressure	bar
$T$	Temperature	°C, °K
$p_o$	Saturation pressure	bar
$A_i$	Antoine coefficient	[-]
$B_i$	Antoine coefficient	[-]
$C_i$	Antoine coefficient	[-]
$y_i$	Gaseous molar fraction	[-]
$x_i$	Liquid molar fraction	[-]
$f_c$	Antoine correction factor	[-]
$V_{measured}$	Volume	ml
$t_{average}$	Time	min
$n_i$	Number of moles	mmol
$A_i$	Integrated peaks area	μV*s
$k_i$	Stoichiometric coefficient	[-]
$\omega_{Ru}$	Ruthenium percentage	%
$m_{Ru}$	Ruthenium mass	mg
$\chi_j$	Acetic acid conversion	%
$x_{areaN_2}$	Fraction of N <sub>2</sub> apparent area	[-]
$\sigma_{C,i}$	C balance	[-]
$f_i$	Area ratio $A_i/A_{N_2i}$	[-]





## Acknowledgments

I would like to dedicate this space to those who, with dedication and patience, contributed to the realisation of this paper.

My first thanks go to my advisor Professor Beretta, who granted me the opportunity to work on this topic. Thanks also to my co-advisor Veronica Piazza, for guiding and helping me through this experience, for the multiple advice and for promptly suggesting the right changes to my thesis.

Thanks to all my engineering colleagues, for always encouraging me from the beginning of my university career. A special mention for Filippo, Paolo and Angelo, who were my co-workers in B18, I wish you all the best.

I am infinitely grateful to my mother and father, without their teaching and support, this thesis work would not even exist. Thanks to my sister, who continually supports and endures me, and whom I wish a great career as a physiotherapist.

A heartfelt thank you to all my friends who have always been there for me over the years: from the “Pungio” and “Zandorlago” boys, to those of “Sette nani” and all those I regard with affection. I have made many joyful memories with all of you, and I hope to continue to do so.

My special thanks go to my love Giulia, who has become my point of reference in everyday life, thank you for always being by my side.

